Universidade Federal da Bahia

Programa de Pós-Graduação em Física

Standard Perturbation Theory (SPT) for models with interaction in the dark sector

Matheus Monteiro Wolney Mello

Thesis submitted as part of the requirements for the degree of Master in Physics.

Supervisor: Prof. Rodrigo von Marttens
Universidade Federal da Bahia (Brazil)

Co-supervisor: Prof. Iuri Baranov
Instituto Federal da Bahia (Brazil)

February 19, 2026

Universidade Federal da Bahia
Grupo de Gravitação e Cosmologia
Programa de Pós-Graduação em Física

Standard Perturbation Theory (SPT) for models with interaction in the dark sector

Matheus Monteiro Wolney Mello

A presente dissertação "*Standard Perturbation Theory (SPT) for models with interaction in the dark sector*" foi submetida no ano de February 19, 2026 ao PPGFIS por *Matheus Monteiro Wolney Mello* como parte dos requisitos para a obtenção do título de Mestre em Cosmologia.

Caso esta dissertação venha a ser aprovada, esta folha deverá ser substituída pela correspondente de aprovação.

Abstract

This dissertation investigates the formation and nonlinear evolution of cosmic structures in cosmological models with an interacting dark sector (IDS), extending the standard ΛCDM framework. Starting from the fluid and perturbation equations governing the density and velocity fields, a fully time-dependent perturbative formalism is developed, going beyond the Einstein–de Sitter (EdS) approximation. Evolution equations for second-, third-, and arbitrary-order perturbative kernels are derived, explicitly incorporating the effects of interactions between dark matter and dark energy. A central result of this work is the critical assessment of the commonly employed approximation in which the ratio between the matter density parameter, Ω_m, and the square of the perturbation growth rate, f^2, is assumed to be approximately unity. In the ΛCDM model, this approximation is motivated by the empirical relation $f \approx \Omega_m^{0.55}$, which implies that Ω_m/f^2 remains close to unity over a significant fraction of cosmic history. This near equality allows the separation of temporal and spatial dependencies in the perturbative equations, rendering nonlinear kernels approximately time-independent and substantially simplifying analytical and numerical calculations. For this reason, the approximation based on the Einstein–de Sitter limit is frequently employed even in cosmologies where it is not strictly valid. It is nevertheless shown that, within the ΛCDM framework, this approximation remains valid even at low redshifts, since deviations from unity remain small in the late Universe. In interacting dark sector models, however, such deviations become significantly larger at late times, indicating that assumptions based on the Einstein–de Sitter limit are no longer reliable when dark sector interactions are present. Using the numerical code `SPTIDS`, developed and implemented by the author as part of this work, the matter power spectrum at one-loop level and the reduced bispectrum are computed for IDS cosmologies. The results show that dark sector interactions enhance the growth of matter perturbations and amplify higher-order correlations relative to the ΛCDM model, providing distinctive nonlinear signatures. These results demonstrate the necessity of a fully time-dependent perturbative treatment for precision modeling of large-scale structure in interacting dark sector scenarios, while also pointing to possible observational deviations from the standard cosmological model.

Resumo

Esta dissertação investiga a formação e a evolução não linear das estruturas cósmicas em modelos cosmológicos com setor escuro interagente (IDS), estendendo o arcabouço padrão do modelo ΛCDM. A partir das equações de fluido e das equações de perturbações que governam os campos de densidade e velocidade, desenvolve-se um formalismo perturbativo completamente dependente do tempo, indo além da aproximação de Einstein–de Sitter (EdS). São derivadas equações de evolução para os núcleos perturbativos de segunda, terceira e ordem arbitrária, incorporando explicitamente os efeitos das interações entre matéria escura e energia escura. Um resultado central do trabalho é a análise crítica da aproximação frequentemente empregada segundo a qual a razão entre o parâmetro de densidade de matéria, Ω_m, e o quadrado da taxa de crescimento das perturbações, f^2, é aproximadamente igual a 1. No modelo ΛCDM, essa aproximação é motivada pela relação empírica $f \approx \Omega_m^{0.55}$, o que implica que Ω_m/f^2 permanece próximo da unidade ao longo de uma fração significativa da história cósmica. Essa proximidade permite separar a dependência temporal e espacial nas equações perturbativas, tornando os núcleos não lineares aproximadamente independentes do tempo e simplificando significativamente os cálculos analíticos e numéricos. Por essa razão, a aproximação baseada no limite de Einstein–de Sitter é frequentemente utilizada mesmo em cosmologias nas quais ela não é estritamente válida. Mostra-se, contudo, que, no contexto do modelo ΛCDM, essa aproximação permanece válida mesmo em baixos redshifts, uma vez que os desvios em relação ao valor unitário permanecem pequenos no Universo recente. Em modelos com setor escuro interagente, tais desvios tornam-se ainda mais pronunciados em épocas tardias, indicando que hipóteses baseadas no limite de Einstein–de Sitter não são confiáveis quando há interações no setor escuro. Utilizando o código numérico `SPTIDS`, desenvolvido e implementado pelo autor no âmbito deste trabalho, são calculados o espectro de potência da matéria em nível de uma volta (*one-loop*) e o biespectro reduzido em cosmologias IDS. Os resultados indicam que interações no setor escuro intensificam o crescimento das perturbações de matéria e amplificam correlações de ordem superior em relação ao modelo ΛCDM, fornecendo assinaturas não lineares distintivas. Esses resultados evidenciam a necessidade de um tratamento perturbativo plenamente dependente do tempo para a modelagem de precisão da estrutura em larga escala em cenários com setor escuro interagente, além de apontarem possíveis desvios observacionais em relação ao modelo cosmológico padrão.

Acknowledgments

I would like to begin by expressing my deepest gratitude to God, for granting me the strength, perseverance, and dedication necessary to pursue my studies and complete this work. I am profoundly grateful to my wife, for her patience, unwavering support, and understanding, and to my son, for his constant encouragement throughout this journey. I extend my sincere thanks to Rodrigo von Marttens for the valuable discussions, guidance, and encouragement that greatly contributed to the progress of this research. I am also indebted to Iuri Baranov and Roberto Menezes for their support and mentorship, which have been instrumental in the development of my scientific career. Special thanks are due to Humberto Borges, whose guidance, constructive feedback, and careful review significantly enhanced the quality of this work. Finally, I gratefully acknowledge CAPES for the financial support that made the realization of this research possible.

Contents

Introduction

Somewhere, something incredible is waiting to be known.
— C. Sagan.

One of the most frequently invoked expressions in contemporary cosmological literature is that we are currently living in the so-called precision era of cosmology. Although this characterization has become something of a cliché, it accurately reflects a profound transformation in the field driven by the unprecedented volume and quality of observational data now available. As emphasized by Turner, cosmology has evolved from a largely speculative and data-limited discipline into a mature, data-driven science capable of delivering high-precision constraints on fundamental physical processes governing the Universe [1]. This transformation has been enabled by a diverse set of observational probes, including large-scale galaxy surveys, high-resolution measurements of the CMB, gravitational-wave detections, and increasingly refined distance-ladder observations [2, 3, 4].

This modern observational landscape stands in sharp contrast to the early stages of cosmology, when empirical input was scarce and theoretical modeling dominated the field. As Turner notes,

> "Only a half century ago cosmology was the province of west-coast astronomers [...] Today, cosmology is mainstream, 'industrial' science [...] the term precision cosmology is a reality." [1]

The transition from a data-starved science to one characterized by massive, high-precision datasets has enabled stringent tests of the standard cosmological model, ΛCDM, while simultaneously exposing potential shortcomings in its ability to fully account for all observational results.

Among the most significant advances of this era are the results delivered by next-generation spectroscopic surveys, most notably the Dark Energy Spectroscopic Instrument (DESI). By providing millions of precise redshift measurements, DESI has substantially improved constraints on the expansion history of the Universe and the growth of cosmic structures [5]. At the same time, DESI and other contemporary experiments have reinforced the existence of persistent tensions in cosmology, including discrepancies in the inferred value of the Hubble-Lemaître constant and in the amplitude of matter clustering inferred from large-scale structure and weak lensing observations [4, 6, 7, 8]. While these tensions may ultimately be resolved through improved control of systematic uncertainties, they may also signal the presence of new physics beyond the ΛCDM paradigm [9, 10].

A crucial component of this renewed effort to test cosmological models lies in the growing emphasis on full-shape analyses of the matter power spectrum and higher-order statistics. Unlike approaches that rely primarily on standard rulers, such as baryon acoustic oscillations (BAO), full-shape analyses exploit the complete scale-dependent information encoded in the clustering of

matter [11, 12]. As a result, they provide direct sensitivity to the underlying dynamics of structure formation, making them particularly powerful probes of modifications to gravity, departures from standard dark energy behavior, and non-standard interactions within the dark sector. With the advent of increasingly precise and extensive surveys, full-shape measurements are expected to play a central role in future efforts to constrain cosmological models and uncover possible extensions of the standard framework.

Within this context, cosmological models featuring interactions in the dark sector have received considerable attention. By allowing energy and/or momentum exchange between dark matter and dark energy, interacting dark sector (IDS) models introduce additional dynamical degrees of freedom that can significantly alter both the background evolution and the growth of cosmic structures [13, 14, 15]. Such models are particularly compelling in the precision era, as they offer potential mechanisms to alleviate existing cosmological tensions while remaining testable with current and forthcoming observational data [16, 17]. However, they also introduce theoretical and phenomenological challenges, including possible instabilities at the level of perturbations, which must be carefully addressed [18, 19].

Understanding the formation and evolution of cosmic structures remains one of the central challenges of modern cosmology. From the discovery of the cosmic microwave background to the three-dimensional mapping of galaxies across cosmic time, the study of the evolution of matter density perturbations has proven essential for reconstructing the history and dynamics of the Universe [20, 21]. In this framework, scalar perturbations play a fundamental role, as they describe the density fluctuations that grow under gravitational instability and ultimately give rise to the observed large-scale structure, particularly on subhorizon scales where gravitational interactions dominate [22, 23].

While conventional cosmological models assume a clear separation between baryonic matter, dark matter, and dark energy, the introduction of interactions within the dark sector provides a broader theoretical framework capable of addressing unresolved issues, such as the nature of cosmic acceleration and the detailed behavior of structure formation [24, 25]. These interactions not only modify the background expansion but can also significantly affect the evolution of perturbations, leaving potentially observable imprints in large-scale structure and weak lensing measurements.

In this work, we investigate scalar perturbations in interacting dark sector cosmologies within the subhorizon limit, adopting the conformal Newtonian gauge. This choice provides a transparent and physically intuitive description of the dynamics on scales where gravitational effects dominate and facilitates direct comparison with observational quantities [23, 26]. By systematically exploring the impact of dark sector interactions on the growth of perturbations, we aim to clarify their role in structure formation and assess their viability in light of modern cosmological data.

This dissertation is organized as follows. In the next section, we present a concise yet comprehensive overview of the theoretical framework underlying modern cosmology, establishing the physical assumptions, fundamental equations, and observational foundations relevant to this study [27, 28]. We then review the formalism of cosmological perturbation theory and discuss its extension to interacting dark sector models. Subsequently, we describe the methodology employed to analyze scalar perturbations in the subhorizon regime and present the main results of our analysis. Finally, we discuss the implications of these findings for contemporary cosmology and outline possible directions for future research.

1.1. Brief summary of the standard cosmological model

This chapter presents a concise overview of the theoretical framework underlying this work. The standard cosmological model, known as the ΛCDM model, constitutes the current paradigm for describing the large-scale structure and dynamical evolution of the Universe. It arises from the interplay between General Relativity and a wide range of high-precision cosmological observations, providing a consistent description of both the background expansion and the growth of cosmic structures.[11]

At its foundation, the model assumes that gravity is governed by Einstein's field equations and that, on sufficiently large scales, the Universe obeys the Cosmological Principle — namely, that it is homogeneous and isotropic. These symmetry assumptions lead to the Friedmann—Lemaître—Robertson—Walker (FLRW) metric, which reduces the dynamics of spacetime to the evolution of a single function, the scale factor $a(t)$. The resulting Friedmann equations relate the expansion rate of the Universe to its total energy content.[26]

Within this framework, the Big Bang scenario emerges naturally as a consequence of an expanding solution of Einstein's equations. Extrapolating backward in time implies that the Universe originated approximately 13.8 billion years ago from a hot and dense state. As it expanded and cooled, it underwent a sequence of physical processes including Big Bang Nucleosynthesis (BBN), recombination, and structure formation. These epochs are strongly supported by independent observational probes.

A central empirical pillar of the ΛCDM model is the CMB, which provides a snapshot of the Universe at the epoch of recombination, roughly 380,000 years after the Big Bang. The near isotropy of the CMB validates the assumption of large-scale homogeneity, while its small anisotropies encode the primordial density perturbations that seeded the formation of galaxies and clusters. The statistical properties of these fluctuations connect early-Universe physics with the present distribution of large-scale structure.

The ΛCDM model is specified by a minimal set of cosmological parameters that completely determine both the background expansion history and the evolution of linear perturbations [2]. In this work, we adopt the parameter values inferred by the *Planck Collaboration* from measurements of the CMB. These values will be consistently used throughout the entire analysis as our fiducial cosmological configuration.

The present-day expansion rate of the Universe is characterized by the Hubble–Lemaître constant,

$$H_0 = 67.66 \pm 0.42\,\mathrm{km\ s^{-1}Mpc^{-1}},$$

which sets the current normalization of the Hubble parameter $H(a)$ and determines the overall time scale of cosmic evolution. Through the Friedmann equations, H_0 fixes the present critical density,

$$\rho_{\mathrm{crit},0} = \frac{3H_0^2}{8\pi G},$$

with respect to which all density parameters are defined.

The total matter density parameter,

$$\Omega_m = 0.3111 \pm 0.00561,$$

represents the fractional contribution of non-relativistic matter to the total energy density of the Universe today. It includes both baryonic matter and cold dark matter components and plays a central role in governing gravitational clustering and structure formation.

The physical baryon density is given by

$$\Omega_b h^2 = 0.02242 \pm 0.00014,$$

where $h \equiv H_0/(100\,\mathrm{km\ s^{-1}Mpc^{-1}})$. This parameter determines the abundance of ordinary matter, influences the physics of recombination, and controls the amplitude of baryon acoustic oscillations.

Cold dark matter contributes

$$\Omega_c h^2 = 0.11933 \pm 0.00091,$$

which quantifies the density of a non-relativistic, non-baryonic component that interacts gravitationally but not electromagnetically. Its cold nature allows small-scale perturbations to grow efficiently, seeding the formation of galaxies and large-scale structure.

Dark energy is modeled as a cosmological constant Λ, contributing

$$\Omega_\Lambda = 0.6889 \pm 0.0056.$$

This component dominates the present energy budget and is responsible for the observed late-time accelerated expansion. The corresponding effective value of the cosmological constant is approximately

$$\Lambda \sim 10^{-52}\,\mathrm{m^{-2}}.$$

Together with the matter density, these values are consistent with spatial flatness, as indicated by the curvature constraint

$$\Omega_k \approx 0,$$

which implies that the total energy density is very close to the critical density.

Additional parameters characterize the statistical properties of primordial perturbations and the growth of cosmic structure. The scalar spectral index,

$$n_s = 0.9665 \pm 0.0038,$$

describes the scale dependence of the primordial power spectrum and indicates a nearly scale-invariant spectrum, consistent with simple inflationary scenarios.

The amplitude of primordial curvature perturbations is given by

$$\ln(10^{10} A_s) = 3.047 \pm 0.014,$$

which sets the initial normalization of density fluctuations. The present-day amplitude of matter fluctuations on scales of $8\,h^{-1}$Mpc is quantified by

$$\sigma_8 = 0.8102 \pm 0.0060,$$

a key observable that directly constrains the growth rate of structures and will be particularly relevant for comparisons involving perturbative predictions.

The optical depth to reionization,

$$\tau_{\mathrm{rei}} = 0.0561 \pm 0.0071,$$

encodes the integrated Thomson scattering probability of CMB photons after recombination and affects the large-scale polarization anisotropies.

Finally, the age of the Universe is tightly constrained at

$$t_0 = 13.787 \pm 0.020 \text{ Gyr},$$

which follows consistently from the background dynamics determined by the above parameters.

Throughout this work, all background quantities, linear growth functions, and perturbative calculations within the ΛCDM framework will be computed using this fiducial parameter set derived from the *Planck Collaboration*[2] results. This ensures internal consistency between the background cosmology and the perturbative analysis developed in the subsequent chapters.

The remarkable success of the ΛCDM model lies in its ability to simultaneously account for multiple independent observables: the acoustic peaks in the CMB, the baryon acoustic oscillation scale in galaxy surveys, the abundances predicted by Big Bang Nucleosynthesis, and the clustering properties of large-scale structure. This concordance across different epochs and physical scales justifies its status as the standard cosmological model.

Nevertheless, despite its empirical success, ΛCDM remains theoretically incomplete as seen in [5]. The fundamental nature of dark matter is still unknown, and the cosmological constant poses deep conceptual challenges related to its extremely small but nonzero value. Moreover, observational tensions — such as the discrepancy in measurements of H_0 — motivate the exploration of extensions beyond the minimal framework. As we will discuss in subsection 1.6.2.

As emphasized in [26], the requirement that dark matter be cold is essential for structure formation. If dark matter were relativistic, its large thermal velocities would suppress small-scale fluctuations via free streaming, in conflict with observed galaxy clustering. The combined evidence from BBN, the CMB, and large-scale structure strongly supports the existence of a non-baryonic, non-relativistic matter component.

From this point onward, we adopt natural units,

$$c = \hbar = k_B = 1,$$

which simplify the expressions that will appear throughout this work.

In the next section, we examine the Cosmological Principle, as it provides the symmetry assumptions that underpin the FLRW description and the geometrical foundation of the standard cosmological model.

1.1.1. The Cosmological Principle

The *Cosmological Principle* is a fundamental assumption upon which modern cosmology is built. It asserts that, when considered on sufficiently large scales, the Universe is both **homogeneous**—the same at every point—and **isotropic**—the same in every direction [27]. Although clearly violated on small scales due to the presence of galaxies, clusters, and voids, the principle is regarded as an excellent approximation at scales larger than approximately 100 megaparsecs [26].

Homogeneity refers to the uniformity of the Universe's large-scale composition and physical properties regardless of location. Isotropy, on the other hand, implies that there is no preferred direction in the Universe; observations made from any vantage point should reveal a statistically similar cosmos in all directions. While these assumptions cannot be proven from first principles, they are strongly supported by a variety of observational data.

One of the most compelling pieces of evidence for isotropy arises from measurements of the CMB radiation. Data from space-based missions such as *COBE*, *WMAP*, and *Planck* have revealed that temperature fluctuations in the CMB are on the order of 10^{-5}, consistent with a

Universe that is remarkably isotropic on the largest observable scales [2]. Homogeneity is more difficult to verify directly, but it is inferred from large-scale galaxy surveys—such as the Sloan Digital Sky Survey (SDSS)—which show that the distribution of matter becomes statistically uniform beyond certain scales [29].

The adoption of the Cosmological Principle enables the derivation of the Friedmann-Lemaître-Robertson-Walker (FLRW) metric, which serves as the geometric foundation for the standard model of cosmology. By assuming homogeneity and isotropy, Einstein's field equations reduce to a set of simpler differential equations that describe the dynamic evolution of the Universe. This framework supports the study of key cosmological phenomena such as the Hubble expansion, structure formation, and the thermal history of the cosmos [20].

Despite being an idealization, this principle has proven to be a remarkably successful and predictive tool. It underlies the interpretation of a wide range of observational data and remains one of the cornerstones of our current understanding of the Universe.

1.1.2. Scale Factor and Hubble Rate

The large-scale dynamics of the Universe are conveniently described in terms of the *scale factor*, $a(t)$, which parametrizes the relative expansion of spatial distances as a function of cosmic time t. Within the framework of homogeneous and isotropic cosmology, all physical length scales evolve proportionally to $a(t)$, making it a fundamental quantity for characterizing cosmic expansion [21, 26].

Observationally, the expansion of the Universe is probed through the redshift z of electromagnetic radiation emitted by distant sources. The redshift is directly related to the scale factor according to

$$1 + z \equiv \frac{\lambda_{\text{obs}}}{\lambda_{\text{emit}}} = \frac{a_0}{a(t)}, \tag{1.1}$$

where λ_{obs} and λ_{emit} denote the observed and emitted wavelengths, respectively. It is conventional to normalize the present-day scale factor to unity, $a_0 \equiv a(t_0) = 1$, so that the redshift provides a direct observational measure of the expansion history of the Universe [26, 21].

The rate at which the scale factor evolves is quantified by the *Hubble parameter*,

$$H(t) \equiv \frac{1}{a(t)} \frac{da(t)}{dt}, \tag{1.2}$$

which sets the characteristic expansion timescale of the Universe. The present value of this quantity, H_0, known as the Hubble-Lemaître constant, plays a central role in observational cosmology and serves as a key parameter in the standard cosmological model [26].

Beyond its kinematical interpretation, the Hubble parameter enters fundamentally into the dynamical description of the Universe. It determines the critical energy density required for spatial flatness and governs the evolution of cosmological fluids through the Friedmann equations [21]. In models that extend beyond ΛCDM, such as interacting dark energy or coupled quintessence scenarios, modifications to the background expansion rate encoded in $H(t)$ directly reflect the presence of non-standard interactions in the dark sector [13].

In the following section, we move from this kinematical description of cosmic expansion to its geometrical formulation. The quantities $a(t)$ and $H(t)$ acquire precise meaning only when embedded in a consistent spacetime geometry, which in General Relativity is specified by the metric tensor. The introduction of the spacetime metric allows the expansion history to be related to the curvature and dynamics of spacetime itself, providing the foundation for the subsequent analysis.

1.1.3. Metric and Symmetries of the Universe

The geometry of spacetime is described by the metric tensor $g_{\mu\nu}$, which determines the infinitesimal interval between two events through the line element

$$ds^2 = g_{\mu\nu} dx^\mu dx^\nu, \tag{1.3}$$

where dx^μ denotes the differentials of the spacetime coordinates. The metric encodes the fundamental geometric properties of the manifold, such as distances, angles, and the causal structure.

To describe the large-scale structure of the universe, we adopt the *Cosmological Principle*, which asserts that on sufficiently large scales the universe is both spatially homogeneous and isotropic. Homogeneity implies invariance under spatial translations, while isotropy requires invariance under spatial rotations about any point. These assumptions severely constrain the form of the metric: the spatial sections of the universe must be maximally symmetric three-dimensional manifolds characterized by constant curvature.

Accordingly, the most general line element consistent with these symmetries is the Friedmann–Lemaître–Robertson–Walker (FLRW) metric, written in comoving spherical coordinates (r, θ, ϕ) and cosmic time t as

$$ds^2 = -dt^2 + a(t)^2 \left[\frac{dr^2}{1 - kr^2} + r^2 d\theta^2 + r^2 \sin^2\theta \, d\phi^2 \right], \tag{1.4}$$

where $a(t)$ is the scale factor and k is the curvature parameter, with

$$k = \begin{cases} 0 & \text{flat (Euclidean)}, \\ +1 & \text{positively curved (spherical)}, \\ -1 & \text{negatively curved (hyperbolic)}. \end{cases}$$

Observational data, particularly from precision measurements of the cosmic microwave background and large-scale structure surveys, provide strong evidence that the spatial curvature parameter satisfies $k \simeq 0$. Current constraints therefore indicate that the Universe is spatially flat to a high degree of accuracy. Motivated by these results, throughout this dissertation we restrict our attention to the flat case of the Friedmann–Lemaître–Robertson–Walker (FLRW) geometry, for which the line element is governed by the metric tensor

$$g_{\mu\nu} = \begin{pmatrix} -1 & 0 & 0 & 0 \\ 0 & a^2(t) & 0 & 0 \\ 0 & 0 & a^2(t) & 0 \\ 0 & 0 & 0 & a^2(t) \end{pmatrix}. \tag{1.5}$$

Within this spacetime, the trajectories of freely falling particles are determined by the geodesic equation,

$$\frac{d^2 x^\mu}{d\lambda^2} + \Gamma^\mu_{\alpha\beta} \frac{dx^\alpha}{d\lambda} \frac{dx^\beta}{d\lambda} = 0, \tag{1.6}$$

which expresses the fact that, in the absence of non-gravitational forces, particles move along paths that extremize the spacetime interval. Here, λ is an affine parameter along the worldline, and the Christoffel symbols $\Gamma^\mu_{\alpha\beta}$ encode the effects of spacetime curvature induced by the cosmic expansion. They are defined in terms of the metric tensor as

$$\Gamma^\mu_{\alpha\beta} = \frac{g^{\mu\nu}}{2} \left(g_{\alpha\nu,\beta} + g_{\beta\nu,\alpha} - g_{\alpha\beta,\nu} \right), \tag{1.7}$$

and therefore vanish in flat Minkowski spacetime, while becoming nonzero in an expanding Universe.

For the spatially flat FLRW metric, the high degree of symmetry greatly simplifies the connection coefficients. The only non-vanishing components of $\Gamma^{\mu}_{\alpha\beta}$ are

$$\Gamma^{0}_{ij} = \delta_{ij}\, a\dot{a}, \tag{1.8}$$

$$\Gamma^{i}_{0j} = \Gamma^{i}_{j0} = \delta^{i}{}_{j}\,\frac{\dot{a}}{a}, \tag{1.9}$$

where $a(t)$ is the scale factor and an overdot denotes a derivative with respect to cosmic time. Physically, these components encode the influence of the Hubble expansion on particle trajectories: Γ^{0}_{ij} accounts for the redshifting of particle energies, while Γ^{i}_{0j} describes the dilution of spatial momenta due to the expansion of space.

It is convenient to introduce the four-momentum of the particle,

$$P^{\alpha} \equiv \frac{dx^{\alpha}}{d\lambda}, \tag{1.10}$$

which can be decomposed as $P^{\alpha} = (E, \vec{P})$, where E represents the particle energy and $\vec{P}$ its comoving spatial momentum. Using the identity

$$\frac{d}{d\lambda} = \frac{dx^{0}}{d\lambda}\frac{d}{dx^{0}} = E\frac{d}{dt}, \tag{1.11}$$

the time component of the geodesic equation can be written as

$$E\,\frac{dE}{dt} = -\Gamma^{0}_{ij}P^{i}P^{j} = -\frac{\dot{a}}{a}\,\delta_{ij}\,a^{2}P^{i}P^{j}. \tag{1.12}$$

This equation explicitly shows that the energy of a particle is not conserved in an expanding Universe: instead, it evolves due to the time dependence of the scale factor, reflecting the cosmological redshift.

For a massive particle, the dynamics are further constrained by the mass–shell condition,

$$P_{\mu}P^{\mu} = -E^{2} + \delta_{ij}\,a^{2}P^{i}P^{j} = -m^{2}, \tag{1.13}$$

which is the relativistic generalization of the energy–momentum relation. Substituting this condition into the energy evolution equation yields

$$E\frac{dE}{dt} + \frac{\dot{a}}{a}\left(E^{2} - m^{2}\right) = 0. \tag{1.14}$$

This differential equation describes how the particle energy redshifts as the Universe expands. Its solution is given by

$$\sqrt{E^{2} - m^{2}} = \frac{1}{a}\sqrt{E_{0}^{2} - m^{2}}, \tag{1.15}$$

where E_0 denotes the present-day energy. The result shows that the magnitude of the spatial momentum scales inversely with the scale factor, a hallmark of cosmological expansion.

Introducing the physical momentum $p^{i} = aP^{i}$, the mass–shell condition assumes the familiar special-relativistic form

$$E^{2} = m^{2} + p^{2}, \tag{1.16}$$

with $p \equiv |\vec{p}|$. These relations, extensively discussed in standard references such as [26, 28], demonstrate how the FLRW geometry governs the redshifting of particle energies and momenta, independently of the microscopic properties of the particles themselves.

In summary, the imposition of the cosmological principle together with maximal spatial symmetry uniquely leads to the FLRW metric. In the spatially flat case, this geometry provides a particularly simple yet powerful framework for describing both the large-scale structure of spacetime and the dynamical evolution of matter and radiation in the Universe.

In the next section, we turn to the observational and kinematical aspects of cosmology, focusing on the definition of cosmological distances and the notion of comoving time. These concepts establish a direct connection between the theoretical framework provided by the FLRW metric and astronomical observations, and are essential for interpreting redshifts, luminosities, and angular scales of distant objects within the standard ΛCDM cosmological model. ‘

1.1.4. Distances and Conformal Time

In relativistic cosmology, the concept of distance is inherently more subtle than in static Euclidean space, owing to the dynamical nature of spacetime described by General Relativity. Within the framework of a homogeneous and isotropic Universe, the Friedmann–Lemaître–Robertson–Walker (FLRW) metric [Eq. (1.4)] provides the geometrical basis for defining physically meaningful distance measures. Because the Universe is expanding, no single notion of distance is universally applicable; instead, different distance definitions are introduced depending on the observational context and the physical quantity being inferred [26, 28].

A particularly useful quantity in observational cosmology is the *comoving distance*, denoted by χ. This quantity measures the separation between an observer and a source along a spatial geodesic at fixed cosmic time, factoring out the effect of the cosmic expansion. In other words, while proper distances change with time as the Universe expands, the comoving distance remains constant for objects that follow the Hubble flow. This makes χ especially convenient for describing the large-scale distribution of cosmic structures and for connecting theoretical predictions with observations expressed in terms of redshift.

The comoving distance can be derived from the FLRW metric by considering radial light propagation. Since photons travel along null geodesics, one imposes the condition $ds^2 = 0$. Restricting the motion to the radial direction and integrating along the line of sight relates the radial coordinate separation to cosmic time. Rewriting the time differential in terms of redshift using the relation $dt = -dz/[(1+z)H(z)]$, one obtains a direct expression for the comoving distance to a source observed at redshift z.

Combining these steps into a single expression, and adopting units in which the speed of light satisfies $c = 1$, the comoving distance can be written compactly as

$$\chi(z) \equiv \int_{r_{\rm emit}}^{r_{\rm obs}} dr = \int_{t_{\rm emit}}^{t_0} \frac{dt}{a(t)} = \int_0^z \frac{dz'}{H(z')}\,, \tag{1.17}$$

where t_0 denotes the present cosmic time, $a(t)$ is the scale factor, and $H(z)$ is the Hubble expansion rate evaluated at redshift z [26]. This relation shows that the comoving distance is entirely determined by the expansion history of the Universe, linking cosmological geometry directly to observable redshift measurements.

The description of distances in an expanding Universe requires a careful distinction between coordinate separations and physically observable quantities. A particularly useful coordinate measure is the *comoving distance*, which factors out the effects of cosmic expansion and remains

fixed for objects that follow the Hubble flow. In the case of radial separations, this quantity is commonly referred to as the *comoving radial distance* and is defined as

$$D_c(z) \equiv \chi(z). \tag{1.18}$$

Although the comoving distance is not directly measurable, it plays a fundamental role in cosmology, as it provides the geometric backbone from which all observational distance measures are constructed.

One such observable quantity is the *angular diameter distance* D_A, which relates the physical transverse size D of an object to the angle it subtends on the sky. In a geometrical description, the transverse physical size is related to the comoving separation and the sine of the observed angle. Thus, the angular diameter distance is defined through

$$D_A(z) \equiv \frac{D}{\sin\theta}. \tag{1.19}$$

This relation expresses the geometrical fact that an object located farther away appears under a smaller angle even if its intrinsic physical size remains the same.

In most cosmological observations, however, the angles involved are very small. In this regime one may use the small-angle approximation,

$$\sin\theta \simeq \theta, \tag{1.20}$$

with θ expressed in radians. Under this approximation, the angular diameter distance reduces to the commonly used expression

$$D_A(z) \simeq \frac{D}{\theta}, \tag{1.21}$$

which provides a simple and accurate relation between physical size and observed angular scale for distant cosmological objects. In an expanding Universe described by the FLRW metric, physical lengths scale with the scale factor $a(t)$, while comoving separations remain constant. As a consequence, the angular diameter distance is related to the comoving distance by

$$D_A(z) = \frac{\chi(z)}{1+z}, \tag{1.22}$$

where the factor $(1+z)^{-1}$ accounts for the conversion between comoving and physical lengths at the time of emission [28]. This relation leads to the well-known behavior that D_A increases with redshift at low z, reaches a maximum, and then decreases at higher redshifts.

Another key observable is the *luminosity distance* D_L, which is defined through the relation between the intrinsic luminosity L of a source and the observed energy flux $\mathcal{F}$,

$$\mathcal{F} = \frac{L}{4\pi D_L^2}. \tag{1.23}$$

In an expanding Universe, the observed flux is reduced not only by the geometric dilution of photons over a spherical surface, but also by the redshifting of photon energies and by time dilation, which decreases the rate at which photons arrive at the observer. Taking these effects into account, the luminosity distance is related to the comoving distance by

$$D_L(z) = (1+z)\chi(z). \tag{1.24}$$

The extra factor of $(1+z)$ relative to D_c encapsulates the combined impact of energy redshift and cosmological time dilation on the observed flux.

These distance measures are not independent, but are related through the cosmological distance duality relation, also known as Etherington's reciprocity relation. This fundamental result connects the luminosity distance and the angular diameter distance through photon number conservation and the geometrical properties of light propagation in FLRW spacetime. As a consequence, one obtains

$$D_c(z) = \frac{D_L(z)}{1+z} = (1+z)\, D_A(z), \tag{1.25}$$

or, equivalently,

$$D_L(z) = (1+z)^2 D_A(z). \tag{1.26}$$

This identity provides a powerful consistency relation for cosmological observations and plays a central role in the interpretation of several observational probes. In particular, it underlies the connection between measurements based on standard candles, such as Type Ia supernovae, standard rulers, such as baryon acoustic oscillations, and the angular structure of anisotropies observed in the cosmic microwave background [26, 28].

In addition to spatial distances, it is often advantageous to redefine the temporal coordinate in cosmology. To this end, one introduces the *conformal time* τ, defined by

$$\tau \equiv \int_0^t \frac{dt'}{a(t')}. \tag{1.27}$$

Conformal time rescales cosmic time in such a way that the FLRW metric becomes conformally equivalent to the Minkowski metric. This transformation greatly simplifies the description of null geodesics, since light rays propagate along straight lines in conformal coordinates. As a result, conformal time is particularly well suited for the analysis of horizon-scale phenomena, the propagation of radiation, and the evolution of cosmological perturbations, especially in the early Universe [28].

In the next section, we turn to the matter content of the Universe and examine how different cosmic components contribute to the total energy–momentum tensor that governs the dynamical evolution of spacetime.

1.2. The Cosmic Substratum

In cosmology, the concept of the cosmic substratum refers to the large-scale distribution of matter and energy that fills the universe. Under the assumption of that, the universe is homogeneous and isotropic on sufficiently large scales, the cosmic substratum can be treated as a continuous medium whose properties evolve with time. The study of this substratum is fundamental to understanding the dynamics of cosmic expansion and the interplay between different forms of energy that govern the evolution of the universe.

The energy content of the universe can be described as a perfect fluid, where the density and pressure determine how the expansion progresses. The laws of general relativity dictate how this energy content influences the curvature and evolution of spacetime. Among the components of the cosmic substratum, there are contributions from radiation, matter, and dark energy, each playing a crucial role in the different epochs of cosmic history.

The expansion of the universe is determined by the balance of these energy components. Radiation was the dominant component in the early universe, when the high temperatures and densities caused photons and other relativistic particles to exert significant pressure. As the universe expanded and cooled, matter became the dominant component, allowing structures such as galaxies and clusters to form. In the current epoch, dark energy, which is associated with the accelerated expansion of the universe, has become the dominant component.

1.2.1. State equations

In order to characterize the dynamical behavior of the different components of the universe, it is common to assume that each of them behaves as a *barotropic fluid*, where the pressure is proportional to the energy density. Under this assumption, the equation of state parameter is defined as

$$\omega_s = \frac{\mathcal{P}_s}{\rho_s}, \tag{1.28}$$

which directly relates the pressure $\mathcal{P}_s$ to the energy density ρ_s of a given cosmic species s.

This parameter plays a fundamental role in cosmology, since it determines how different fluids contribute to the expansion history of the universe. For instance, relativistic particles such as photons and neutrinos are characterized by $\omega = 1/3$, non-relativistic matter by $\omega \approx 0$, while a cosmological constant corresponds to $\omega = -1$. In more general scenarios, ω may vary with time, but the barotropic approximation provides a simple and powerful framework to describe the main cosmic epochs.

Therefore, the equation of state parameter not only unifies the description of distinct forms of energy content but also allows us to study their dynamical impact on the evolution of the scale factor.

In the next section we will discuss the structure and properties of the energy-momentum tensor, which generalizes these concepts to a covariant formulation.

1.2.2. Energy-Momentum Tensor

The energy-momentum tensor, $T_{\mu\nu}$, plays a central role in cosmology as it encapsulates all forms of energy and momentum that act as sources of spacetime curvature through Einstein's field equations. Within the framework of the standard cosmological model, this tensor aggregates the contributions of the different constituents of the universe—radiation, baryonic matter, dark matter, and dark energy—each characterized by distinct dynamical and thermodynamical properties. Although physically diverse, these components enter the gravitational field equations in a unified manner through their inclusion in $T_{\mu\nu}$, which ultimately governs the evolution of spacetime geometry and cosmic expansion.

Assuming that each cosmic component can be modeled as a perfect fluid, the energy-momentum tensor takes the well-known form

$$T^{\mu}_{\ \nu} = (\rho + \mathcal{P})u^{\mu}u_{\nu} + \mathcal{P}\delta^{\mu}_{\ \nu}, \tag{1.29}$$

where ρ is the energy density, $\mathcal{P}$ is the isotropic pressure, u^{μ} is the four-velocity of the fluid, and $\delta^{\mu}_{\ \nu}$ is the Kronecker delta. This formulation ensures the local conservation of energy and momentum, embedding gravitational attraction, radiation pressure, and vacuum repulsion within the dynamics of spacetime.

In a flat, homogeneous and isotropic universe described by the Friedmann–Lemaître–Robertson–Walker (FLRW) metric, the comoving frame is privileged. In this frame, the four-velocity takes the simple form $u^{\mu} = (-1, 0, 0, 0)$, and the energy-momentum tensor becomes diagonal:

$$T^{\mu}_{\ \nu} = \begin{pmatrix} -\rho & 0 & 0 & 0 \\ 0 & \mathcal{P} & 0 & 0 \\ 0 & 0 & \mathcal{P} & 0 \\ 0 & 0 & 0 & \mathcal{P} \end{pmatrix}. \tag{1.30}$$

This explicit structure highlights how the energy density drives the cosmic expansion, while pressure influences whether the expansion accelerates or decelerates, depending on its sign. Thus, the tensor not only encodes the physical characteristics of each cosmic component but also provides the mathematical foundation for describing the different eras of cosmic evolution: radiation domination, matter domination, and the current dark energy domination.

For specific cosmic fluids, the energy-momentum tensor reduces to the following forms:

- Pressureless matter ($\mathcal{P}_m = 0$):
$$T^{\mu}_{\ \nu}|_m = \rho_m u^{\mu} u_{\nu}. \tag{1.31}$$
- Radiation ($3\mathcal{P}_r = \rho_r$):
$$T^{\mu}_{\ \nu}|_r = \frac{\rho_r}{3}\left(4u^{\mu}u_{\nu} + \delta^{\mu}_{\nu}\right). \tag{1.32}$$
- Dark energy ($\mathcal{P}_\Lambda = -\rho_\Lambda$):
$$T^{\mu}_{\ \nu}|_\Lambda = -\rho_\Lambda\, \delta^{\mu}_{\nu}. \tag{1.33}$$

1.2.3. Density parameters

It is important to introduce the density parameter, defined as

$$\Omega_s \equiv \frac{\rho_s}{\rho_{cr}}, \tag{1.34}$$

which measures the energy density of a given component s in units of the critical density of the universe. The critical density is defined by

$$\rho_{cr} = \frac{3H^2}{8\pi G}, \tag{1.35}$$

and represents the precise energy density required for a spatially flat universe in the framework of General Relativity. Therefore, Ω_s provides a dimensionless and convenient way to compare the relative contribution of different components (such as matter, radiation, and dark energy) to the total energy budget of the universe. The sum over all species, $\sum_s \Omega_s$, directly encodes the geometry of the universe, with values greater than, equal to, or less than unity corresponding to closed, flat, or open spatial geometries, respectively.

In the next section we will discuss the theoretical framework of General Relativity, which provides the fundamental description of spacetime dynamics and the gravitational interaction.

1.3. General Relativity

General relativity, formulated by Albert Einstein in 1915, stands as one of the cornerstones of modern physics and provides the essential framework for understanding the universe on large scales. This theory revolutionized the concepts of space, time, and gravity, establishing a mathematical description of how matter and energy determine the curvature of spacetime. General relativity not only redefined the notion of gravity but also laid the foundation for much of modern cosmology in the 20th and 21st centuries. Its implications, particularly in the study of the expanding universe, the Big Bang, and the fundamental nature of spacetime, remain profound and far-reaching.

At the heart of general relativity lies the principle that gravity is not a force acting at a distance, as described by Newtonian mechanics, but rather a manifestation of the curvature of

spacetime produced by mass and energy. Massive objects such as stars, planets, and galaxies distort the fabric of spacetime, and this curvature dictates the trajectories of other objects. In the absence of non-gravitational forces, particles and radiation follow geodesics—curves that represent the straightest possible paths in a curved geometry. This concept is crucial for understanding planetary motion, the deflection of light by massive bodies, and the propagation of radiation across the universe.

The dynamics of spacetime in general relativity are governed by the Einstein Field Equations (EFE), which are expressed as

$$G_{\mu\nu} = R_{\mu\nu} - \frac{1}{2}R\, g_{\mu\nu} + \Lambda g_{\mu\nu} = 8\pi G T_{\mu\nu}. \tag{1.36}$$

These ten coupled nonlinear differential equations encapsulate the interplay between geometry and energy. The left-hand side describes the geometric structure of spacetime, with $R_{\mu\nu}$ representing the Ricci tensor, R the Ricci scalar, $g_{\mu\nu}$ the metric tensor, and Λ the cosmological constant. The right-hand side contains the energy-momentum tensor $T_{\mu\nu}$, which encodes the distribution of matter and energy. The cosmological constant Λ may be interpreted either as a purely geometric term or as an effective energy component of the universe. In this work, we adopt the energetic interpretation.

To make the structure of the field equations more explicit, it is instructive to recall the definitions of the curvature tensors. The Ricci tensor is obtained by contracting the first and third indices of the Riemann curvature tensor:

$$R_{\mu\nu} = R^{\rho}{}_{\mu\rho\nu}. \tag{1.37}$$

where the Ricci tensor is obtained by contraction:

$$R_{\mu\nu} = \Gamma^{\alpha}_{\mu\nu,\alpha} - \Gamma^{\alpha}_{\mu\alpha,\nu} + \Gamma^{\alpha}_{\beta\alpha}\Gamma^{\beta}_{\mu\nu} - \Gamma^{\alpha}_{\beta\nu}\Gamma^{\beta}_{\mu\alpha}, \tag{1.38}$$

and the Ricci scalar follows from contracting the Ricci tensor with the metric,

$$R = g^{\mu\nu}R_{\mu\nu}. \tag{1.39}$$

By applying the Einstein equations to a homogeneous and isotropic universe described by the Friedmann–Lemaître–Robertson–Walker (FLRW) metric, one arrives at the fundamental equations of cosmology. Considering separately the temporal component ($\mu = \nu = 0$) and the spatial components ($\mu = \nu = i$, with $i = 1, 2, 3$), we obtain

$$G_{00} = 8\pi G T_{00}, \tag{1.40}$$

where

$$G_{00} = R_{00} - \frac{1}{2}g_{00}R. \tag{1.41}$$

For the FLRW metric, the relevant curvature components are

$$R_{00} = -3\frac{\ddot{a}}{a}, \tag{1.42}$$

$$R_{ij} = \delta_{ij}\left[2\dot{a}^2 + a\ddot{a}\right], \tag{1.43}$$

and the Ricci scalar is

$$R = -R_{00} + \frac{1}{a^2}R_{ii} = 6\left[\frac{\ddot{a}}{a} + \left(\frac{\dot{a}}{a}\right)^2\right]. \tag{1.44}$$

Substituting these expressions into Eq. (1.40), one finds the first Friedmann equation,

$$\left(\frac{\dot{a}}{a}\right)^2 = \frac{8\pi G}{3}\rho, \tag{1.45}$$

where ρ is the total energy density. This result can be written in terms of the Hubble parameter $H = \dot{a}/a$ as

$$H^2 = \frac{8\pi G}{3}\sum_{b,c,r,\Lambda}\rho_i. \tag{1.46}$$

Introducing the density parameters $\Omega_i = \rho_i/\rho_0$, with the critical density $\rho_0 = \frac{3H_0^2}{8\pi G}$, the Hubble parameter takes the form

$$H = H_0 E(a), \tag{1.47}$$

where

$$E^2_{\Lambda\mathrm{CDM}}(a) = \Omega_{m0}a^{-3} + \Omega_{\Lambda 0} + \Omega_{r0}a^{-4}. \tag{1.48}$$

In this work, we neglect the contribution of neutrinos, as their effect is negligible in the late-time evolution of the universe.

Equivalently, the Friedmann equation may be expressed in terms of the density parameters as

$$\frac{H^2}{H_0^2} = \sum_{s=m,r,\,\Lambda}\Omega_s a^{-3(1+\omega_s)}. \tag{1.49}$$

Einstein's theory also predicted the possibility of a non-static universe. Although Einstein originally introduced the cosmological constant to ensure a static solution, subsequent observations by Edwin Hubble demonstrated that galaxies are receding from one another, implying an expanding universe. This discovery led Einstein to abandon the static model, embracing the dynamic nature of cosmology.

Beyond cosmic expansion, general relativity predicts extreme phenomena such as black holes, regions of spacetime where curvature becomes so strong that nothing can escape. The detection of gravitational waves by LIGO in 2015 further confirmed the theory, enabling direct observation of events like black hole and neutron star mergers.

General relativity currently provides the most successful theoretical framework for describing gravitation on cosmological scales and plays a central role in modeling phenomena associated with dark matter and dark energy, two dominant yet still poorly understood components of the Universe. Dark matter is inferred through its gravitational effects on visible matter and on the dynamics of galaxies and large-scale structures, while dark energy, commonly modeled through the cosmological constant, is introduced to account for the observed accelerated expansion of the Universe. Together, these ingredients form the basis of the ΛCDM model, which presently offers the most consistent phenomenological description of a wide range of cosmological observations.

In summary, general relativity constitutes an extremely successful and useful theoretical framework for modern cosmology, providing the foundation for interpreting cosmic expansion, structure formation, gravitational lensing, and compact objects such as black holes. Nevertheless, it is understood as an effective theory whose domain of validity may eventually be superseded or extended, particularly in regimes where quantum effects become important. Ongoing theoretical and observational efforts therefore aim to test its limits and to develop a more fundamental description of gravity capable of consistently unifying general relativity with quantum mechanics.

1.3.1. Bianchi Identities

The Bianchi identities are fundamental geometric relations in differential geometry and play a crucial role in the formulation of Einstein's field equations. These identities arise from the symmetries of the Riemann curvature tensor. Emerging from the mathematical structure of Riemannian geometry, the Bianchi identities reflect the inherent consistency of how curvature behaves in a differentiable manifold endowed with a metric connection. They are a consequence of the properties of parallel transport and the behavior of vectors under infinitesimal loops in curved space. Specifically, they ensure that the curvature derived from the connection is coherent with the underlying geometry.

These identities are essential for establishing the conservation laws in general relativity. When applied to the geometry of spacetime, they guarantee that the field equations are compatible with the principle of local conservation of energy and momentum. This compatibility is achieved through the vanishing divergence of the Einstein tensor, which in turn implies that the energy-momentum tensor describing matter and fields must also be covariantly conserved.

In this way, the Bianchi identities bridge the geometric description of gravity with the physical requirement that energy and momentum are preserved in a curved spacetime, ensuring that Einstein's theory remains self-consistent and physically meaningful.

The Riemann tensor satisfies the differential (second) Bianchi identity:

$$R^{\rho}{}_{\sigma\mu\nu\,;\lambda} + R^{\rho}{}_{\sigma\nu\lambda\,;\mu} + R^{\rho}{}_{\sigma\lambda\mu\,;\nu} = 0. \tag{1.50}$$

By contracting the indices appropriately, one obtains a contracted version of the Bianchi identity involving the Ricci tensor $R_{\mu\nu}$ and the Ricci scalar R. This leads to the identity:

$$\nabla^{\mu}\left(R_{\mu\nu} - \frac{1}{2}Rg_{\mu\nu}\right) = 0. \tag{1.51}$$

The expression inside the parentheses is known as the Einstein tensor:

$$G_{\mu\nu} \equiv R_{\mu\nu} - \frac{1}{2}Rg_{\mu\nu}. \tag{1.52}$$

Therefore, the contracted Bianchi identities imply that the Einstein tensor has zero covariant divergence:

$$\nabla^{\mu}G_{\mu\nu} = \nabla^{\mu}(8\pi G\, T_{\mu\nu}) = 0. \tag{1.53}$$

This property is essential in general relativity, as it ensures the consistency of Einstein's field equations with the local conservation of energy and momentum, expressed by the vanishing divergence of the energy-momentum tensor

$$\nabla^{\mu}T_{\mu\nu} = 0. \tag{1.54}$$

In this context, each component of the Einstein tensor must have vanishing covariant derivative, meaning that the geometry itself respects a kind of conservation law. This property is essential in general relativity, as it ensures the consistency of Einstein's field equations with the local conservation of energy and momentum, expressed mathematically by the condition $\nabla^{\mu}T^{(s)}_{\mu\nu} = 0$. This relation affirms that the flow of energy and momentum in spacetime, represented by the energy-momentum tensor, must be conserved in a covariant sense within any local region of the universe.

1.3.2. Background equations in LCDM model

Within the framework of General Relativity, the evolution of the Universe is governed by the Einstein field equations (EFE) [Eq. 1.36]. A key mathematical property of the Einstein tensor is that it obeys the Bianchi identities [Eq. 1.53]. When these identities are applied to the Einstein field equations, they directly imply the covariant conservation of the total energy–momentum tensor [Eq. 1.54]. This conservation law expresses the local conservation of energy and momentum and provides the fundamental starting point for deriving the fluid equations that describe the individual components of the ΛCDM model. For notational convenience, partial derivatives will be denoted by a comma; for instance, $,\mu$ represents $\partial\mu$.

The ΛCDM model consists of three main energy components: radiation (r), matter (m), and the cosmological constant (Λ), which acts as dark energy with constant density. An important property of the energy-momentum tensor is that its covariant divergence vanishes,

$$\nabla_\mu T^\mu_{\ \nu} \equiv T^\mu_{\ \nu,\mu} + \Gamma^\mu_{\alpha\mu} T^\alpha_{\ \nu} - \Gamma^\alpha_{\nu\mu} T^\mu_{\ \alpha} = 0. \tag{1.55}$$

As discussed in Sec. 1.3, this condition reflects the conservation of energy and momentum under parallel transport. For the moment, we adopt this result and explore its implications.

Expanding the conservation equation for the temporal component ($\nu = 0$) yields

$$T^\mu_{\ 0,\mu} + \Gamma^\mu_{\alpha\mu} T^\alpha_{\ 0} - \Gamma^\alpha_{0\mu} T^\mu_{\ \alpha} = 0. \tag{1.56}$$

Substituting the explicit forms of the energy-momentum tensor for each cosmic fluid, we obtain the following conservation laws:

- For pressureless matter:

$$\frac{\partial(\rho_m a^3)}{\partial t} = 0. \tag{1.57}$$

- For radiation:

$$\frac{\partial(\rho_r a^4)}{\partial t} = 0. \tag{1.58}$$

- For dark energy:

$$\frac{\partial(\rho_\Lambda)}{\partial t} = 0. \tag{1.59}$$

These relations encapsulate the expected scaling behaviors of the cosmic components: matter density scales as a^{-3}, radiation as a^{-4}, and dark energy remains constant throughout cosmic history. Assuming these components interact only gravitationally (no energy exchange between fluids), each satisfies an independent conservation equation:

$$\text{Radiation:} \quad \frac{\partial \rho_r}{\partial t} + 4H\rho_r = 0, \tag{1.60}$$

$$\text{Pressureless Matter:} \quad \frac{\partial \rho_m}{\partial t} + 3H\rho_m = 0, \tag{1.61}$$

$$\text{Cosmological Constant:} \quad \frac{\partial \rho_\Lambda}{\partial t} = 0. \tag{1.62}$$

The conservation equations arise naturally from the Bianchi identities applied to the Einstein Field Equations, imposing local conservation of the energy-momentum tensor. Within the ΛCDM model, this leads to distinct continuity equations for each perfect cosmic fluid component, governing their time evolution and influencing the universe's expansion dynamics.

1.4. Horizons

In cosmology, the concept of a horizon is fundamental for understanding which regions of the Universe can be in causal contact and how cosmological perturbations evolve over time. Because physical signals propagate at finite speed, there exists at any cosmic time a maximum distance over which physical processes could have influenced one another since the beginning of cosmic evolution. This causal limitation introduces characteristic length scales that separate regions able to exchange information from those that remain causally disconnected. In the context of Standard Perturbation Theory (SPT), distinguishing between perturbations that lie inside or outside the relevant horizon scale is particularly important, since the equations governing their evolution simplify significantly once modes are well within the horizon.

One important notion is the particle horizon, which defines the maximum comoving distance that light could have traveled since the beginning of the Universe up to a given cosmic time t. It therefore marks the boundary of the region that has been in causal contact with a given observer since the earliest times. In an expanding Universe described by the FLRW metric, the comoving particle horizon is given by

$$\chi_p(t) = \int_0^t \frac{dt'}{a(t')}, \tag{1.63}$$

where $a(t)$ is the scale factor. This expression accumulates the comoving distance traveled by light since the initial cosmic epoch. Regions separated by distances larger than $\chi_p(t)$ could not have exchanged causal signals since the Big Bang. The existence of this horizon is closely related to the classical horizon problem, which provided one of the main motivations for the introduction of cosmic inflation.

Another related concept is the event horizon, which instead characterizes the maximum distance from which light emitted at the present time can ever reach an observer in the future. Its comoving size is given by

$$\chi_e(t) = \int_t^\infty \frac{dt'}{a(t')}. \tag{1.64}$$

In cosmological models undergoing accelerated expansion, such as the late-time ΛCDM Universe, this integral converges, implying that some regions will eventually move permanently outside causal contact. Although this notion is important for understanding the long-term fate of the Universe, it plays a less direct role in the dynamics of cosmological perturbations.

In perturbation theory, the most relevant scale is instead associated with the Hubble expansion rate. The physical Hubble radius is defined as

$$R_H = \frac{1}{H(t)}, \tag{1.65}$$

while the corresponding comoving Hubble radius is

$$r_H = \frac{1}{aH}. \tag{1.66}$$

This scale represents approximately the distance over which causal microphysical processes can operate within one Hubble time. In practice, it serves as the effective dynamical horizon separating different regimes of perturbation evolution. When perturbations are much smaller than this scale, causal processes such as gravitational collapse and velocity flows can efficiently operate across them. Conversely, perturbations larger than this scale evolve differently because causal processes cannot act across their full extent.

A perturbation mode characterized by comoving wavenumber k corresponds to a comoving wavelength

$$\lambda = \frac{2\pi}{k}. \tag{1.67}$$

Comparing this wavelength with the comoving Hubble radius allows one to classify perturbations according to their dynamical regime. A mode is said to lie in the super-horizon regime when its physical wavelength is larger than the Hubble radius, corresponding to

$$\frac{k}{aH} \ll 1. \tag{1.68}$$

In this regime, causal processes cannot redistribute matter efficiently across the perturbation scale, and curvature perturbations often remain approximately constant in time. This behavior plays a crucial role in inflationary cosmology, where quantum fluctuations are stretched beyond the horizon and later re-enter it to seed cosmic structure.

Conversely, perturbations lie in the sub-horizon regime when

$$\frac{k}{aH} \gg 1, \tag{1.69}$$

meaning that their physical wavelength is much smaller than the Hubble radius. In this regime, gravitational collapse, pressure forces, and velocity flows can act across the perturbation scale, allowing the dynamical growth of cosmic structures. Standard Perturbation Theory is primarily concerned with this sub-horizon regime, where Newtonian-like fluid equations coupled to the Poisson equation provide an excellent approximation to the full relativistic dynamics.

As the Universe evolves, the comoving Hubble radius changes with time, causing perturbation modes to transition between super-horizon and sub-horizon regimes. The condition

$$k = aH \tag{1.70}$$

defines the moment of horizon crossing for a given mode. During inflation, the comoving Hubble radius decreases, causing quantum fluctuations to exit the horizon. After inflation, during radiation and matter domination, the comoving Hubble radius grows, allowing these perturbation modes to re-enter the horizon and subsequently evolve into the structures observed today.

Understanding these horizon scales and their relation to perturbation evolution is therefore essential for connecting early-Universe initial conditions with the late-time nonlinear growth of cosmic structures. In particular, it establishes the domain of validity of the perturbative treatment employed in this work, which focuses on modes well inside the horizon where Standard Perturbation Theory can be consistently applied.

1.5. Einstein Equations for Scalar Perturbations

In this section, we study scalar perturbations around a homogeneous and isotropic Friedmann–Lemaître–Robertson–Walker (FLRW) background. Scalar modes are of particular relevance for structure formation, as they are directly sourced by matter density fluctuations. We work in the Newtonian (or longitudinal) gauge, in which gauge ambiguities are eliminated and the physical interpretation of the perturbations is particularly transparent.

Restricting attention to scalar perturbations, the perturbed metric takes the form

$$\begin{aligned} g_{00} &= -1 - 2\Psi(\vec{x}, t), \\ g_{0i} &= g_{i0} = 0, \\ g_{ij} &= a^2(t)\, \delta_{ij} \big[1 + 2\Phi(\vec{x}, t)\big]. \end{aligned} \tag{1.71}$$

Here, $a(t)$ denotes the cosmic scale factor, while Ψ and Φ are the gauge-invariant Bardeen potentials. The potential Ψ plays the role of the Newtonian gravitational potential governing the motion of non-relativistic particles, whereas Φ characterizes scalar perturbations of the spatial curvature. Throughout this section, partial derivatives are denoted by commas, e.g. $\Phi_{,0} \equiv \partial_t \Phi$.

Starting from the perturbed metric, one can compute the Ricci tensor, which encodes the local curvature of spacetime. The time–time component reads

$$R_{00} = -3\frac{\ddot{a}}{a} - \frac{k^2}{a^2}\Psi - 3\Phi_{,00} + 3H(\Psi_{,0} - 2\Phi_{,0}), \tag{1.72}$$

where $H \equiv \dot{a}/a$ is the Hubble rate. The first term corresponds to the homogeneous background contribution, while the remaining terms arise from scalar perturbations. The Laplacian term proportional to $k^2\Psi$ reflects spatial inhomogeneities in the gravitational potential, whereas the time-derivative terms describe the dynamical evolution of the metric perturbations.

The spatial components of the Ricci tensor are given by

$$\begin{aligned} R_{ij} = \delta_{ij}\Big[&(2a^2H^2 + a\ddot{a})(1 + 2\Phi - 2\Psi) + a^2H(6\Phi_{,0} - \Psi_{,0}) + a^2\Phi_{,00} + k^2\Phi\Big] \\ &+ k_i k_j(\Phi + \Psi). \end{aligned} \tag{1.73}$$

The terms proportional to δ_{ij} contribute to the trace of the spatial curvature, while the term proportional to $k_i k_j$ captures anisotropic spatial variations. The combination $\Phi + \Psi$ will later be identified as the quantity sourcing anisotropic stress.

Contracting the Ricci tensor with the metric yields the Ricci scalar,

$$\begin{aligned} R = {}&[-1 + 2\Psi]\Big[-3\frac{\ddot{a}}{a} - \frac{k^2}{a^2}\Psi - 3\Phi_{,00} + 3H(\Psi_{,0} - 2\Phi_{,0})\Big] \\ &+ \frac{1 - 2\Phi}{a^2}\Big[3(2a^2H^2 + a\ddot{a})(1 + 2\Phi - 2\Psi) + a^2H(6\Phi_{,0} - \Psi_{,0}) + a^2\Phi_{,00} + k^2\Phi\Big] \\ &+ k^2(\Phi + \Psi). \end{aligned} \tag{1.74}$$

At zeroth order in perturbations, this expression reduces to

$$R^{(0)} = 6\left(H^2 + \frac{\ddot{a}}{a}\right), \tag{1.75}$$

which depends solely on the background expansion and characterizes the curvature of the unperturbed FLRW spacetime.

Retaining only terms linear in the scalar perturbations, the first-order correction to the Ricci scalar becomes

$$\delta R = -12\Psi\left(H^2 + \frac{\ddot{a}}{a}\right) + \frac{2k^2}{a^2}\Psi + 6\Phi_{,00} - 6H(\Psi_{,0} - 4\Phi_{,0}) + 4\frac{k^2}{a^2}\Phi. \tag{1.76}$$

This expression explicitly shows how scalar metric perturbations modify the spacetime curvature through both spatial gradients and time evolution.

The Einstein tensor, defined as $G^{\mu}{}_{\nu} = R^{\mu}{}_{\nu} - \frac{1}{2}\delta^{\mu}_{\nu}R$, governs the coupling between geometry and matter. The time–time component is given by

$$G^0{}_0 = g^{00}\left(R_{00} - \frac{1}{2}g_{00}R\right) = (-1 + 2\Psi)R_{00} - \frac{R}{2}, \tag{1.77}$$

where we have used $g^{0i} = 0$. Extracting the linear contribution yields

$$\delta G^0{}_0 = -6H\Phi_{,0} + 6H^2\Psi - 2\frac{k^2}{a^2}\Phi. \tag{1.78}$$

This component plays a central role in relating scalar metric perturbations to matter density fluctuations.

The corresponding source term is provided by the energy–momentum tensor. For a generic particle species s, the time–time component is

$$T^0{}_0(\vec{x},t) = -\sum_s g_s \int \frac{d^3p}{(2\pi)^3} E_s(p)\, f_s(p,\vec{x},t), \tag{1.79}$$

where g_s denotes the number of internal degrees of freedom and f_s is the phase-space distribution function. At late times, the dominant contribution arises from non-relativistic matter, for which $E_m \simeq m$. Writing $f_s = f^{(0)} + \delta f$, one obtains

$$T^0{}_0\big|_m = -\rho_m(1+\delta_m), \tag{1.80}$$

where ρ_m is the background matter density and δ_m its density contrast.

Combining the Einstein equations with this expression leads to a Poisson-like equation for the potential Φ,

$$k^2\Phi + 3\frac{a'}{a}\left(\Phi' - \Psi\frac{a'}{a}\right) = 4\pi G a^2 \rho_m \delta_m, \tag{1.81}$$

where primes denote derivatives with respect to conformal time. The additional terms proportional to a'/a encode relativistic corrections associated with the expansion of the Universe.

To obtain a second relation between the scalar potentials, we consider the spatial components of the Einstein tensor,

$$G^i{}_j = g^{ik}\left(R_{kj} - \frac{1}{2}g_{kj}R\right) = \frac{\delta^{ik}(1-2\Phi)}{a^2}R_{kj} - \frac{\delta^i_j}{2}R. \tag{1.82}$$

This expression can be decomposed into trace and traceless parts as

$$G^i{}_j = F(\Phi,\Psi)\,\delta^i_j + \frac{k^i k_j}{a^2}(\Phi+\Psi), \tag{1.83}$$

where $F(\Phi,\Psi)$ collects the trace contributions. Projecting onto the traceless longitudinal component yields

$$\left(\hat{k}_i\hat{k}^j - \frac{1}{3}\delta^j_i\right) G^i{}_j = \frac{2}{3a^2}k^2(\Phi+\Psi). \tag{1.84}$$

For non-relativistic matter, the anisotropic stress is negligible, implying

$$\left(\hat{k}_i\hat{k}^j - \frac{1}{3}\delta^j_i\right) T^i{}_j\big|_m \simeq 0. \tag{1.85}$$

Consequently, the traceless Einstein equation enforces

$$\Phi = -\Psi, \tag{1.86}$$

a relation characteristic of standard late-time cosmology in the absence of anisotropic stress.

Finally, in the sub-horizon[1] limit $k \gg \mathcal{H}$, the Poisson-like equation simplifies to

$$\nabla^2\Psi = 4\pi G a^2 \rho_m \delta_m. \tag{1.87}$$

Using the Friedmann equation,

$$\mathcal{H}^2 = \frac{8\pi G}{3}\rho a^2, \tag{1.88}$$

$$4\pi G a^2 \rho_m = \frac{3}{2}\Omega_m \mathcal{H}^2, \tag{1.89}$$

one arrives at the standard cosmological Poisson equation,

$$\nabla^2\Psi = \frac{3}{2}\Omega_m \mathcal{H}^2 \delta_m. \tag{1.90}$$

This equation governs the evolution of scalar perturbations on sub-horizon scales and provides the theoretical foundation for the study of structure formation in the ΛCDM cosmological model.

1.6. Current Status of ΛCDM model

The Λ Cold Dark Matter (ΛCDM) model is currently the standard paradigm in cosmology, providing a remarkably successful framework to describe the large-scale structure and evolution of the universe. It combines a cosmological constant Λ, representing dark energy responsible for the accelerated expansion of the universe, with cold dark matter (CDM) as the dominant form of matter driving structure formation. The model is built on the foundation of General Relativity and the Cosmological Principle, assuming a homogeneous and isotropic universe at large scales. Over the past decades, ΛCDM has been extensively tested and refined through increasingly precise cosmological observations.

1.6.1. Observational Success

The standard ΛCDM cosmological model has achieved an extraordinary level of success in describing the observable Universe across a wide range of physical scales and cosmic epochs. With a minimal set of parameters, it provides a coherent and internally consistent framework that connects the physics of the early Universe to the formation and evolution of large-scale structures observed today. This success is most strikingly illustrated by its ability to simultaneously fit diverse and independent cosmological datasets with high precision.

One of the most compelling demonstrations of the predictive power of the ΛCDM model is its agreement with observations of the CMB temperature anisotropies. As shown in Fig. 1.1, the theoretical angular power spectrum predicted by ΛCDM accurately reproduces the observed acoustic peak structure over a broad range of multipoles. The precise locations, relative heights, and damping tail of these peaks encode detailed information about the contents and geometry of the Universe, including the baryon density, cold dark matter abundance, spatial curvature, and the properties of primordial fluctuations. The remarkable level of agreement between the model and the high-precision CMB data, with residuals consistent with statistical noise, underscores the robustness of the ΛCDM scenario as a description of the early Universe.

The ΛCDM model is also strongly supported by observations of baryon acoustic oscillations (BAO), which provide a standard ruler for probing the expansion history of the Universe. Measurements of the BAO scale from galaxy redshift surveys are fully consistent with the expansion

[1] See Sec 1.4

history inferred from CMB data when interpreted within the ΛCDM framework. Likewise, observations of Type Ia supernovae, which act as standardizable candles, independently confirm the late-time accelerated expansion of the Universe driven by dark energy, a central component of the model.

On intermediate and late-time scales, ΛCDM successfully accounts for the observed distribution of galaxies and the growth of cosmic structures. The model predicts the hierarchical formation of structures through gravitational instability, starting from nearly Gaussian primordial fluctuations and evolving into the complex web of galaxies and clusters observed today. Measurements of large-scale galaxy clustering, redshift-space distortions, and weak gravitational lensing are broadly consistent with these predictions, further reinforcing the validity of the ΛCDM paradigm.

Taken together, these observational successes establish ΛCDM as the cornerstone of modern cosmology. Its ability to explain phenomena ranging from the physics of the early Universe to the large-scale structure of matter with a unified theoretical framework is unparalleled. However, the very precision with which cosmological parameters are now measured has also revealed a number of persistent discrepancies between different observational probes. In the following subsections, we discuss these emerging tensions—most notably those associated with the Hubble-Lemaître constant and the amplitude of matter fluctuations—and examine their potential implications for extensions or modifications of the standard ΛCDM model.

1.6.2. Cosmological Tensions

Despite its remarkable success in accounting for a wide range of cosmological observations, the standard ΛCDM model currently faces several persistent observational tensions that may point either to unresolved systematic effects or to the need for extensions beyond the minimal cosmological framework. With the advent of high-precision cosmological data, these discrepancies have become increasingly significant and now constitute one of the central challenges in modern cosmology.

The most prominent of these discrepancies is the so-called *Hubble tension*, which refers to the statistically significant mismatch between determinations of the Hubble-Lemaître constant H_0 obtained from local, late-Universe probes and those inferred from early-Universe observations under the assumption of ΛCDM. A comprehensive overview of recent measurements of H_0 and their mutual inconsistencies is presented in Fig. 1.2 and Fig. 1.3. Early-Universe estimates, primarily derived from observations of the CMB by the *Planck* satellite, yield a value of $H_0 \simeq 67.66 \pm 0.42\ \mathrm{km\,s^{-1}\,Mpc^{-1}}$ within the ΛCDM framework [2]. In contrast, late-Universe measurements based on local distance-ladder techniques—most notably those reported by the SH0ES collaboration using Cepheid-calibrated Type Ia supernovae—consistently favor higher values, $H_0 \simeq 72.51 \pm 1.54\ \mathrm{km\,s^{-1}\,Mpc^{-1}}$ [4]. The discrepancy between these determinations has now reached a significance of approximately 5σ, making it one of the most robust and persistent tensions in contemporary cosmology.

In addition to the Hubble tension, significant discrepancies have also emerged in measurements related to the amplitude of matter fluctuations at late times. This is commonly quantified by the parameter σ_8, which measures the root-mean-square amplitude of matter density fluctuations smoothed on scales of $8\,h^{-1}\,\mathrm{Mpc}$, or by the derived combination

$$S_8 \equiv \sigma_8 \sqrt{\Omega_m/0.3}.$$

Low-redshift observations, particularly those based on weak gravitational lensing and redshift-space distortions, tend to prefer lower values of S_8 than those inferred from CMB measurements

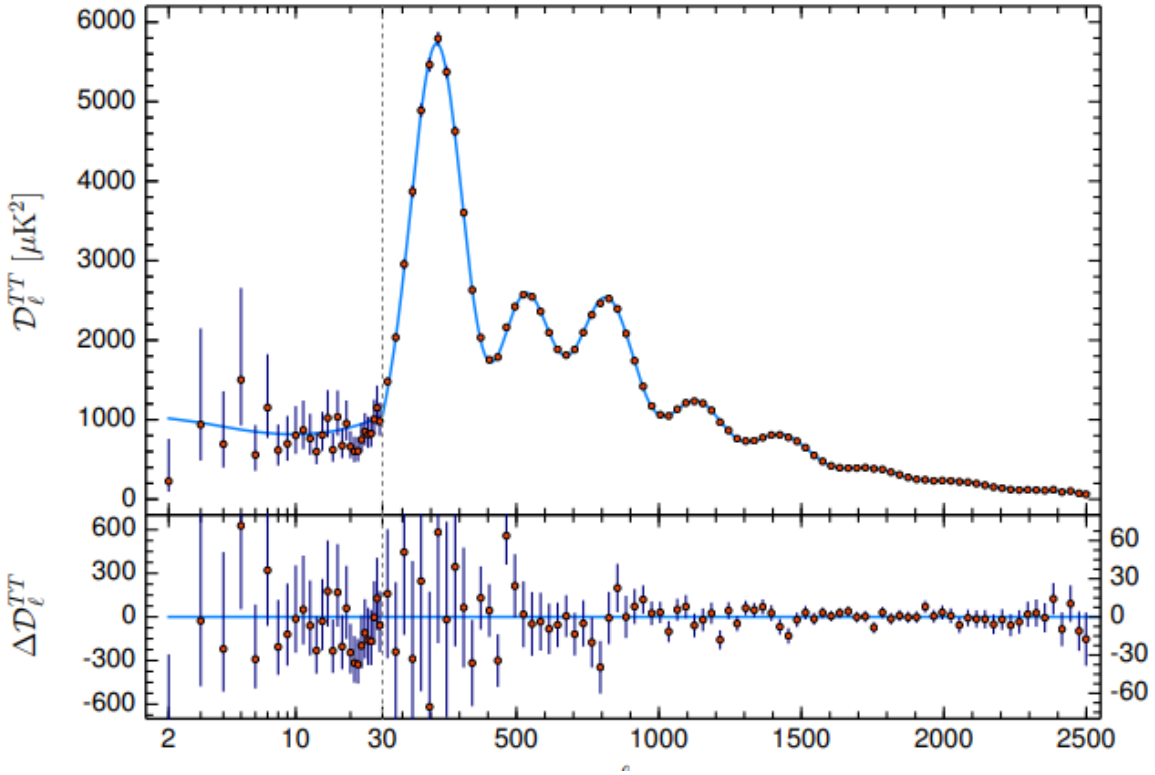

Figure 1.1.: Angular power spectrum of temperature anisotropies of the CMB, $D_\ell^{TT} \equiv \ell(\ell+1)C_\ell^{TT}/2\pi$, compared with observational data. The data points with error bars represent the measured CMB temperature fluctuations, while the solid curve shows the best-fit prediction of the standard ΛCDM model. The excellent agreement between the theoretical curve and the observed acoustic peak structure over a wide range of multipoles demonstrates the remarkable success of ΛCDM in describing the physics of the early Universe, including the dynamics of the photon–baryon fluid, gravitational potentials, and the initial conditions of primordial perturbations. The lower panel displays the residuals between the data and the ΛCDM prediction, which are consistent with statistical noise, further highlighting the precision with which the ΛCDM model reproduces the observed CMB temperature anisotropies.[2]

assuming ΛCDM. This discrepancy, known as the S_8 *(or* σ_8*) tension*, where late-time large-scale structure measurements systematically fall below the predictions extrapolated from early-Universe data. Although currently less statistically significant than the Hubble tension, the S_8 tension is of particular interest because it directly probes the growth of cosmic structures and the underlying gravitational dynamics.

The simultaneous presence of tensions in both the expansion history (H_0) and the growth of structure (σ_8 or S_8) suggests that these discrepancies may be physically connected. In particular, any modification to the cosmological model that alters either the background expansion or the growth rate of density perturbations has the potential to impact both observables. This has motivated extensive theoretical efforts aimed at identifying possible resolutions, including modifications to the early-Universe expansion history—such as early dark energy scenarios [9]—as well as extensions of the dark sector involving interactions between dark matter and dark energy or departures from general relativity on cosmological scales [8].

More fundamentally, some studies have questioned the validity of the underlying assumptions of large-scale isotropy and homogeneity. In particular, Ref. [30] investigates whether the observable Universe is fully consistent with the cosmological principle, arguing that the persistence of large-scale structures beyond expected scales could signal deviations from statistical homogeneity. Such considerations further emphasize that the current cosmological tensions may not merely reflect parameter-level inconsistencies, but could point to deeper issues related to the foundations of the standard cosmological paradigm.

Taken together, the Hubble and S_8 tensions highlight the importance of exploring extensions to ΛCDM and developing more flexible theoretical frameworks capable of accommodating high-precision cosmological data across multiple probes and redshifts. In this context, observables related to the growth of structure play a crucial role, providing complementary and highly sensitive tests of both the background expansion and the dynamics of cosmic perturbations.

One of the most relevant current tensions within the ΛCDM framework is associated with the recent results reported by the DESI Collaboration, which suggest a possible deviation from a strictly constant dark energy equation of state. In particular, combined analyses involving DESI data indicate a preference for a dynamical dark energy scenario, as illustrated in Fig. 1.4.

Although not yet conclusive, this potential deviation from the ΛCDM limit opens new avenues for theoretical exploration. The degeneracy inherent to the dark sector allows for multiple physical interpretations of an effective dynamical behavior. Among the possible alternatives, interactions within the dark sector constitute a well-motivated extension, capable of mimicking or generating departures from a cosmological constant while preserving consistency with large-scale structure observations.

In this context, the hypothesis of an interacting dark sector provides a natural framework to investigate whether the observed indications of dynamical dark energy may arise from underlying couplings between dark matter and dark energy, rather than from a fundamental modification of the equation of state alone.

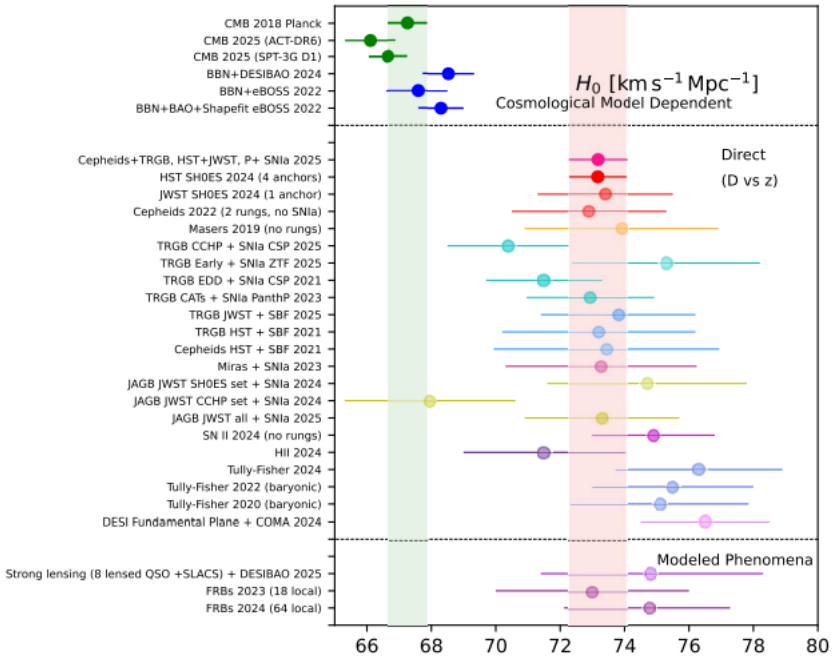

Figure 1.2.: Recent determinations of the Hubble-Lemaître constant H_0 obtained using a wide range of observational probes. Local, late-Universe measurements based on distance-ladder techniques—including Cepheid- and TRGB-calibrated Type Ia supernovae, surface-brightness fluctuations, Type II supernovae, the Tully–Fisher relation, Mira variables, carbon stars, strong-lensing time-delay cosmography, fast radio bursts, the DESI fundamental plane calibrated with the Coma cluster, and water megamaser distances—consistently favor higher values of the Hubble constant, typically in the range $H_0 \simeq 71$–$77\ \mathrm{km\,s^{-1}\,Mpc^{-1}}$. In contrast, early-Universe determinations inferred from CMB and BAO data within the ΛCDM framework yield significantly lower values, $H_0 \simeq 66$–$68\ \mathrm{km\,s^{-1}\,Mpc^{-1}}$. This discrepancy highlights the current Hubble tension. Updated from Ref. [10].

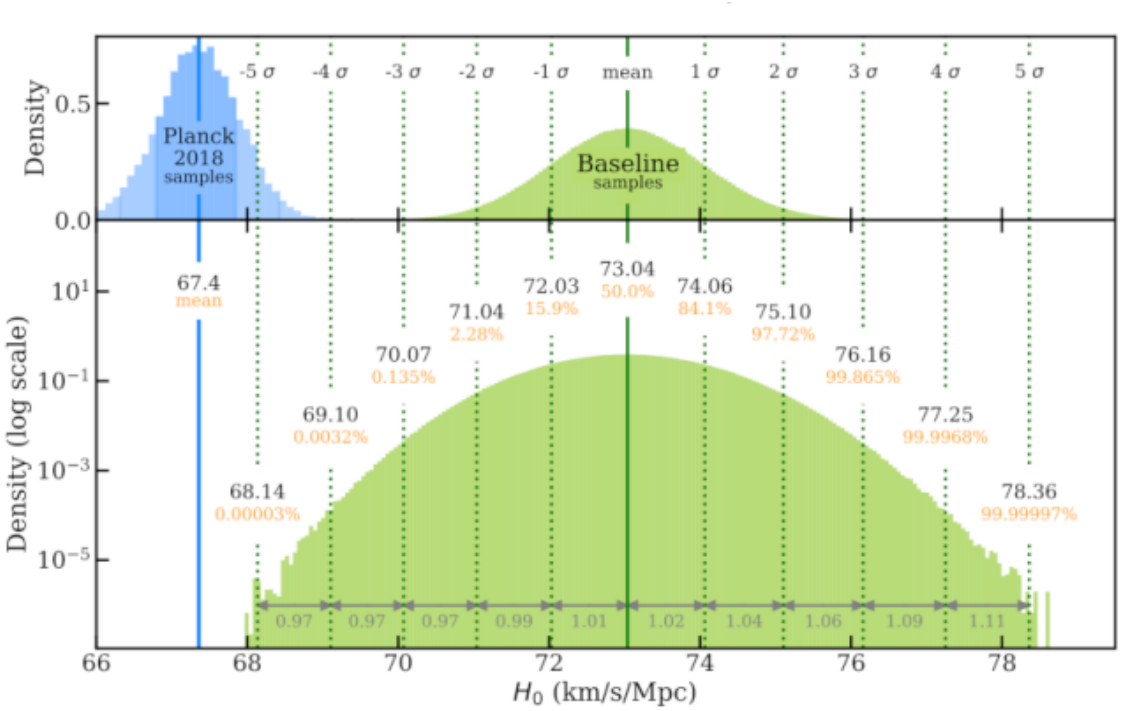

Figure 1.3.: An extended Markov Chain Monte Carlo (MCMC) sampling of the posterior distribution of H_0 was performed in order to probe confidence regions out to the $\pm 5\sigma$ level. The upper panel displays the probability density corresponding to the baseline SH0ES analysis, together with the chains from the Planck Collaboration et al. (2020). The lower panel presents the logarithm of the probability density, which enhances the visibility of the distribution tails and allows for a clearer comparison at large deviations from the mean. A mild asymmetry in the posterior distribution can be observed: the confidence intervals on the low-H_0 side are slightly narrower than those on the high-H_0 side. This asymmetry arises because the underlying measurements are Gaussian in magnitudes and in $5 \log H_0$, which induces a small skewness when expressed directly in terms of H_0. Updated from Ref. [4]

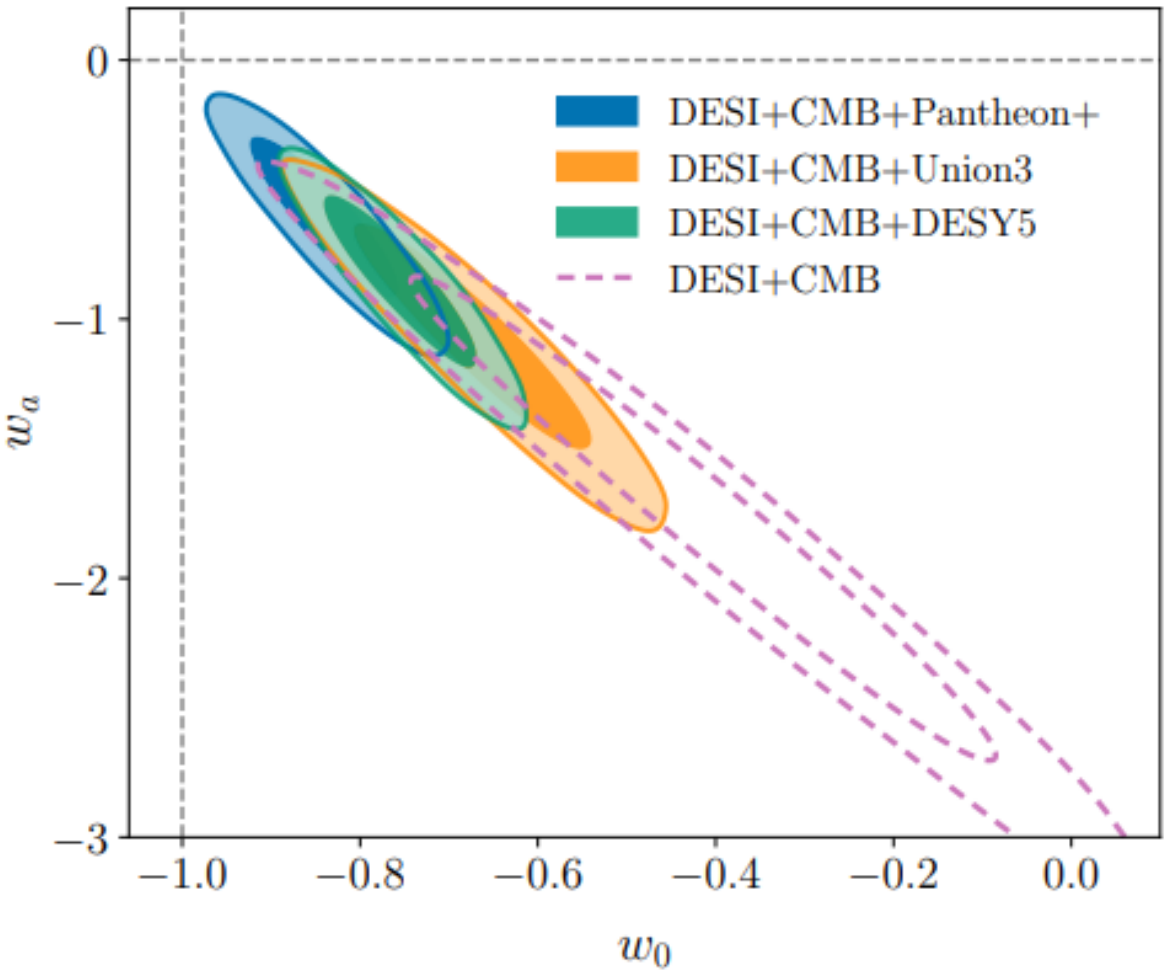

Figure 1.4.: Posterior distributions of the parameters w_0 and w_a, obtained from fits of the w_0w_aCDM model to DESI data in combination with CMB measurements and three supernova (SNe) datasets, as indicated. For comparison, we also display the constraints derived from the combination of DESI with CMB data alone. The contours enclose 68% and 95% credible regions of the posterior probability distribution. The gray dashed lines correspond to $w_0 = -1$ and $w_a = 0$, whose intersection defines the ΛCDM limit. The statistical significance for rejecting the ΛCDM model is found to be 2.8σ, 3.8σ, and 4.2σ when DESI and CMB data are combined with the Pantheon+, Union3, and DESY5 SNe samples, respectively. For the DESI+CMB combination without supernova data, the rejection significance is 3.1σ. These results correspond to the most recent cosmological constraints reported by the DESI Collaboration.

Statistical Description of the dynamics of the Universe

In the context of the standard cosmological framework, the statistical description of cosmology plays a central role in connecting theoretical predictions with observational data. Rather than focusing on individual galaxies or structures, the Universe is treated as a statistical ensemble where the distribution of matter and radiation is described in terms of averaged quantities and correlation functions. This perspective is motivated by the fact that the primordial fluctuations generated in the early Universe are inherently random in nature, and their evolution leads to the large-scale structure observed today.

Within this approach, statistical tools allow us to characterize the clustering of matter, the anisotropies of the cosmic microwave background, and the formation of cosmic structures on a wide range of scales. These statistical descriptors provide a bridge between theory and observation, enabling rigorous tests of the ΛCDM paradigm. They also serve as the foundation for comparing numerical simulations, perturbative calculations, and high-precision cosmological surveys.

The strength of this statistical framework lies in its capacity to reduce the apparent complexity of the Universe into measurable quantities that can be systematically analyzed. In doing so, it allows cosmology to advance as a precision science, turning the randomness of initial conditions into a coherent picture of cosmic evolution.

The possibility of an interaction between dark matter and dark energy has received considerable attention as a natural extension of the standard cosmological model. In such scenarios, the dark sectors are not conserved independently but exchange energy and/or momentum through a coupling term introduced at the level of the continuity equations. This interaction is typically motivated by the absence of a symmetry that would forbid it, and by the potential to alleviate persistent cosmological tensions such as the Hubble tension and the σ_8 discrepancy.

The phenomenological modeling of the interaction term Q in the continuity equations for dark matter and dark energy is a common starting point. A frequently studied class of models assumes $Q = 3\gamma H\rho_i$, where γ is a dimensionless coupling constant, H is the Hubble parameter, and ρ_i is the energy density of one of the dark components, typically chosen to be dark matter or dark energy [14, 18].

In this chapter, we present the theoretical framework and observational implications of interacting dark sector models. We begin by introducing a modified Boltzmann-Poisson equation that incorporates possible interactions between dark matter and dark energy. The zeroth-order moment of this equation provides the evolution of the background density, while the first-order moment describes the dynamics of the velocity field, allowing us to analyze perturbations and momentum transfer.

Next, we discuss the Bianchi identities and their role in constraining viable interaction models, ensuring the consistency of the modified cosmological framework. Building on these results, we derive new evolution equations for the density contrast and velocity divergence, which form the basis for studying structure formation under interactions.

We then examine the background dynamics of the interaction model, highlighting its effects on the expansion rate, matter content, and dark energy evolution. Finally, we explore how current observational data constrain these models, using measurements from the cosmic microwave background, large-scale structure, and supernovae surveys to set bounds on the interaction parameters.

These models lead to modified background evolution and impact the growth of perturbations. Depending on the sign of γ, the interaction may transfer energy from dark energy to dark matter or vice versa. This affects both the expansion history and structure formation, which can be tested with cosmological observables such as the CMB anisotropies, baryon acoustic oscillations (BAO), Type Ia supernovae, and redshift-space distortions (RSD) [16].

However, not all interaction models are viable. For instance, early studies revealed that models where the momentum transfer is not carefully treated can lead to large-scale instabilities in the evolution of perturbations [18]. These instabilities can be avoided by adopting models with specific couplings or by considering the interaction in the rest frame of dark matter or dark energy [19].

From the observational standpoint, interacting dark sector models are subject to increasingly stringent constraints. Yet, some studies suggest that mild interactions may still be allowed and even preferred when considering combined cosmological datasets [25].

In recent years, the idea of interaction in the dark sector has also been revisited in light of the Hubble tension, as such models can modify the late-time dynamics and potentially reconcile the local and early-time measurements of H_0 [10].

In the following section, we turn our attention to the Boltzmann equations, which provide a fundamental framework for describing the evolution of particle distribution functions in an expanding universe. These equations play a central role in cosmology, as they allow us to track the statistical properties of different species, including matter, radiation, and neutrinos, while also incorporating the effects of collisions and interactions. By formulating the Boltzmann equations in the context of perturbation theory, we will be able to establish the link between microscopic particle dynamics and macroscopic cosmological observables.

2.1. Boltzmann equations

These equations plays a fundamental role in statistical mechanics and kinetic theory, as it governs how the distribution function evolves over time. This function characterizes the density of particles in phase space, encompassing both their positions and momenta. By connecting the microscopic motion of individual particles with the emergent macroscopic properties of a system, the Boltzmann equation serves as a powerful tool for studying systems away from equilibrium.

In its general form, the Boltzmann equations is written as:

$$\frac{df}{dt} = \frac{\partial f}{\partial t} + \frac{\partial f}{\partial x^i}\frac{dx^i}{dt} + \frac{\partial f}{\partial p^i}\frac{dp^i}{dt} \tag{2.1}$$

Here, $\frac{\partial f}{\partial t}$ accounts for explicit time dependence, $\frac{\partial f}{\partial x^i}\frac{dx^i}{dt}$ describes spatial transport, and $\frac{\partial f}{\partial p^i}\frac{dp^i}{dt}$ represents momentum changes due to external forces. In practice, an additional **collision term** is often included on the right-hand side to model interactions between particles.

The equation is fundamental for understanding the behavior of gases and plasmas, providing a microscopic basis for macroscopic properties like pressure and temperature. Solutions to the Boltzmann equation lead to conservation laws and fluid dynamics equations, such as the Navier-Stokes equations. Applications of the Boltzmann equation extend beyond classical gases to fields like astrophysics, plasma physics, and semiconductor transport, making it a powerful tool in both theoretical and applied physics. The Boltzmann equation gains practical significance when combined with the equations governing the motion of particles in a given spacetime. These are expressed through the equations for the evolution of spatial coordinates and momenta. For a relativistic context, these equations are:

The motion of particles in an expanding and perturbed Universe is governed by the geodesic equations, which describe how freely falling particles move under the influence of gravity alone. In General Relativity, gravity is not treated as a force but rather as a manifestation of spacetime curvature, and particles follow geodesics determined by the metric. In the presence of scalar perturbations, the geodesic equations for the spatial coordinates and momenta of particles take the form

$$\frac{dx^i}{dt} = \frac{p^i}{aE}(1-\phi+\Psi), \tag{2.2}$$

$$\frac{dp^i}{dt} = -(H+\dot{\phi})p^i - \frac{E}{a}\Psi_{,i} - \frac{1}{a}\frac{p^i}{E}p^k\phi_{,k} + \frac{p^2}{aE}\phi_{,i}. \tag{2.3}$$

These expressions correspond to the spatial components of the geodesic equations written in terms of the particle momenta, making explicit how the background expansion and metric perturbations affect particle trajectories. Here, x^i and p^i denote the spatial coordinates and momenta of the particles, respectively, while E represents the total particle energy, related to the momentum through $E = \sqrt{p^2 + m^2}$ for massive particles. The factor $a(t)$ denotes the cosmological scale factor, and the Hubble parameter $H = \dot{a}/a$ accounts for the effect of cosmic expansion on particle motion. The scalar perturbations ϕ and Ψ describe gravitational potential fluctuations in the perturbed metric, introducing corrections to both particle trajectories and momentum evolution.

By inserting these geodesic relations for dx^i/dt and dp^i/dt into the Boltzmann equation, one establishes a direct connection between the microscopic dynamics of particles moving along geodesics and the statistical evolution of the distribution function $f(t, x^i, p^i)$. This procedure allows one to derive macroscopic evolution equations from the underlying particle dynamics. In cosmological applications, this framework is essential for describing the evolution of photons, neutrinos, and dark matter particles, providing the bridge between gravitational dynamics and the kinetic description of cosmic fluids in the early Universe.

2.2. Sub-horizon Approximation

The sub-horizon approximation[1] is commonly employed in cosmology when studying the dynamics of perturbations on scales much smaller than the cosmological horizon. In this regime, perturbation wavelengths are sufficiently small compared to the Hubble radius such that local gravitational dynamics dominate over purely relativistic, large-scale effects associated with the expansion of the Universe. As a consequence, spatial gradients become more important than terms suppressed by factors of the Hubble scale, and the evolution equations simplify considerably.

[1] See Sec. 1.4

An important implication of this limit is that the relativistic evolution equations smoothly reduce to their Newtonian counterparts while preserving the hydrodynamic structure of the system. In other words, although the equations originate from a fully relativistic treatment, their form in the sub-horizon regime coincides with the standard hydrodynamical description of a self-gravitating fluid. Therefore, the continuity and Euler equations retain their usual interpretation, and the dynamics can be consistently described within the hydrodynamic limit without loss of accuracy on the scales relevant for structure formation.

Under this approximation, particle motion follows the geodesic equations in a form that directly leads to the familiar hydrodynamic equations governing density and velocity perturbations. In this regime, the motion of particles is governed by:

$$\frac{dx^i}{dt} = \frac{p^i}{am}, \tag{2.4}$$

$$\frac{dp^i}{dt} = -Hp^i - \frac{m}{a}\Psi_{,i}. \tag{2.5}$$

The subhorizon approximation is particularly relevant for studying non-relativistic matter, such as cold dark matter, where the dynamics are influenced by the competition between the Hubble expansion and gravitational clustering. These simplified equations provide a clear framework for analyzing local interactions without the complexities introduced by relativistic effects or large-scale curvature.

2.3. The Boltzmann-Poisson Equation

The Boltzmann–Poisson equation is a key framework in kinetic theory, describing the dynamics of the matter distribution function $f(t, x^i, p^i)$ under the influence of self-consistent gravitational fields. In this context, the equation governs the evolution of non-relativistic matter, where the statistical properties of a large ensemble of particles are encoded in the phase-space distribution. The evolution of the distribution function is determined by:

$$\frac{df}{dt} = \frac{\partial f}{\partial t} + \frac{\partial f}{\partial x^i}\frac{p^i}{am} + \frac{\partial f}{\partial p^i}\left[-Hp^i - \frac{m}{a}\Psi_{,i}\right] = C\left[f\right]. \tag{2.6}$$

This kind of system is widely used in cosmology to model the evolution of large-scale structures, such as dark matter distributions as we can see in [26] and [28]. It captures the competition between the expansion of the universe, represented by the Hubble term, and the gravitational clustering driven by perturbations in Ψ. The term $C[f]$ is related to possible interactions between different components of the dark sector, such as dark matter and dark energy. It encodes the exchange of energy and momentum at the microscopic level, modifying the standard Boltzmann evolution. This term can give rise to additional source terms in the moments of the distribution function, affecting both the background dynamics and the growth of perturbations.

In the following subsection, we will show that the zeroth-order moment of the equation determines how the mean matter density evolves in the presence of interactions, while the first-order moment, discussed in the subsequent subsection, governs the evolution of the velocity field, introducing corrections to the standard continuity and Euler equations. By including the collision term, the modified Boltzmann-Poisson system provides a consistent framework to study the impact of dark sector interactions on structure formation and the overall expansion history of the universe.

2.3.1. Zeroth Order Moment of Boltzmann Equation

The zeroth-order moment of the Boltzmann equation provides a macroscopic description of the conservation of mass or particle number density in a collisional system. It is derived by integrating the Boltzmann equation over the momentum space of the particle distribution function. The resulting continuity equation is expressed as:

$$\frac{\partial \rho_m}{\partial t} + \frac{1}{a}\partial_i \left(\rho_m u^i\right) + 3H\rho_m = \int \frac{d^3p}{(2\pi)^3} C\left[f\right] E\,. \tag{2.7}$$

where ρ_m is the mass density of the particles, u^i is their bulk velocity, and H is the Hubble parameter accounting for the effect of cosmic expansion. The right-hand side contains an integral over momentum space, involving the collision term $C[f]$ and the particle energy E, which accounts for non-conservation effects due to particle interactions.

The three terms on the left-hand side represent distinct physical processes. The first term, $\partial\rho_m/\partial t$, describes the explicit time evolution of the mass density. The second term, $\partial_i \left(\rho_m u^i\right)/a$, accounts for mass transport due to particle bulk flow. The third term, $3H\rho_m$, represents the dilution of mass density caused by the expansion of the universe.

When $C[f] = 0$, corresponding to a collisionless system, the equation simplifies, enforcing the conservation of mass within the context of an expanding spacetime. This zeroth-order moment is fundamental in cosmological models, describing how matter densities evolve and interact with the Hubble flow and gravitational clustering processes. In interaction models, we define that,

$$\int \frac{d^3p}{(2\pi)^3} C\left[f\right] E \equiv -u^\mu Q_\mu = Q\,. \tag{2.8}$$

In summary, by imposing this relationship, the equation states that the integral describing energy exchange due to collisions is equal to a quantity Q, which defines the dissipation or energy transfer rate in the system. This rate is determined by the interaction between the particles and the gravitational field (or other external fields), suggesting that the behavior of the particles is influenced by this dissipation term.

2.3.2. First Order Moment of Boltzmann Equation

The first moment of the Boltzmann equation is crucial for understanding the dynamics of a system of particles, as it describes how the momentum density evolves due to both the expansion of the universe and any internal interactions. This moment is a key ingredient in deriving the fluid-like behavior of matter in cosmology, especially when studying the evolution of structures such as dark matter and galaxy formation. It links the microscopic particle distribution to macroscopic observables like velocity fields, momentum transfer, and stress-energy tensors. We can obtain integrating Boltzmann equation multiplied for the velocity field.

$$\frac{\partial u^i}{\partial t} + \frac{1}{a}u^j\partial_j u^i + Hu^i + \frac{1}{a}\partial^i\Psi = \frac{1}{\rho_m}\left(Q^i - Qu^i\right)\,, \tag{2.9}$$

imposing the equation

$$\int \frac{d^3p}{(2\pi)^3}\; C\left[f\right] p^i \equiv Q^i\,. \tag{2.10}$$

has a specific physical meaning in the context of the Boltzmann-Poisson system and kinetic theory. This equation states that the momentum exchange rate between particles due to collisions

or interactions is given by a quantity Q^i, which can be interpreted as a macroscopic force or momentum transfer. Where,

$$Q^i = Qu^i, \tag{2.11}$$

where u^i denotes the spatial components of the fluid four-velocity and Q characterizes the interaction strength responsible for energy exchange between the dark sector components. Physically, this relation states that the interaction current is aligned with the fluid four-velocity, so that the energy–momentum transfer follows the bulk motion of the fluid.

In general, the vector Q^μ describes the exchange of energy and momentum between interacting components and therefore appears as a source term in the conservation equations of each species. Its spatial components Q^i would, in principle, represent a transfer of momentum density induced by the interaction, thereby modifying the dynamical evolution of the fluid motion.

However, in the present model the interaction vector is assumed to be parallel to the four-velocity, implying that there is no momentum transfer in the rest frame of the fluid. As a consequence, the interaction corresponds to a purely energetic exchange between the components, leaving the momentum density unaffected. In practical terms, this means that the coupling modifies the energy densities of the interacting species without introducing an additional force term capable of accelerating the fluid. This assumption significantly simplifies the perturbation equations while still capturing the essential impact of energy exchange in the dark sector.

2.4. On the covariant modeling of a dark sector interaction

In cosmological contexts, the Boltzmann–Poisson framework can be employed to describe how the momentum of particles (such as dark matter or baryons) evolves under the influence of both self-interactions and external fields, most notably gravity. This description is essential for understanding the evolution of structures and the large-scale dynamics of the universe.

However, when dealing with relativistic settings, the Boltzmann–Poisson approach must be generalized. *A covariant formulation becomes crucial*, since it ensures that the physical laws governing particle interactions and energy–momentum conservation hold independently of the chosen reference frame or coordinate system. Such a description is particularly important in cosmology, where spacetime curvature and the expansion of the universe cannot be neglected.

Within this context, the interaction between different components of the dark sector can be effectively characterized by a covariant interaction vector Q^μ. One proposed form for this interaction vector is given by

$$Q^\mu = -\frac{\gamma}{4}\Theta^\nu{}_\nu \, T_\Lambda{}^\sigma \, u^\mu \,, \tag{2.12}$$

where Q^μ represents the exchange of energy-momentum between different cosmic fluids, such as dark matter and dark energy. The parameter γ is a dimensionless coupling constant that governs the strength of the interaction. The term $\Theta^\nu{}_\nu$ denotes the covariant derivative of the four–velocity or expansion scalar, while $T_\Lambda{}^\sigma$ is the trace of the energy-momentum tensor associated with the dark energy component, often modeled as a cosmological constant. The vector u^μ represents the four-velocity of the matter component, describing its motion in spacetime.

In much of the phenomenological literature, a simplified version of the interaction term is adopted:

$$Q = 3H\gamma\rho_\Lambda \,, \tag{2.13}$$

where H is the Hubble parameter, and ρ_Λ is the energy density of the dark energy component. This form is widely used due to its analytical simplicity and compatibility with observational

constraints [13, 24, 15]. In this work, we employ the simplified form given by (2.13) to derive and interpret our results. However, the broader objective is to develop a framework capable of encompassing a variety of interaction models, including those that cannot be directly reduced to the form of (2.13).

In the next section, we discuss the role of the Bianchi identities in the context of interacting dark sector models. These identities, which arise from the geometric properties of spacetime, ensure the conservation of the total energy-momentum tensor. By applying the Bianchi identities, we derive consistency conditions that constrain the form of possible interactions between dark matter and dark energy, ensuring that the modified cosmological equations remain self-consistent. This framework allows us to construct physically viable interaction models and analyze their implications for both the background evolution and the growth of perturbations.

The equation

$$\nabla_\mu T^{\mu\nu}_\Lambda = -\nabla_\mu T^{\mu\nu}_c = Q^\nu \,, \tag{2.14}$$

is a direct consequence of the **Bianchi identities**, which ensure the conservation of the total energy-momentum tensor in general relativity. According to the Bianchi theorem, the divergence of the Einstein tensor vanishes, implying that the total energy-momentum tensor, accounting for all cosmic components, satisfies the conservation equation:

$$\nabla_\mu T^{\mu\nu}_{total} = 0. \tag{2.15}$$

In cosmological models involving interactions between different components, such as dark energy and dark matter, the energy-momentum tensor for each component is not conserved individually. Instead, their divergences are linked through an interaction term represented by the vector Q^ν. Specifically, $T^{\mu\nu}_\Lambda$ denotes the energy-momentum tensor of the dark energy component, while $T^{\mu\nu}_c$ represents that of the dark matter component.

The Q quantifies the exchange of energy and momentum between these two components. A positive Q-term corresponds to a transfer of energy from dark matter to dark energy, while a negative interaction term signifies the reverse flow. This interaction modifies the dynamics of the universe, influencing its expansion rate and the evolution of cosmic structures.

Thus, this equation encapsulates a crucial aspect of interacting dark energy models, highlighting the non-conservation of individual components and the role of interaction in shaping the cosmic evolution. Oppening the temporal term of the tensorial equation, we obtain that for the background,

$$\begin{aligned} \frac{\partial \rho_c}{\partial t} + 3H\rho_c &= Q \,, \\ \frac{\partial \rho_\Lambda}{\partial t} &= -Q \,. \end{aligned} \tag{2.16}$$

In the next section, we derive the modified evolution equations for the density contrast and velocity divergence in the presence of dark sector interactions. Building on the moments of the modified Boltzmann-Poisson equation and the constraints imposed by the Bianchi identities, these equations describe how matter perturbations and fluid velocities evolve under the influence of an interacting dark energy component. The resulting system generalizes the standard continuity and Euler equations, providing a framework to study the growth of cosmic structures and the impact of energy-momentum exchange on the dynamics of the universe.

2.5. Equations for Density Constrast and Velocity Divergence

The spatial distribution of matter density in an inhomogeneous universe can be expressed as

$$\rho_m(\vec{x}, a) \equiv \rho_m(a)\big(1 + \delta_m(\vec{x}, a)\big), \tag{2.17}$$

where $\rho_m(\vec{x}, a)$ denotes the local matter density at position $\vec{x}$ and scale factor a, while $\rho_m(a)$ represents the homogeneous background matter density at the same cosmic time.

The quantity $\delta_m(\vec{x}, a)$ is the matter density contrast, defined as

$$\delta_m(\vec{x}, a) = \frac{\rho_m(\vec{x}, a) - \rho_m(a)}{\rho_m(a)}\,, \tag{2.18}$$

which quantifies the relative deviation of the local density from the cosmological mean. Positive values of δ_m ($\delta_m > 0$) correspond to overdense regions, such as those that eventually evolve into galaxies or clusters of galaxies. Conversely, negative values ($\delta_m < 0$) describe underdense regions, or voids.

This formulation is central to modern cosmology, as it provides the starting point for investigating the growth of cosmic structures. The time evolution of δ_m, governed by gravitational instability, reveals how small initial fluctuations in the matter density field grow into the nonlinear structures observed in the present-day universe.

By inserting this definition, together with $\theta = \nabla \cdot \vec{u}$, into the zeroth- and first-order moments of the Boltzmann equations, one obtains the fluid equations for the evolution of matter perturbations. In the context of interacting dark sector (IDS) cosmologies, these equations are modified by the presence of an energy exchange between dark matter and dark energy. Within the fluid approximation, the coupled dynamics of density fluctuations and velocity fields can be described by the following system.

The first equation governs the evolution of the matter density contrast, δ_m. In addition to the standard terms describing advection and nonlinear couplings between density and velocity, it includes a contribution proportional to the interaction term Q, which encodes the energy transfer between dark matter and dark energy:

$$\delta_m' + \theta_m = -u^i \partial_i \delta_m - \delta_m \theta_m - \frac{aQ}{\rho_m}\delta_m\,. \tag{2.19}$$

The second equation describes the evolution of the velocity divergence, θ_m. Besides the usual Hubble damping term, the gravitational source term driven by matter overdensities, and nonlinear convective contributions, the interaction affects the dynamics indirectly through the modified evolution of δ_m:

$$\theta_m' + \mathcal{H}\theta_m + \nabla^2\Psi = -\big(\partial_i u^j\big)\big(\partial_j u^i\big) - u^i \partial_i \theta_m\,. \tag{2.20}$$

Equations (2.19) and (2.20) provide a self-consistent framework for describing the evolution of large-scale structures in interacting dark sector cosmologies, capturing both linear and mildly nonlinear effects.

For convenience in the subsequent analysis, we introduce the dimensionless interaction function

$$g \equiv \frac{aQ}{\mathcal{H}\rho_m}\,, \tag{2.21}$$

which parametrizes the strength of the interaction relative to the Hubble expansion rate. This quantity will play a central role in the following sections, where we investigate the implications of dark sector interactions for the growth of cosmic structures.

2.6. Background dynamics of interaction model

Understanding the background dynamics of cosmological models with dark sector interactions is essential for assessing their physical viability and observational signatures. In the standard ΛCDM scenario, the universe undergoes distinct evolutionary phases dominated first by radiation, then by matter, and finally by dark energy. Introducing an interaction between dark matter and dark energy can significantly alter the timing and duration of these epochs.

In particular, the matter-dominated era plays a crucial role in structure formation, while the dark energy-dominated era governs the current accelerated expansion of the universe. Any deviation from the standard background evolution must be carefully examined to ensure consistency with cosmological observations.

In this section, we investigate how the background cosmological evolution is modified in the presence of an interaction term between dark matter and dark energy. Specifically, we analyze the evolution of the corresponding energy densities as functions of both redshift and scale factor. Starting from the continuity equations 2.16 with the interaction term defined as $Q = 3\gamma H \rho_\Lambda$, the system becomes

$$\frac{d\rho_c}{dt} = -3H(\rho_c - \gamma\rho_\Lambda), \tag{2.22}$$

$$\frac{d\rho_\Lambda}{dt} = -3\gamma H \rho_\Lambda. \tag{2.23}$$

The solution to this system of equations is given by

$$\rho_c(a) = \rho_{0c}a^{-3} + \frac{\gamma}{\gamma - 1}\rho_{0\Lambda}\left(a^{-3} - a^{-3\gamma}\right), \tag{2.24}$$

$$\rho_\Lambda(a) = \rho_{0\Lambda}a^{-3\gamma}. \tag{2.25}$$

It is important to emphasize that the Friedmann equation is modified in the interacting scenario. For a spatially flat universe composed of baryonic matter, radiation, interacting cold dark matter, and interacting dark energy, the normalized Hubble parameter can be expressed as

$$E^2_{\rm IDS}(a) = \Omega_{r0}a^{-4} + \Omega_{m0}a^{-3} + \Omega_{\Lambda 0}a^{-3}\left(\frac{a^{3(1-\gamma)} - \gamma}{1 - \gamma}\right), \tag{2.26}$$

where $\Omega_{m0} = \Omega_{b0} + \Omega_{c0}$. In the limit $\gamma \to 0$, the standard ΛCDM relation is recovered:

$$\lim_{\gamma \to 0} E^2_{\rm IDS} = E^2_{\Lambda\rm CDM}. \tag{2.27}$$

By plotting the density parameters and their evolution as functions of redshift or scale factor, we are able to visualize the impact of the interaction on the overall cosmic history. Of particular interest are the onset and duration of the matter- and dark energy-dominated eras, as illustrated in Figure 2.1. Such plots serve as diagnostic tools to determine whether the interaction model preserves the essential features of the standard cosmological scenario or introduces deviations that could be constrained through observational data.

Within this specific interaction model, the interaction function $g(a)$ can be defined as

$$g(a) = 3\gamma\frac{\Omega_\Lambda}{\Omega_m} = 3\gamma\,\Omega_{\Lambda 0}a^{-3\gamma}\left[\Omega_{m0}a^{-3} + \frac{\gamma}{\gamma - 1}\Omega_{\Lambda 0}\left(a^{-3} - a^{-3\gamma}\right)\right]^{-1}. \tag{2.28}$$

The evolution of this function can be analyzed for different values of γ, as shown in Figure 2.2. These results highlight how the strength and sign of the interaction modify the relative contribution of dark matter and dark energy across cosmic time. Even when the parameter γ assumes relatively small values and the interaction term g remains small when compared to the growth rate f, the interaction must still be regarded as strong within this model, since it produces significant modifications in the evolution of f itself. This demonstrates that , in this model, even weak interaction parameters can lead to substantial changes in the growth of cosmic structures.

Using the definition of $g(a)$ together with the distance relations introduced in Section 1 with (1.25), we compare the predictions of the interacting dark sector model with those of the ΛCDM framework. The differences are displayed in Figures 2.3, 2.4 and 2.5, which illustrate the impact of the interaction term on cosmological distance measures.

In the next section, we focus on the observational constraints of interacting dark sector models. This analysis is essential to test the theoretical consistency of such models and to determine whether the interaction between dark matter and dark energy leaves detectable imprints on cosmological observables. By comparing theoretical predictions with current data, we can place bounds on the strength and functional form of the interaction. These constraints allow us to assess the viability of interacting scenarios with respect to the standard ΛCDM model and to explore potential deviations that might alleviate existing cosmological tensions.

In this work, we choose to adopt interaction parameters fixed at $\gamma = \pm 0.05$, as values within this range have already been explored in the literature and shown to be phenomenologically viable. This choice allows for a meaningful comparison with previous studies while ensuring that the interaction strength remains within observationally acceptable bounds.

In some instances, the results corresponding to $\gamma = -0.05$ are not explicitly displayed. This is because a more detailed investigation of the significant redshift-space distortions generated in this scenario is still required. A comprehensive analysis of these effects lies beyond the scope of the present dissertation and will be addressed in future work.

2.7. Observational constraints

Interacting dark sector models propose that dark matter and dark energy may exchange energy or momentum through mechanisms beyond standard gravitational interaction. These models have been extensively studied as extensions to the ΛCDM paradigm, offering possible explanations for persistent cosmological tensions, such as the discrepancies in measurements of the Hubble-Lemaître constant and the growth rate of cosmic structures. In such scenarios, the interaction is typically introduced phenomenologically, with its strength quantified by a dimensionless coupling parameter. Even small values of this coupling can induce noticeable effects on the expansion history and structure formation, making the models testable with current observational data.

A variety of cosmological probes are used to constrain interactions in the dark sector. The high-precision temperature and polarization spectra from the *Planck* mission, provides information about the early Universe and serves as a strong anchor for cosmological parameters. Type Ia supernovae, as standardizable candles, contribute to distance measurements at low to intermediate redshifts, especially through the Pantheon and Pantheon+ compilations. Baryon acoustic oscillations (BAO), measured by surveys like BOSS, eBOSS, and DESI, trace the cosmic distance scale and the Hubble parameter at different epochs. Additionally, redshift-space distortions (RSD) and weak gravitational lensing offer constraints on the growth of structure, which can be sensitive to the presence of interactions in the dark sector.

Analyses of these data are often performed using modified Boltzmann solvers, such as `CLASS`

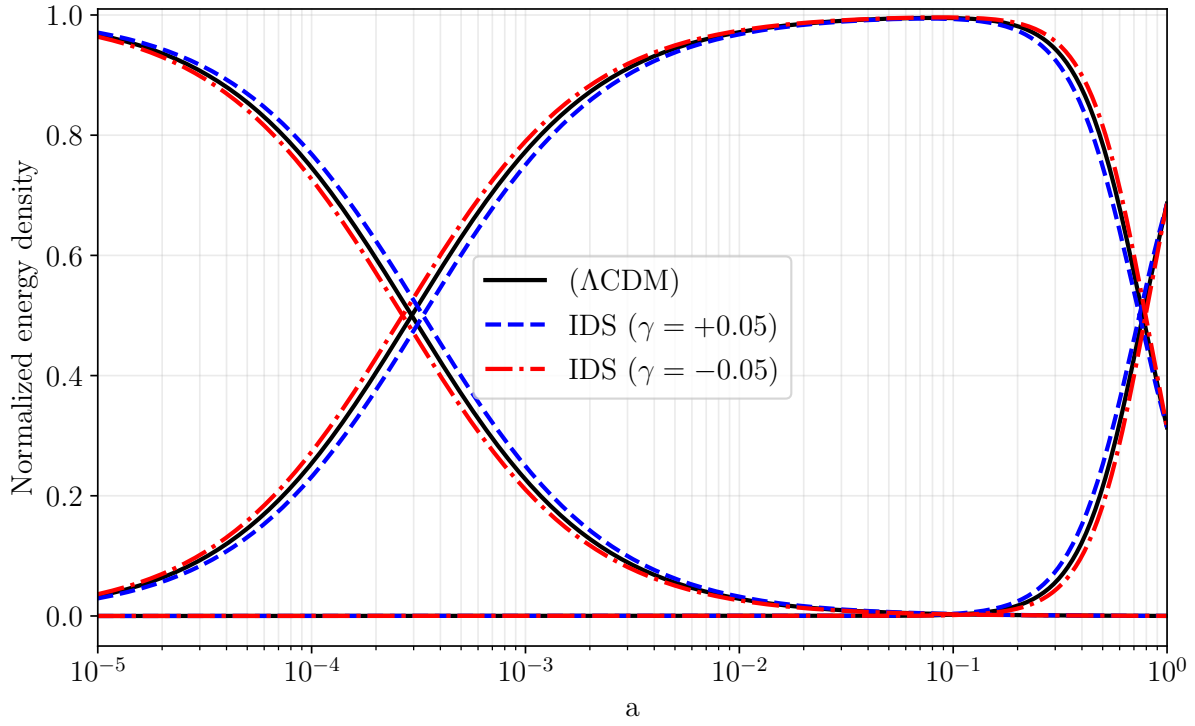

Figure 2.1.: Comparison of normalized energy density components (radiation, matter, and dark energy) as functions of the scale factor a, for the standard ΛCDM model ($\gamma = 0$, black lines) and interacting dark sector models with $\gamma = -0.05$ (red dash-dotted) and $\gamma = +0.05$ (blue dashed). The main panel displays the evolution of each component. The figure illustrates how interactions in the dark sector modify the relative contribution of each component across cosmic time.

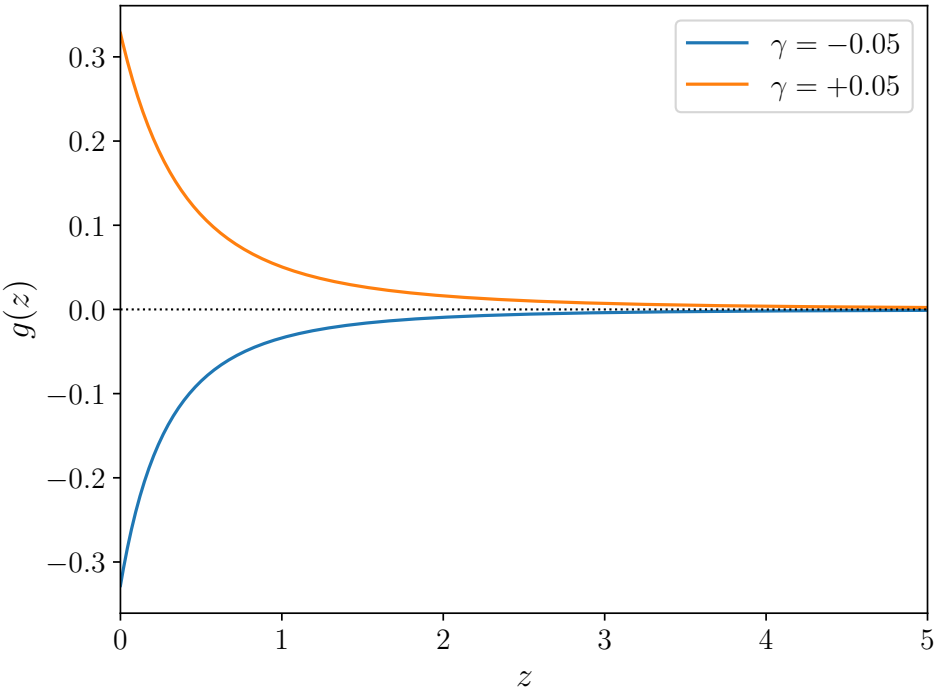

Figure 2.2.: Evolution of the interaction term $g(z)$ as a function of the redshift z for different values of the coupling parameter γ. The cases $\gamma = -0.05$ (blue) and $\gamma = +0.05$ (orange) are shown for comparison. The dotted line corresponds to the standard ΛCDM scenario without interaction.

or `CAMB`, with interaction terms implemented into the energy-momentum conservation equations. Monte Carlo Markov Chain (MCMC) techniques are employed to explore the parameter space, fitting for the interaction strength alongside standard cosmological parameters. Studies using combined datasets—such as CMB, BAO, supernovae, and RSD—typically find that the interaction parameter is consistent with zero within uncertainties, with current upper bounds in the range $|\gamma| \lesssim 0.05$. However, in some analyses, especially those focusing on resolving the Hubble tension, a small negative interaction (energy transfer from dark energy to dark matter) is mildly favored, as it can lead to higher values of H_0 compatible with local distance ladder measurements.

Despite these promising features, interacting models face theoretical and observational challenges. Degeneracies with other parameters, such as the dark energy equation-of-state or neutrino masses, can weaken constraints. Some forms of interaction may also lead to instabilities in the evolution of cosmological perturbations unless properly regularized. Statistical model comparison using techniques such as the Akaike Information Criterion (AIC) or Bayesian Evidence often suggests that current data do not decisively favor interacting models over ΛCDM, though they may alleviate specific tensions.

Looking ahead, next-generation surveys like Euclid, LSST, the Roman Space Telescope, and CMB-S4 will significantly improve the precision of cosmological measurements. These missions will enable tighter constraints on possible interactions in the dark sector, especially through joint analyses of expansion history and structure growth. If dark matter and dark energy are indeed coupled, the imprint of this interaction may become detectable in the coming decade.

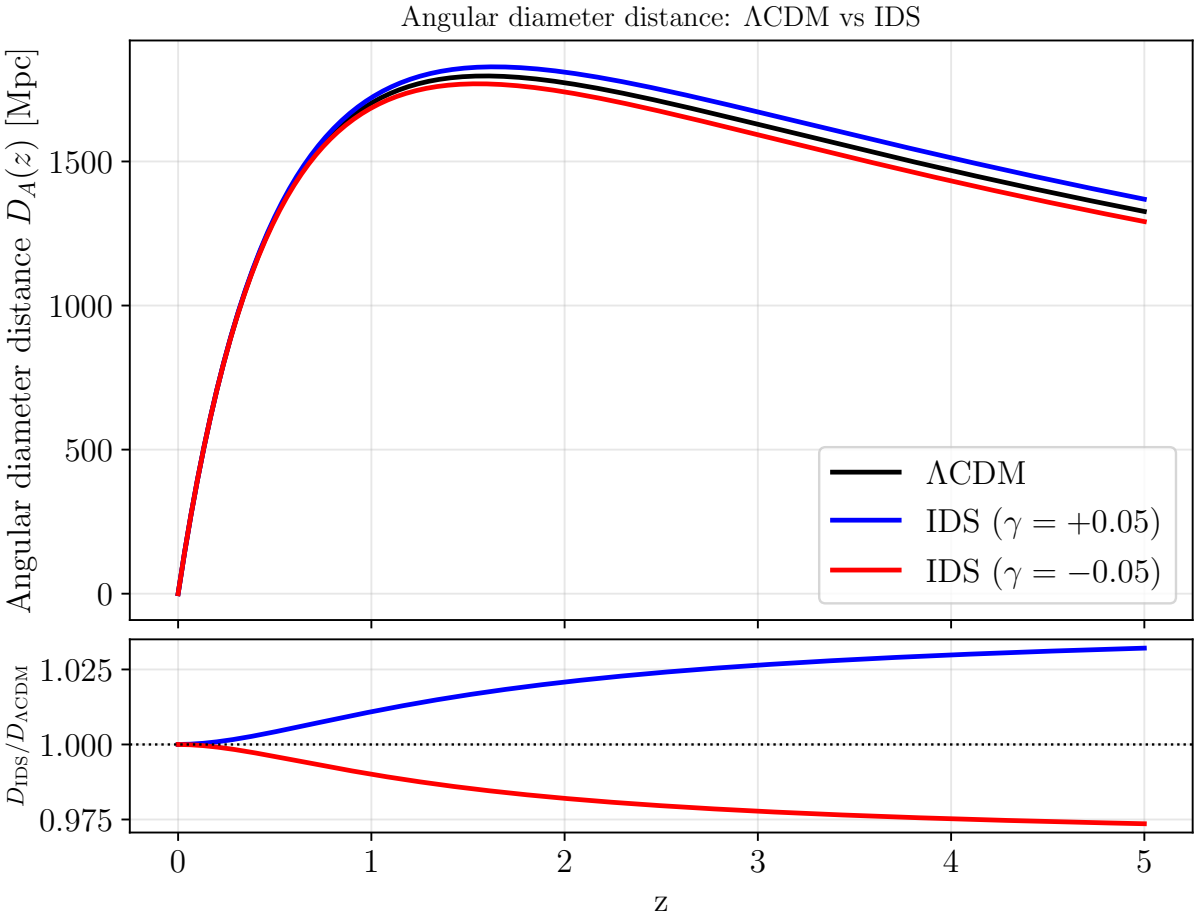

Figure 2.3.: Angular diameter distance $D_A(z)$ as a function of redshift for ΛCDM and interacting dark sector (IDS) models with interaction parameters $\gamma = \pm 0.05$. The upper panel displays the angular diameter distance in each scenario, while the lower panel shows the ratio $D_A^{IDS}/D_A^{\Lambda CDM}$, emphasizing the impact of dark sector interactions on distance measures relevant for observations such as baryon acoustic oscillations and gravitational lensing.

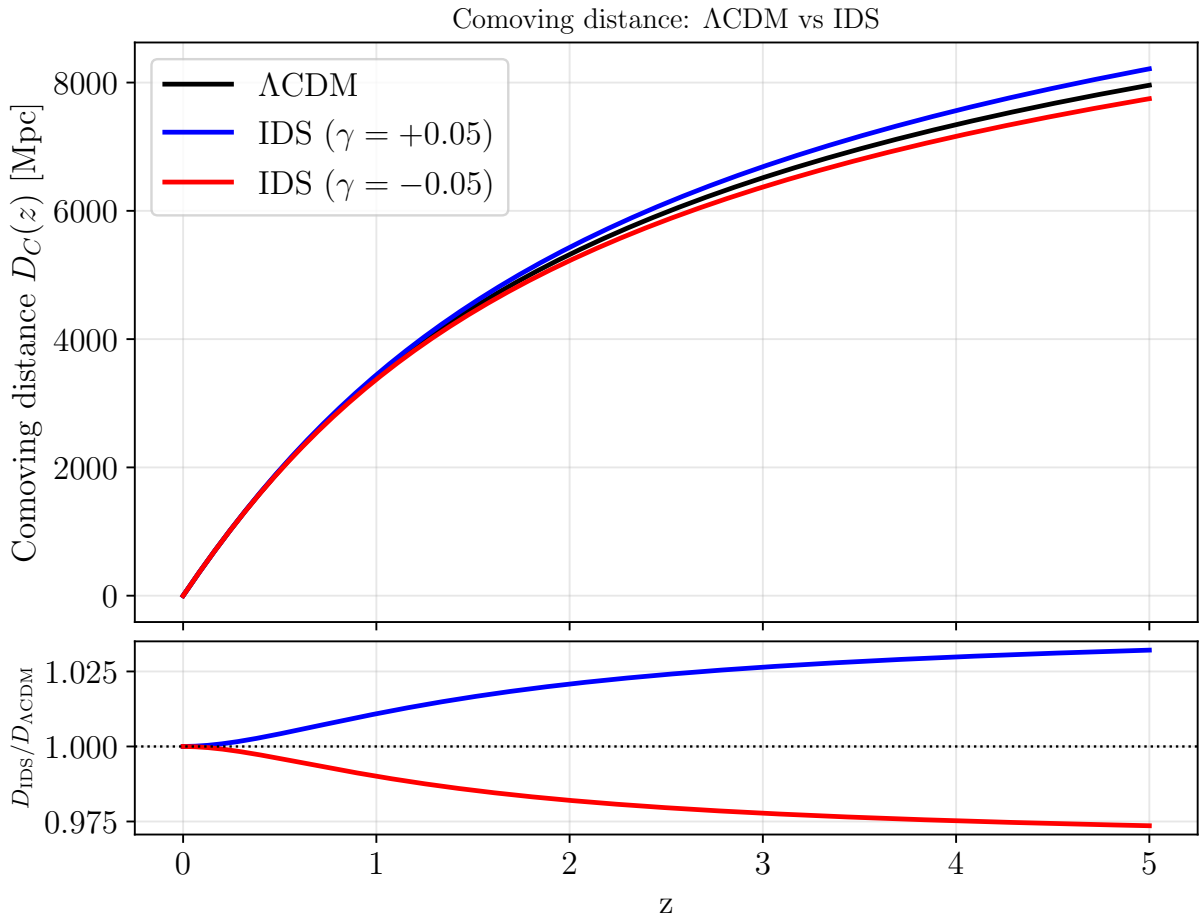

Figure 2.4.: Comoving distance $D_C(z)$ as a function of redshift in the ΛCDM model and in interacting dark sector (IDS) scenarios with $\gamma = \pm 0.05$. The upper panel presents the comoving distance in each model, while the lower panel shows the ratio $D_C^{IDS}/D_C^{\Lambda CDM}$. This representation isolates the effect of the interaction on the background expansion, revealing systematic deviations from the standard cosmological prediction that grow with increasing redshift.

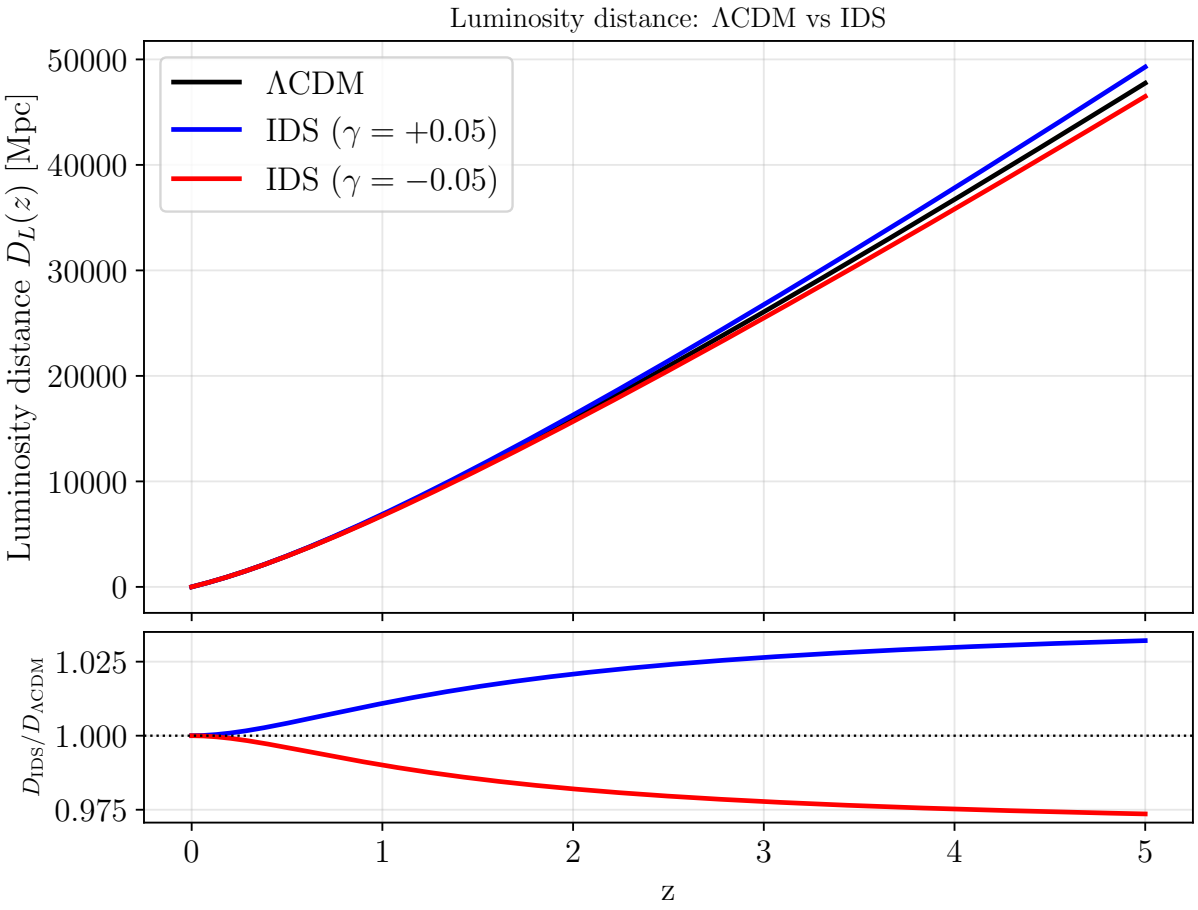

Figure 2.5.: Luminosity distance $D_L(z)$ as a function of redshift for the standard ΛCDM model and for interacting dark sector (IDS) models with interaction parameters $\gamma = \pm 0.05$. The upper panel shows the absolute distances predicted by each cosmological scenario, while the lower panel displays the ratio $D_L^{IDS}/D_L^{\Lambda CDM}$, highlighting the relative deviations induced by the dark sector interaction. The departures from unity increase with redshift, reflecting the cumulative impact of modified expansion histories in the interacting models.

Standard Perturbation Theory

All truths are easy to understand once they are discovered; the point is to discover them.
— G. Galileo.

In order to connect the linear description of cosmological perturbations with the mildly non-linear regime relevant for large-scale structure observations, it is necessary to go beyond first-order perturbation theory. In this context, Standard Perturbation Theory (SPT) provides a systematic framework to study the non-linear evolution of density and velocity perturbations by expanding the fluid equations in powers of the density contrast. Originally developed within the Einstein–de Sitter and later extended to the ΛCDM cosmology, SPT allows one to compute higher-order corrections to observables such as the matter power spectrum and bispectrum. As will be discussed in Sec.5.2, the EdS formulation can be used with sub-percentual deviations for the ΛCDM model, however, in IDS models, the presence of energy–momentum exchange between dark matter and dark energy modifies both the background evolution and the perturbation equations, leading to a non-trivial corrections to the standard SPT kernels.

This section presents the formalism of Standard Perturbation Theory adapted to interacting dark sector models, emphasizing the modifications induced by the dark sector interaction and establishing the framework for the computation of non-linear kernels and loop corrections to the matter power spectrum. In general, the standard ΛCDM limit is recovered by setting $g(a) = 0$, corresponding to the absence of interaction, while the Einstein–de Sitter (EdS) limit is obtained by imposing $\Omega_{\rm m} = 1$.

Revisiting the fluid equations previously derived from the Boltzmann equation(2.19), and substituting the Poisson equation (1.90) into the Euler equation (2.20), we obtain a coupled system governing the evolution of the matter density contrast and the velocity divergence. Explicitly, the continuity and Euler equations can be written as

$$\delta_m' + \theta_m + \mathcal{H} g\, \delta_m = -u_m^i \partial_i \delta_m - \delta_m \theta_m \,, \tag{3.1}$$

$$\theta_m' + \mathcal{H}\theta_m + \frac{3}{2}\mathcal{H}^2 \Omega_m \delta_m = -\left(\partial_i u_m^j\right)\left(\partial_j u_m^i\right) - u_m^i \partial_i \theta_m \,. \tag{3.2}$$

The perturbative approach consists in assuming that both the matter density contrast and the velocity divergence can be expressed as perturbative expansions in powers of the density field. In what follows, we truncate these expansions at third order, such that

$$\begin{aligned} \delta_m &= \delta^{(1)} + \delta^{(2)} + \delta^{(3)} + \dots \,, \\ \theta_m &= \theta^{(1)} + \theta^{(2)} + \theta^{(3)} + \dots \,, \\ u_m^i &= u^{i(1)} + u^{i(2)} + u^{i(3)} + \dots \,. \end{aligned} \tag{3.3}$$

In the following sections, the perturbative framework based on these expansions is developed in detail, and their role in describing the nonlinear evolution of cosmic structures is discussed. This formalism provides a systematic approach to account for mode coupling effects and higher-order corrections, which are essential for an accurate description of structure formation in the mildly nonlinear regime.

3.1. First-order perturbation equations

Retaining only terms up to first order in the perturbative expansion, the continuity and Euler equations simplify to a closed system of linear differential equations for the matter density contrast and the velocity divergence,

$$\begin{aligned} \delta^{(1)\prime} + \theta^{(1)} + \mathcal{H} g\, \delta^{(1)} &= 0\,, \\ \theta^{(1)\prime} + \mathcal{H}\theta^{(1)} + \frac{3}{2}\mathcal{H}^2\Omega_m\delta^{(1)} &= 0\,. \end{aligned} \tag{3.4}$$

These equations describe the linear evolution of matter perturbations in the IDS model and will serve as the foundation for the analysis that follows. To solve this system, the continuity equation is differentiated with respect to conformal time and the Euler equation is used to eliminate the velocity divergence. This procedure leads to a single second-order differential equation governing the linear evolution of the matter density contrast,

$$\delta^{(1)\prime\prime} + [\mathcal{H}(1+g)]\ \delta^{(1)\prime} + \left[\mathcal{H}^2 g + (\mathcal{H}g)' - \frac{3}{2}\,\mathcal{H}^2\,\Omega_m\right]\ \delta^{(1)} = 0\,. \tag{3.5}$$

In the absence of the interaction term ($g = 0$), the above equation reduces to the standard linear growth equation governing the evolution of matter perturbations in the ΛCDM model,

$$\delta^{(1)\prime\prime} + \mathcal{H}\,\delta^{(1)\prime} - \tfrac{3}{2}\,\mathcal{H}^2\,\Omega_m\,\delta^{(1)} = 0\,. \tag{3.6}$$

This equation describes the ΛCDM linear evolution of density perturbations written in conformal time and provides the reference case against which the effects of dark sector interactions are assessed. As it is well-known, the general solution of Eq. (3.6) can be expressed as a linear superposition of two independent modes,

$$\delta^{(1)}(\tau,\vec{x}) = A(\vec{x})\,D_+(\tau) + B(\vec{x})\,D_-(\tau)\,, \tag{3.7}$$

where $D_+(\tau)$ and $D_-(\tau)$ denote the growing and decaying mode functions, respectively. The spatially dependent coefficients $A(\vec{x})$ and $B(\vec{x})$ are determined by the initial conditions and encode the spatial shape of each mode. The velocity divergence immediately follows from the ΛCDM limit of Eq. (3.4),

$$\theta^{(1)}(\tau,\vec{x}) = -\delta^{(1)\prime}(\tau,\vec{x}) = -A(\vec{x})\,D_+'(\tau) - B(\vec{x})\,D_-'(\tau). \tag{3.8}$$

Under the assumptions of an Einstein-de Sitter (EdS) universe, where the background is matter dominated, the linear growth equation (3.6) admits simple power-law solutions. Written in terms of the scale factor a, the two independent modes are $D_+(a) \propto a$, corresponding to the growing mode, and $D_-(a) \propto a^{-3/2}$, corresponding to the decaying mode. The linear density contrast therefore takes the form

$$\delta^{(1)}(a,\vec{x}) = A(\vec{x})\,a + B(\vec{x})\,a^{-3/2} \quad \text{(EdS)} \tag{3.9}$$

Although this case will not be explored further here, it is worth mentioning that for a general ΛCDM background the growing mode does not admit a simple closed-form expression. Instead, it can be written in terms of a well-known integral representation, normalized such that $D_+(a) \to a$ at matter-dominatted times,

$$D_+(a) \;=\; \frac{5}{2} H_0^2 \Omega_{\rm m}\, H(a) \int_{a_{\rm ini}}^{a} \frac{da'}{a'^3 H^3(a')}\,. \tag{3.10}$$

The second independent solution of the linear growth equation, corresponding to the decaying mode, can be constructed using the standard reduction-of-order method once the growing mode D_+ is known. In practical applications, however, initial conditions are typically chosen so as to isolate the pure growing mode, which is the physically relevant solution for large-scale structure formation. This amounts to setting $B(\vec{x}) = 0$, in which case the linear density contrast and velocity divergence reduce to

$$\delta^{(1)}(\vec{x},\tau) = D_+(\tau)\,\delta_0(\vec{x}) \qquad \text{and} \qquad \theta^{(1)}(\tau,\vec{x}) = -D'_+(\tau)\,\delta_0(\vec{x})\,, \tag{3.11}$$

where, for convenience, the general function $A(\vec{x})$ is now denoted by $\delta_0(\vec{x})$. As the function $\delta^{(1)}(\vec{x},\tau)$ represents the linear-order matter density contrast, the growing mode D_+ determines how primordial perturbations are amplified by gravitational instability and therefore governs the formation of cosmic structures, while the decaying mode D_- rapidly becomes negligible for typical initial conditions and is usually discarded.

Since Eqs. (3.5) and (3.6) share the same mathematical structure, it is natural to assume that the variable separation introduced in Eq. (3.11) remains valid in interacting dark sector (IDS) models. This assumption is well motivated, as the interaction only introduces additional time-dependent contributions to the coefficients of the evolution equation, without altering its overall form. Under this hypothesis, Eq. (3.5) can be rewritten for the growing mode in an IDS scenario as,

$$D''_+ + [\mathcal{H}(1+g)]\; D'_+ + \left[\mathcal{H}^2 g + (\mathcal{H}g)' - \frac{3}{2}\mathcal{H}^2\,\Omega_m\right]\; D_+ = 0\,. \tag{3.12}$$

Equivalently, using the scale factor as the time variable, the growth equation can be expressed as,

$$\ddot{D}^{(1)}_+ + \dot{D}^{(1)}_+ \left(\frac{3}{a} + \frac{\dot{H}}{H} + \frac{g}{a}\right) + D^{(1)}_+ \left(\frac{\dot{g}}{a} + \frac{2g}{a^2} + \frac{g\dot{H}}{aH} - \frac{3\Omega_m}{2a^2}\right) = 0\,. \tag{3.13}$$

Another closely related quantity is the linear growth rate f, which measures how rapidly matter density perturbations evolve as the Universe expands. This function plays a central role in cosmology, as it directly connects the growth of structure to the underlying theory of gravity and the background expansion history. The growth rate is defined as,

$$f \equiv \frac{d\ln D_+}{d\ln a} = \frac{1}{D_+\mathcal{H}}\frac{dD_+}{d\tau} = \frac{\delta'^{(1)}}{\mathcal{H}\delta^{(1)}} \tag{3.14}$$

where the last equality follows from the assumption that the linear density contrast evolves proportionally to the growing mode.

Physically, the growth rate quantifies the response of the matter distribution to gravitational instability: larger values of f correspond to a more efficient growth of overdensities, while smaller

values indicate a suppression of structure formation, for instance due to dark energy domination or interactions in the dark sector. Observationally, f is tightly connected to the peculiar velocities of galaxies, which distort clustering measurements in redshift space. These redshift-space distortions arise because galaxy velocities along the line of sight add to the Hubble flow, leading to anisotropies in the observed power spectrum or correlation function. As a consequence, measurements of redshift-space distortions provide direct constraints on the product $f\sigma_8$, making the growth rate a powerful probe of both the dynamics of structure formation and the underlying cosmological model.

With this definition, the linear velocity divergence can be written as

$$\theta^{(1)}(\vec{x},\tau) = -\mathcal{H}\,(f+g)\,D_+(\tau)\delta(\vec{x}) \tag{3.15}$$

This expression highlights an important difference with respect to the standard ΛCDM case. In the presence of an interaction in the dark sector, the linear velocity divergence is no longer determined solely by the logarithmic growth rate f, but receives an additional contribution proportional to the coupling function g. As a result, the peculiar velocity field responds not only to the growth of matter perturbations but also to the explicit energy exchange between dark matter and dark energy. The standard ΛCDM limit is recovered by setting $g = 0$, in which case Eq. (3.15) reduces to the familiar relation,

$$\theta^{(1)}_{\Lambda CDM}(\vec{x},\tau) = -\mathcal{H}fD_+(\tau)\delta(\vec{x})\,, \tag{3.16}$$

which is widely used in linear perturbation theory and in the analysis of redshift-space distortions.

This modification has important implications for the usual Einstein–de Sitter (EdS) approximation commonly employed in standard perturbation theory[1]. In the ΛCDM framework, it is often assumed that the combination Ω_m/f^2 is approximately unity, reflecting the fact that $f \approx \Omega_m^{0.55}$ in the matter-dominated regime. This approximation underlies the time independence of the EdS perturbative kernels and greatly simplifies the nonlinear analysis. In interacting dark sector models, however, the appearance of the additional coupling term g alters the relation between the growth rate and the matter density parameter. For this reason, it is convenient to introduce the effective growth rate,

$$f_Q \equiv f + g\,, \tag{3.17}$$

which leads to

$$\theta^{(1)}(\vec{x},\tau) = -\mathcal{H}f_QD_+(\tau)\delta(\vec{x})\,. \tag{3.18}$$

The Eq. (3.18) naturally governs the evolution of the velocity divergence in interacting dark sector scenarios. This quantity plays a central role in the perturbative analysis developed in the following sections, replacing the standard growth rate in the construction of nonlinear kernels and highlighting the impact of dark sector interactions on structure formation.

In cosmology, it is often convenient to express the perturbation equations in Fourier space. At linear order, this representation greatly simplifies the analysis, since different Fourier modes evolve independently and the dynamics reduces to a set of ordinary differential equations in time for each wavenumber. By transforming the continuity and Euler equations into momentum space, one obtains evolution equations for the Fourier components of the density contrast and velocity divergence, in which spatial derivatives become simple algebraic factors. This formulation not only provides a clearer physical interpretation of the growth of cosmic structures but also establishes a direct connection with observable quantities, such as the matter power spectrum.

[1] See Sec. 3.6

Moreover, the Fourier-space description is essential beyond linear order, where nonlinearities introduce mode coupling through convolution integrals, making momentum space the natural framework for the development of perturbation theory.

To derive the first-order equations in Fourier space, it is convenient to start from their real-space counterparts, given in Eqs. (3.4). Entering Fourier space amounts to expanding the density contrast and the velocity divergence in terms of their Fourier modes and substituting these expansions into the real-space evolution equations. Adopting standard Fourier transform conventions, the first-order continuity and Euler equations can be written as

$$\int \frac{d^3k}{(2\pi)^3} e^{i\vec{k}\cdot\vec{x}} \left[\delta_k^{(1)\prime} + \theta_k^{(1)} + \mathcal{H}g\,\delta_k^{(1)}\right] = 0 \tag{3.19}$$

$$\int \frac{d^3k}{(2\pi)^3} e^{i\vec{k}\cdot\vec{x}} \left[\theta_k^{(1)\prime} + \mathcal{H}\theta_k^{(1)} + \frac{3}{2}\mathcal{H}^2\Omega_m\delta_{k_1}^{(1)}\right] = 0 \tag{3.20}$$

At linear order, these expressions make explicit that the Fourier-space equations retain the same structure as their real-space counterparts for each individual mode, with no spatial derivatives or convolution integrals appearing. Consequently, different Fourier modes evolve independently and the dynamics reduces to a set of ordinary differential equations in time for each wavenumber k. The Fourier transformations are written out explicitly here for clarity, as this notation will become essential at higher orders, where nonlinear terms introduce mode coupling through convolution integrals in momentum space. Thus, in the Fourier space, each mode satisfy,

$$\delta_k^{(1)\prime} + \theta_k^{(1)} + \mathcal{H}g\,\delta_k^{(1)} = 0 \tag{3.21}$$

$$\theta_k^{(1)\prime} + \mathcal{H}\theta_k^{(1)} + \frac{3}{2}\mathcal{H}^2\Omega_m\delta_{k_1}^{(1)} = 0 \tag{3.22}$$

Analogously to the real-space case, the first-order solutions for the matter density contrast and the velocity divergence can be written in Fourier space in a separable form, where the time dependence is fully captured by the linear growth function. Explicitly, one finds

$$\delta_k^{(1)} = D_+(\tau)\,\delta_0(\vec{k})\,, \qquad \theta_k^{(1)} = -\mathcal{H}f_Q D_+(\tau)\,\delta_0(\vec{k})\,. \tag{3.23}$$

The impact of the interaction in the in the growing factor D_+ and in the growth rate f is shown in Fig. 3.1 and Fig. 3.2.

Although the background expansion and the linear growth of density perturbations in interacting dark sector models can be consistently characterized at the level presented in this work, a detailed and systematic analysis of redshift-space distortion (RSD) effects remains an open problem. In particular, the mapping between the real-space matter distribution and the observed galaxy clustering in redshift space is expected to be modified by the interaction, through changes in both the growth rate of structures and the velocity field of matter. Since RSD observables are directly sensitive to the combination of the growth rate and peculiar velocities, a proper treatment of these effects in interacting models requires a careful reformulation of the standard RSD framework.

This issue is especially relevant for models with negative interaction strength, such as the case $B = -0.05$, where the effective growth rate exhibits significant deviations from the ΛCDM prediction. In such scenarios, the additional interaction-induced contribution to the growth rate may lead to nontrivial modifications the nonlinear velocity corrections, potentially impacting the interpretation of current and forthcoming large-scale structure measurements.

A comprehensive and self-consistent study of redshift-space distortions in interacting dark sector models, including both linear and nonlinear regimes, is therefore left for future work. Such

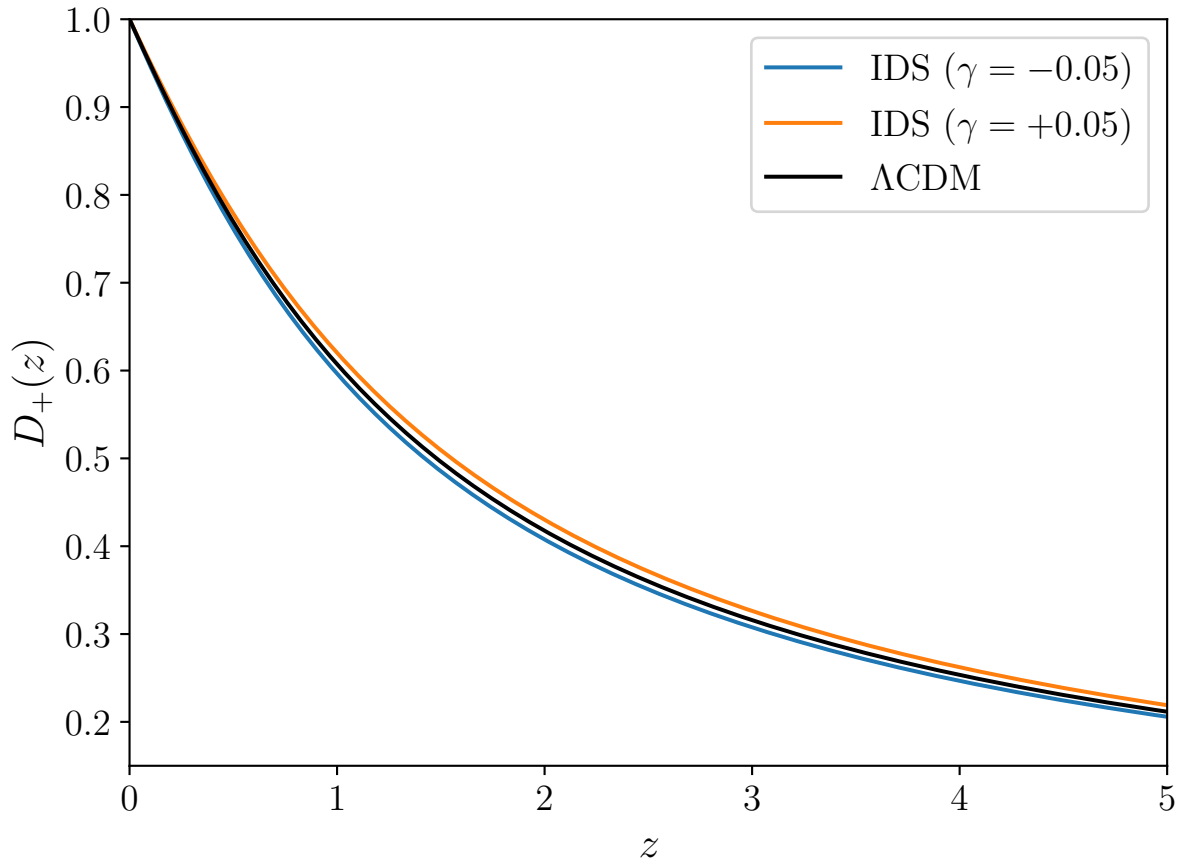

Figure 3.1.: Linear growth factor $D_+(z)$ as a function of redshift for the standard ΛCDM model and for interacting dark sector (IDS) scenarios with interaction parameters $B = \pm 0.05$. The growth factor is normalized to unity at $z = 0$. Deviations from the ΛCDM prediction reflect the impact of dark sector interactions on the growth of matter density perturbations, with positive and negative interaction strengths leading to systematically enhanced or suppressed growth histories relative to the standard cosmological model.

an analysis constitutes one of the main objectives of the continuation of the present research and will be essential for confronting these models with precision galaxy clustering data from upcoming surveys.

3.2. Second-order perturbation equations

Extending the perturbative expansion to second order allows the derivation of evolution equations for the second-order density contrast $\delta^{(2)}$ and velocity divergence $\theta^{(2)}$. These equations are obtained by inserting the first-order solutions into the nonlinear terms of the continuity and Euler equations and retaining all contributions that are quadratic in the linear perturbations. For notational convenience, partial derivatives are denoted by a comma, $,_i \equiv \partial_i$. The resulting

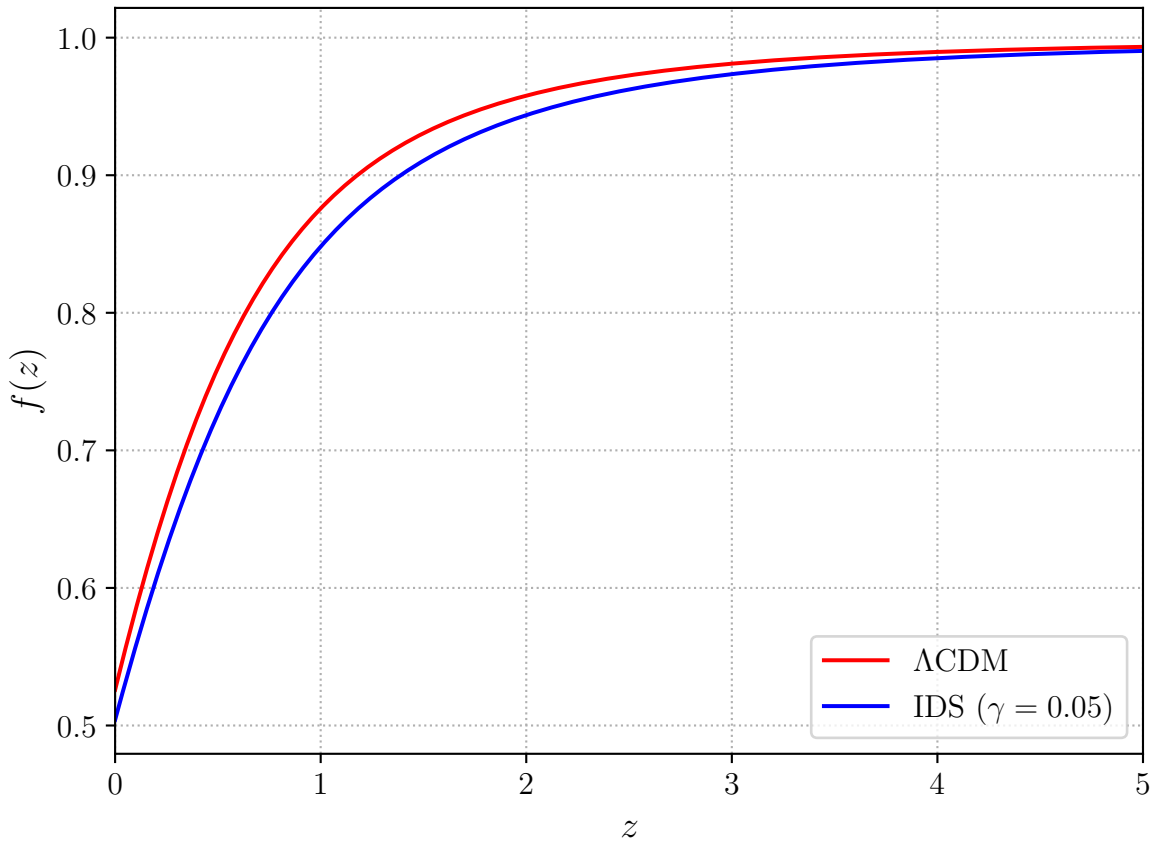

Figure 3.2.: Evolution of the linear growth rate $f(z)$ as a function of redshift z for the standard ΛCDM model (red curve) and for the Interacting Dark Sector (IDS) model with interaction parameter $B = 0.05$ (blue curve). The presence of dark sector interactions modifies the growth rate of cosmic structures relative to the ΛCDM prediction, with deviations becoming more pronounced at low redshifts. The case $B = -0.05$ is not displayed, as significant distortions arise in redshift space for this parameter choice. These effects are currently under detailed investigation and will be analyzed in future work.

second-order equations can be written as

$$\delta^{(2)\prime} + \theta^{(2)} + \mathcal{H}g\,\delta^{(2)} = -u^{i(1)}\delta^{(1)}_{,i} - \delta^{(1)}\theta^{(1)} \tag{3.24}$$

$$\theta^{(2)\prime} + \mathcal{H}\theta^{(2)} + \frac{3}{2}\mathcal{H}^2\Omega_m\delta^{(2)} = -u^{j(1)}_{,i}\,u^{i(1)}_{,j} - u^{i(1)}\theta^{(1)}_{,i} \tag{3.25}$$

For pedagogical clarity, it is useful to rewrite these equations explicitly in real space, making the spatial-derivative operators ∇ and ∇^{-1} manifest. In this formulation, the inverse-gradient operator ∇^{-1} is introduced to express the velocity field $\vec{u}$ in terms of its divergence θ, while the gradient operator ∇ accounts for the spatial derivatives acting on the perturbations. A detailed discussion of the Fourier-space representation and physical interpretation of these operators is provided in Appendix A. This representation makes the structure of the nonlinear couplings between density and velocity perturbations transparent,

$$\delta^{(2)\prime} + \theta^{(2)} + \mathcal{H}g\,\delta^{(2)} = -(\nabla^{-1})^i\theta^{(1)}\nabla_i\delta^{(1)} - \delta^{(1)}\theta^{(1)} \tag{3.26}$$

$$\theta^{(2)\prime} + \mathcal{H}\theta^{(2)} + \frac{3}{2}\mathcal{H}^2\Omega_m\delta^{(2)} = -\nabla_i(\nabla^{-1})^j\theta^{(1)}\nabla_j(\nabla^{-1})^i\theta^{(1)} - (\nabla^{-1})^i\theta^{(1)}\nabla_i\theta^{(1)} \tag{3.27}$$

With these expressions at hand, the equations can now be transformed to Fourier space by expanding the perturbation fields into their Fourier modes and applying the Fourier transform to each term in the real-space equations. In contrast to the linear case, the quadratic nonlinearities present at second order give rise to products of fields evaluated at the same spatial point, which translate into convolution integrals in momentum space. As a result, different Fourier modes become coupled, and the evolution of a given mode depends on pairs of modes with wavevectors $\vec{k}_1$ and $\vec{k}_2$. Carrying out this procedure, the second-order continuity and Euler equations can be written in momentum space as

$$\int \frac{d^3k}{(2\pi)^3} e^{i\vec{k}\cdot\vec{x}} \left[\delta^{(2)\prime}_k + \theta^{(2)}_k + \mathcal{H}g\,\delta^{(2)}_k\right] = \mathcal{H}f_Q D_+^2 \int \frac{d^3k_1}{(2\pi)^3}\int \frac{d^3k_2}{(2\pi)^3} e^{i(\vec{k}_1+\vec{k}_2)\cdot\vec{x}} \times \alpha(\vec{k}_1,\vec{k}_2)\delta_0(\vec{k}_1)\delta_0(\vec{k}_2)\,, \tag{3.28}$$

$$\int \frac{d^3k}{(2\pi)^3} e^{i\vec{k}\cdot\vec{x}} \left[\theta^{(2)\prime}_k + \mathcal{H}\theta^{(2)}_k + \frac{3}{2}\mathcal{H}^2\Omega_m\delta^{(2)}_k\right] = -\mathcal{H}^2 f_Q^2 D_+^2 \int \frac{d^3k_1}{(2\pi)^3}\int \frac{d^3k_2}{(2\pi)^3} e^{i(\vec{k}_1+\vec{k}_2)\cdot\vec{x}} \times \beta(\vec{k}_1,\vec{k}_2)\delta_0(\vec{k}_1)\delta_0(\vec{k}_2)\,, \tag{3.29}$$

where the functions $\alpha(\vec{k}_1,\vec{k}_2)$ and $\beta(\vec{k}_1,\vec{k}_2)$ are the standard mode-coupling kernels arising from the nonlinear terms in the continuity and Euler equations, respectively,

$$\begin{aligned}\alpha(\vec{k}_1,\vec{k}_2) &= (\nabla^{-1})^i(\vec{k}_1)\nabla_i(\vec{k}_2) + 1 \\ \beta(\vec{k}_1,\vec{k}_2) &= \nabla_i(\vec{k}_1)(\nabla^{-1})^j(\vec{k}_1)\nabla_j(\vec{k}_2)(\nabla^{-1})^i(\vec{k}_2) + (\nabla^{-1})^i(\vec{k}_1)\nabla_i(\vec{k}_2)\end{aligned} \tag{3.30}$$

Using the definition of ∇_i and $(\nabla^{-1})^i$ in the Fourier Space as explained in Appendix A. We obtain that,

$$\begin{aligned}\alpha(\vec{k}_1,\vec{k}_2) &= -\frac{ik_1^i}{k_1^2}ik_{2i} + 1 \\ \beta(\vec{k}_1,\vec{k}_2) &= ik_{1i}\left[-\frac{ik_1^j}{k_1^2}\right]ik_{2j}\left[-\frac{ik_2^i}{k_2^2}\right] + \left[-\frac{ik_1^i}{k_1^2}\right]ik_{2i}\end{aligned} \tag{3.31}$$

Finally,

$$\begin{aligned}\alpha(\vec{k}_1,\vec{k}_2) &= 1+\frac{\vec{k}_1\cdot\vec{k}_2}{k_1^2}\\ \beta(\vec{k}_1,\vec{k}_2) &= \frac{\vec{k}_1\cdot\vec{k}_2}{k_1^2}+\frac{(\vec{k}_1\cdot\vec{k}_2)^2}{k_1^2k_2^2}\end{aligned} \tag{3.32}$$

These kernels encode the geometric dependence of the nonlinear interactions between different Fourier modes, describing how perturbations with wavevectors $\vec{k}_1$ and $\vec{k}_2$ combine to source a mode with wavevector $\vec{k}=\vec{k}_1+\vec{k}_2$. The explicit dependence on scalar products of the wavevectors emphasizes the role played by their relative orientation in determining the strength of mode coupling, which is a central aspect of nonlinear structure formation. Importantly, these kernels are purely kinematic in origin and are therefore identical to those obtained in the standard ΛCDM framework, which means that the effects of the interacting dark sector enter exclusively through the time-dependent coefficients that multiply these kernels, leaving their momentum dependence unchanged.

At this point, one must recalling the identity,

$$e^{i(\vec{k_1}+\vec{k_2})\cdot\vec{x}}=\int d^3k\, e^{i\vec{k}\cdot\vec{x}}\delta_D(\vec{k}-\vec{k}_1-\vec{k}_2)\,. \tag{3.33}$$

It is convenient to introduce the Dirac delta distribution in order to make explicit the relation between the wavevector $\vec{k}$ appearing on the left-hand side and the pair of wavevectors $\vec{k}_1$ and $\vec{k}_2$ that source it through nonlinear mode coupling. This representation enforces momentum conservation in Fourier space and allows the convolution structure of the second-order equations to be written in a compact form. As a result, the second-order continuity and Euler equations for the IDS model can be expressed as

$$\begin{aligned}\delta_k^{(2)\prime}+\theta_k^{(2)}+\mathcal{H}g\,\delta_k^{(2)} = \mathcal{H}f_Q D_+^2\int\frac{d^3k_1}{(2\pi)^3}\int\frac{d^3k_2}{(2\pi)^3}(2\pi)^3\delta_D(\vec{k}-\vec{k}_1-\vec{k}_2)\\ \times\,\alpha(k_1,k_2)\delta_0(\vec{k}_1)\delta_0(\vec{k}_2)\,,\end{aligned} \tag{3.34}$$

$$\begin{aligned}\theta_k^{(2)\prime}+\mathcal{H}\theta_k^{(2)}+\frac{3}{2}\mathcal{H}^2\Omega_m\delta_k^{(2)} = -\mathcal{H}^2f_Q^2D_+^2\int\frac{d^3k_1}{(2\pi)^3}\int\frac{d^3k_2}{(2\pi)^3}(2\pi)^3\delta_D(\vec{k}-\vec{k}_1-\vec{k}_2)\\ \times\,\beta(k_1,k_2)\delta_0(\vec{k}_1)\delta_0(\vec{k}_2)\,,\end{aligned} \tag{3.35}$$

Here, it is convenient to identify the right-hand side terms in Eqs. (3.34) and (3.35) as source terms $S_\delta(\vec{k})$ and $S_\theta(\vec{k})$, which encapsulate the nonlinear mode-coupling contributions appearing in the second-order equations. These terms arise from convolution integrals over products of first-order perturbations and encode the quadratic interactions between Fourier modes. In particular, they describe how pairs of modes with wavevectors $\vec{k}_1$ and $\vec{k}_2$ combine to source a mode with wavevector $\vec{k}=\vec{k}_1+\vec{k}_2$, as enforced by the Dirac delta function. Explicitly, the source terms are given by

$$S_\delta(\vec{k}) = \int\frac{d^3k_1}{(2\pi)^3}\int\frac{d^3k_2}{(2\pi)^3}(2\pi)^3\delta_D(\vec{k}-\vec{k}_1-\vec{k}_2)\alpha(\vec{k}_1,\vec{k}_2)\delta_0(\vec{k}_1)\delta_0(\vec{k}_2)\,, \tag{3.36}$$

$$S_\theta(\vec{k}) = -\int\frac{d^3k_1}{(2\pi)^3}\int\frac{d^3k_2}{(2\pi)^3}(2\pi)^3\delta_D(\vec{k}-\vec{k}_1-\vec{k}_2)\beta(\vec{k}_1,\vec{k}_2)\delta_0(\vec{k}_1)\delta_0(\vec{k}_2)\,. \tag{3.37}$$

With these definitions, the system of equations given in Eqs. (3.34) and (3.35) can be written in a compact form. The second-order continuity and Euler equations then reduce to

$$\delta_k^{(2)\prime} + \theta_k^{(2)} + \mathcal{H}g\,\delta_k^{(2)} = \mathcal{H}f_Q D_+^2 S_\delta \tag{3.38}$$

$$\theta_k^{(2)\prime} + \mathcal{H}\theta_k^{(2)} + \frac{3}{2}\mathcal{H}^2\Omega_m\delta_k^{(2)} = \mathcal{H}^2 f_Q^2 D_+^2 S_\theta \tag{3.39}$$

At this point, another key conceptual element of this Master's thesis is introduced. The second-order contributions to the density contrast and velocity divergence are written in the form

$$\delta_k^{(2)} = D_+^2(\tau)\,A_\delta(\vec{k}_1,\vec{k}_2,\tau)\,, \qquad \theta_k^{(2)} = -\mathcal{H}f_Q D_+^2(\tau)\,B_\theta(\vec{k}_1,\vec{k}_2,\tau)\,, \tag{3.40}$$

where $\delta_k^{(2)}$ and $\theta_k^{(2)}$ denote the second-order density and velocity perturbations, respectively. This parametrization separates the dominant time dependence, governed by the square of the linear growth function, from the remaining scale- and time-dependent structure encoded in A_δ and B_θ.

In the standard ΛCDM literature, these functions are typically assumed to depend only on the wavevectors, with no explicit time dependence. This assumption is strictly valid only in the Einstein–de Sitter (EdS) limit, where the perturbative kernels are time independent. In practice, however, ΛCDM is known to be well approximated by the EdS case over a wide range of redshifts, which explains the success of this simplification in many applications. As will be seen, a central result of this thesis is to demonstrate that this approximation breaks down in IDS models. In such scenarios, the EdS limit fails to capture the correct nonlinear dynamics, and the time dependence of A_δ and B_θ becomes non-negligible. Retaining this time dependence is therefore essential for an accurate perturbative description of structure formation in the presence of dark sector interactions.

In order to express both the second-order density contrast and the velocity divergence in a unified convolutional form, it is convenient to introduce the second-order perturbative kernels. With this definition, the second-order solutions can be written as,

$$\delta_k^{(2)} = D_+^2(\tau)\int\frac{d^3k_1}{(2\pi)^3}\int\frac{d^3k_2}{(2\pi)^3}(2\pi)^3\delta_D(\vec{k}-\vec{k}_1-\vec{k}_2)\,F_2(\vec{k}_1,\vec{k}_2,\tau)\,\delta_0(\vec{k}_1)\,\delta_0(\vec{k}_2)\,, \tag{3.41}$$

$$\theta_k^{(2)} = -\mathcal{H}f_Q D_+^2(\tau)\int\frac{d^3k_1}{(2\pi)^3}\int\frac{d^3k_2}{(2\pi)^3}(2\pi)^3\delta_D(\vec{k}-\vec{k}_1-\vec{k}_2)\,G_2(\vec{k}_1,\vec{k}_2,\tau)\,\delta_0(\vec{k}_1)\,\delta_0(\vec{k}_2)\,, \tag{3.42}$$

where F_2 and G_2 are the time-varying second-order kernels.

Writing the second-order perturbations in terms of kernel functions provides a convenient description of the nonlinear dynamics. In this formulation, all mode-coupling effects are absorbed into the kernels, while the convolution integrals explicitly show how pairs of linear modes combine to generate second-order perturbations. From a practical perspective, this separation is particularly advantageous, as it allows the evolution of the kernels to be computed directly, avoiding the need to repeatedly evaluate the full convolution integrals appearing in the perturbation equations.

By comparing Eq. (3.40) with Eqs. (3.41) and (3.42), the functions A_δ and B_θ can be expressed explicitly in terms of the second-order perturbative kernels,

$$A_\delta(\vec{k},\tau) = \int\frac{d^3k_1}{(2\pi)^3}\int\frac{d^3k_2}{(2\pi)^3}(2\pi)^3\delta_D(\vec{k}-\vec{k}_1-\vec{k}_2)\,F_2(\vec{k}_1,\vec{k}_2,\tau)\,\delta_0(\vec{k}_1)\,\delta_0(\vec{k}_2)\,, \tag{3.43}$$

$$B_\theta(\vec{k},\tau) = \int\frac{d^3k_1}{(2\pi)^3}\int\frac{d^3k_2}{(2\pi)^3}(2\pi)^3\delta_D(\vec{k}-\vec{k}_1-\vec{k}_2)\,G_2(\vec{k}_1,\vec{k}_2,\tau)\,\delta_0(\vec{k}_1)\,\delta_0(\vec{k}_2)\,. \tag{3.44}$$

Substituting the kernel-based expressions for the second-order density contrast and velocity divergence into the fluid equations leads to a closed, coupled system of ordinary differential equations for the functions A_δ and B_θ. In this formulation, all nonlinear interactions between Fourier modes are captured by the source terms S_δ and S_θ, which act as driving terms for the evolution of the kernels,

$$\frac{A'_\delta}{\mathcal{H} f_Q} + \left[\frac{2f+g}{f_Q}\right] A_\delta - B_\theta = S_\delta \,, \tag{3.45}$$

$$-\frac{B'_\theta}{\mathcal{H} f_Q} - \left[\frac{3}{2}\frac{\Omega_m}{f_Q^2} + \frac{f}{f_Q}\right] B_\theta + \frac{3}{2}\frac{\Omega_m}{f_Q^2} A_\delta = S_\theta \,. \tag{3.46}$$

It is important to emphasize that, if one wishes to switch off the interaction, this can be achieved by taking the limit $g \to 0$, in which case f_Q consistently reduces to the standard growth rate f.

In Fig. 3.4, we present the deviation with respect to the ΛCDM behavior for each term appearing in the coupled evolution equation. This constitutes one of the main theoretical results of this dissertation, as it demonstrates that the time dependence becomes significantly modified in models with interaction in the dark sector.

As a consequence, the functions A_δ and B_θ can be identified with the second-order perturbative kernels, and their evolution is governed by a closed system of differential equations. This leads directly to the following coupled equations for the second-order kernels F_2 and G_2 in interacting dark sector models,

$$\frac{F'_2}{\mathcal{H} f_Q} + \left[\frac{2f+g}{f_Q}\right] F_2 - G_2 = \alpha \,, \tag{3.47}$$

$$-\frac{G'_2}{\mathcal{H} f_Q} - \left[\frac{3}{2}\frac{\Omega_m}{f_Q^2} + \frac{f}{f_Q}\right] G_2 + \frac{3}{2}\frac{\Omega_m}{f_Q^2} F_2 = -\beta \,. \tag{3.48}$$

The structure of Eqs. (3.47) and (3.48) makes explicit that, in IDS models, the second-order kernels F_2 and G_2 must in general be time dependent. Unlike the standard Einstein–de Sitter case, where the coefficients of the kernel equations are constant and the kernels admit time-independent solutions, the presence of explicitly time-dependent coefficients in the IDS scenario prevents such a simplification. In particular, the evolution of the kernels is driven not only by the usual growth rate f and the matter density parameter Ω_m, but also by the coupling function g, which introduces additional time dependence through both friction and source terms. As a result, the temporal evolution of F_2 and G_2 becomes sensitive to the specific form of the dark sector interaction, implying that their behavior is strongly model dependent. This enhanced time dependence reflects the fact that, in IDS models, nonlinear mode coupling is directly influenced by the interaction between dark matter and dark energy, and can not be accurately captured by time-independent kernels or by the standard EdS approximation. The ΛCDM limit and the EdS approximation will be discussed in Sec. 3.5 and Sec. 3.6

It is also important to note that the mode-coupling functions $\alpha(\vec{k}_1, \vec{k}_2)$ and $\beta(\vec{k}_1, \vec{k}_2)$ are not symmetric under the exchange $\vec{k}_1 \leftrightarrow \vec{k}_2$. As a consequence, the kernels F_2 and G_2 obtained from the evolution equations do not, in general, possess the correct permutation symmetry required by the convolution integrals appearing in the second-order solutions. To ensure that the resulting expressions are invariant under the interchange of the two wavevectors, it is therefore convenient

to introduce symmetrized versions of the kernels. These are defined as,

$$F_2^{(\mathrm{s})}(\vec{k}_1,\vec{k}_2,\tau) = \tfrac{1}{2}\left[F_2(\vec{k}_1,\vec{k}_2,\tau) + F_2(\vec{k}_2,\vec{k}_1,\tau)\right] \tag{3.49}$$

and

$$G_2^{(\mathrm{s})}(\vec{k}_1,\vec{k}_2,\tau) = \tfrac{1}{2}\left[G_2(\vec{k}_1,\vec{k}_2,\tau) + G_2(\vec{k}_2,\vec{k}_1,\tau)\right] . \tag{3.50}$$

From this point onward, the superscript (s) will be omitted for simplicity, with the understanding that all kernels are implicitly symmetrized unless stated otherwise.

3.3. Third-order perturbation equations

Following the same strategy adopted in the second-order analysis, the perturbative expansion can be extended to third order in order to describe higher-order nonlinear corrections to the evolution of matter perturbations. At this order, the density contrast $\delta^{(3)}$ and the velocity divergence $\theta^{(3)}$ are sourced by products involving first- and second-order perturbations, reflecting the hierarchical structure of Standard Perturbation Theory.

The third-order evolution equations are obtained by substituting the first- and second-order solutions into the nonlinear terms of the continuity and Euler equations and retaining all contributions that are cubic in the perturbations. As before, primes denote derivatives with respect to conformal time. The resulting equations read,

$$\delta^{(3)\prime} + \theta^{(3)} + \mathcal{H}g\,\delta^{(3)} = -(u^{i(1)}\delta^{(2)}_{,i} + u^{i(2)}\delta^{(1)}_{,i}) - (\delta^{(1)}\theta^{(2)} + \delta^{(2)}\theta^{(1)}) , \tag{3.51}$$

$$\theta^{(3)\prime} + \mathcal{H}\theta^{(3)} + \frac{3}{2}\mathcal{H}^2\Omega_m\delta^{(3)} = -(u^{j(1)}_{,i}\,u^{i(2)}_{,j} + u^{j(2)}_{,i}\,u^{i(1)}_{,j}) - (u^{i(1)}\theta^{(2)}_{,i} + u^{i(2)}\theta^{(1)}_{,i}) . \tag{3.52}$$

As in the second-order case, it is instructive to rewrite these equations explicitly in real space in order to make the structure of the nonlinear couplings transparent. Using the relation between the velocity field and its divergence, the third-order equations can be expressed in terms of gradient and inverse-gradient operators as

$$\begin{aligned}
\delta^{(3)\prime} + \theta^{(3)} + \mathcal{H}g\,\delta^{(3)} &= -\left[(\nabla^{-1})^i\theta^{(1)}\nabla_i\delta^{(2)} + (\nabla^{-1})^i\theta^{(2)}\nabla_i\delta^{(1)}\right] - \left[\delta^{(1)}\theta^{(2)} + \delta^{(2)}\theta^{(1)}\right] \\
\theta^{(3)\prime} + \mathcal{H}\theta^{(3)} + \frac{3}{2}\mathcal{H}^2\Omega_m\delta^{(3)} &= -\left[\nabla_i(\nabla^{-1})^j\theta^{(1)}\nabla_j(\nabla^{-1})^i\theta^{(2)} + \nabla_i(\nabla^{-1})^j\theta^{(2)}\nabla_j(\nabla^{-1})^i\theta^{(1)}\right] \\
&\quad - \left[(\nabla^{-1})^i\theta^{(1)}\nabla_i\theta^{(2)} + (\nabla^{-1})^i\theta^{(2)}\nabla_i\theta^{(1)}\right]
\end{aligned} \tag{3.53}$$

In close analogy with the second-order treatment, these expressions reveal that third-order perturbations are sourced by mode-coupling terms involving lower-order fields. Transforming the equations to Fourier space leads to convolution integrals that describe the coupling of three linear modes, providing the natural framework for the definition of third-order kernels.

The third-order equations can also be transformed to Fourier space by expanding all perturbation fields in Fourier modes and inserting these expansions into the real-space evolution equations. Now, the nonlinearities involve products of first- and second-order fields, which give rise to convolution integrals over three independent wavevectors. Carrying out the usual procedure to move to Fourier space, the third-order continuity and Euler equations can be written as

$$\int \frac{d^3k}{(2\pi)^3} e^{i\vec{k}\cdot\vec{x}} \left[\delta_k^{(3)\prime} + \theta_k^{(3)} + \mathcal{H}g\,\delta_k^{(3)}\right] = \mathcal{H} f_Q D_+^3 \int \frac{d^3k_1}{(2\pi)^3} \int \frac{d^3k_2}{(2\pi)^3} \int \frac{d^3k_3}{(2\pi)^3} e^{i(\vec{k}_1+\vec{k}_2+\vec{k}_3)\cdot\vec{x}} \times \phi(k_1,k_2,k_3,\tau)\delta_0(\vec{k}_1)\delta_0(\vec{k}_2)\delta_0(\vec{k}_3)\,, \tag{3.54}$$

$$\int \frac{d^3k}{(2\pi)^3} e^{i\vec{k}\cdot\vec{x}} \left[\theta_k^{(3)\prime} + \mathcal{H}\theta_k^{(3)} + \frac{3}{2}\mathcal{H}^2\Omega_m\delta_k^{(3)}\right] = -\mathcal{H}^2 f_Q^2 D_+^3 \int \frac{d^3k_1}{(2\pi)^3} \int \frac{d^3k_2}{(2\pi)^3} \int \frac{d^3k_3}{(2\pi)^3} e^{i(\vec{k}_1+\vec{k}_2+\vec{k}_3)\cdot\vec{x}} \times \psi(k_1,k_2,k_3,\tau)\delta_0(\vec{k}_1)\delta_0(\vec{k}_2)\delta_0(\vec{k}_3)\,. \tag{3.55}$$

The functions ϕ and ψ encode the effective three-mode couplings generated by the nonlinear evolution and are constructed from combinations of the second-order kernels F_2 and G_2. In this sense, they play a role analogous to the mode-coupling functions α and β that appear at second order. However, in contrast to the second-order case, where α and β depend only on the wavevectors, the functions ϕ and ψ inherit an explicit time dependence through the kernels F_2 and G_2. This reflects the fact that, at third order, the nonlinear coupling between modes is sensitive not only to their geometric configuration but also to the time evolution of the lower-order perturbations.

$$\phi(\vec{k}_1,\vec{k}_2,\vec{k}_3,\tau) = F_2(\vec{k}_1,\vec{k}_2,\tau) + \frac{\vec{k}_1\cdot\vec{k}_{23}}{k_1^2}F_2(\vec{k}_2,\vec{k}_3,\tau) + G_2(\vec{k}_2,\vec{k}_3,\tau) + \frac{\vec{k}_{12}\cdot\vec{k}_3}{k_{12}^2}G_2(\vec{k}_1,\vec{k}_2,\tau) \tag{3.56}$$

$$\psi(\vec{k}_1,\vec{k}_2,\vec{k}_3,\tau) = G_2(\vec{k}_1,\vec{k}_2,\tau)\left[\frac{\vec{k}_{12}\cdot\vec{k}_3}{k_{12}^2} + \frac{(\vec{k}_{12}\cdot\vec{k}_3)^2}{k_{12}^2k_3^2}\right] + G_2(\vec{k}_2,\vec{k}_3,\tau)\left[\frac{\vec{k}_1\cdot\vec{k}_{23}}{k_1^2} + \frac{(\vec{k}_1\cdot\vec{k}_{23})^2}{k_1^2k_{23}^2}\right] \tag{3.57}$$

As was done at second order, it is convenient to make explicit use of the Dirac delta distribution when writing the third-order equations in Fourier space, now involving three wavevectors. In this case, the relevant identity reads

$$e^{i(\vec{k}_1+\vec{k}_2+\vec{k}_3)\cdot\vec{x}} = \int d^3k\, e^{i\vec{k}\cdot\vec{x}}\delta_D(\vec{k}-\vec{k}_1-\vec{k}_2-\vec{k}_3) \tag{3.58}$$

Introducing the Dirac delta in this way allows the exponential factor arising from the product of three Fourier modes to be rewritten in terms of a single integration over the wavevector $\vec{k}$ appearing on the left-hand side of the evolution equations. This procedure enforces the condition $\vec{k} = \vec{k}_1 + \vec{k}_2 + \vec{k}_3$, expressing momentum conservation in Fourier space and making explicit that a given mode is sourced by the nonlinear coupling of three linear modes.

Using this identity, the third-order continuity and Euler equations can be written in a compact convolution form as

We can write that,

$$\begin{aligned}
\delta_k^{(3)\prime} + \theta_k^{(3)} + \mathcal{H}g\,\delta_k^{(3)} &= \int \frac{d^3k_1}{(2\pi)^3}\int \frac{d^3k_2}{(2\pi)^3}\int \frac{d^3k_3}{(2\pi)^3}(2\pi)^3\delta_D(\vec{k}-\vec{k}_1-\vec{k}_2-\vec{k}_3) \\
&\times \mathcal{H} f_Q D_+^3 \phi(\vec{k}_1,\vec{k}_2,\vec{k}_3,\tau)\delta_0(\vec{k}_1)\delta_0(\vec{k}_2)\delta_0(\vec{k}_3) \\
\theta_k^{(2)\prime} + \mathcal{H}\theta_k^{(2)} + \frac{3}{2}\mathcal{H}^2\Omega_m\delta_k^{(2)} &= -\int \frac{d^3k_1}{(2\pi)^3}\int \frac{d^3k_2}{(2\pi)^3}\int \frac{d^3k_3}{(2\pi)^3}(2\pi)^3\delta_D(\vec{k}-\vec{k}_1-\vec{k}_2-\vec{k}_3) \\
&\times \mathcal{H}^2 f_Q^2 D_+^3 \psi(\vec{k}_1,\vec{k}_2,\vec{k}_3,\tau)\delta_0(\vec{k}_1)\delta_0(\vec{k}_2)\delta_0(\vec{k}_3)
\end{aligned} \tag{3.59}$$

Here, the source terms $T_\delta(\vec{k})$ and $T_\theta(\vec{k})$ encapsulate the nonlinear mode-coupling contributions for third order. They arise from convolution integrals over products of first-order and second-order perturbations, and their structure reflects the cubic interactions between modes with wavevectors $\vec{k}_1$, $\vec{k}_2$ and $\vec{k}_3$ such that $\vec{k} = \vec{k}_1 + \vec{k}_2 + \vec{k}_3$:

$$\begin{aligned} T_\delta(\vec{k}) &= \int \frac{d^3k_1}{(2\pi)^3} \int \frac{d^3k_2}{(2\pi)^3} \int \frac{d^3k_3}{(2\pi)^3} (2\pi)^3 \delta_D(\vec{k} - \vec{k}_1 - \vec{k}_2 - \vec{k}_3) \\ &\times \phi(\vec{k}_1, \vec{k}_2, \vec{k}_3, \tau)\, \delta_0(\vec{k}_1)\, \delta_0(\vec{k}_2)\, \delta_0(\vec{k}_3) \qquad (3.60) \\ T_\theta(\vec{k}) &= -\int \frac{d^3k_1}{(2\pi)^3} \int \frac{d^3k_2}{(2\pi)^3} \int \frac{d^3k_3}{(2\pi)^3} (2\pi)^3 \delta_D(\vec{k} - \vec{k}_1 - \vec{k}_2 - \vec{k}_3) \\ &\times \psi(\vec{k}_1, \vec{k}_2, \vec{k}_3, \tau)\, \delta_0(\vec{k}_1)\, \delta_0(\vec{k}_2)\, \delta_0(\vec{k}_3) \qquad (3.61) \end{aligned}$$

With this definition, the equation (3.59) turn into

$$\begin{aligned} \delta_k^{(3)\prime} + \theta_k^{(3)} + \mathcal{H} g\, \delta_k^{(3)} &= \mathcal{H} f_Q D_+^3 T_\delta \\ \theta_k^{(3)\prime} + \mathcal{H}\theta_k^{(3)} + \frac{3}{2}\mathcal{H}^2 \Omega_m \delta_k^{(3)} &= \mathcal{H}^2 f_Q^2 D_+^3 T_\theta \end{aligned} \qquad (3.62)$$

Next, we assume a separable structure between time evolution and scale dependence by postulating that the third-order perturbative solutions can be factorized into a purely time-dependent component and a kernel that depends on both time and spatial scales. To cast the third-order density contrast and velocity divergence into a unified convolutional form, it is convenient to introduce the third-order perturbative kernels. With this definition, the third-order solutions can be expressed as

$$\begin{aligned} \delta_k^{(3)} &= D_+^3 \int \frac{d^3k_1}{(2\pi)^3} \int \frac{d^3k_2}{(2\pi)^3} \int \frac{d^3k_3}{(2\pi)^3} (2\pi)^3 \delta_D(\vec{k} - \vec{k}_1 - \vec{k}_2 - \vec{k}_3) \\ &\times F_3(\vec{k}_1, \vec{k}_2, \vec{k}_3, \tau) \times \delta_0(\vec{k}_1)\delta_0(\vec{k}_2)\delta_0(\vec{k}_3) \\ \theta_k^{(3)} &= -\mathcal{H} f_Q D_+^3 \int \frac{d^3k_1}{(2\pi)^3} \int \frac{d^3k_2}{(2\pi)^3} \int \frac{d^3k_3}{(2\pi)^3} (2\pi)^3 \delta_D(\vec{k} - \vec{k}_1 - \vec{k}_2 - \vec{k}_3) \\ &\times G_3(\vec{k}_1, \vec{k}_2, \vec{k}_3, \tau) \times \delta_0(\vec{k}_1)\delta_0(\vec{k}_2)\delta_0(\vec{k}_3) \qquad (3.63) \end{aligned}$$

where F_3 and G_3 are the time-varying third-order kernels.

Expressing the third-order perturbations in terms of kernel functions provides a convenient and systematic description of the nonlinear dynamics. In this formulation, the mode-coupling effects are fully encoded in the kernels, while the convolution integrals explicitly illustrate how products of lower-order perturbations contribute to the third-order solutions. In particular, the presence of second-order terms multiplying first-order perturbations highlights the hierarchical structure of perturbation theory, wherein nonlinear corrections arise from successive couplings between different perturbative orders. From a practical standpoint, this separation is advantageous, as it allows the evolution of the kernels to be computed directly, thereby avoiding the repeated evaluation of the full convolution integrals appearing in the perturbative equations.

By comparing Eq. (3.63) with Eqs. (3.59), the functions C_δ and D_θ can be expressed explicitly

in terms of the third-order perturbative kernels,

$$\begin{aligned} C_\delta(\vec{k},\tau) &= \int \frac{d^3k_1}{(2\pi)^3}\int \frac{d^3k_2}{(2\pi)^3}\int \frac{d^3k_3}{(2\pi)^3}(2\pi)^3\delta_D(\vec{k}-\vec{k}_1-\vec{k}_2-\vec{k}_3) \\ &\times \; F_3(\vec{k}_1,\vec{k}_2,\vec{k}_3,\tau)\;\times\delta_0(\vec{k}_1)\delta_0(\vec{k}_2)\delta_0(\vec{k}_3) \\ D_\theta(\vec{k},\tau) &= \int \frac{d^3k_1}{(2\pi)^3}\int \frac{d^3k_2}{(2\pi)^3}\int \frac{d^3k_3}{(2\pi)^3}(2\pi)^3\delta_D(\vec{k}-\vec{k}_1-\vec{k}_2-\vec{k}_3) \\ &\times \; G_3(\vec{k}_1,\vec{k}_2,\vec{k}_3,\tau)\;\times\delta_0(\vec{k}_1)\delta_0(\vec{k}_2)\delta_0(\vec{k}_3) \end{aligned} \tag{3.64}$$

Upon inserting the kernel-based representations of the third-order density contrast and velocity divergence into the fluid equations, one obtains a closed and coupled system of ordinary differential equations governing the functions C_δ and D_θ. Within this framework, the nonlinear interactions among Fourier modes are entirely encoded in the source terms T_δ and T_θ, which serve as driving contributions to the kernel evolution. As a result, Eq. (3.62) can be recast in the form

$$\begin{aligned} \frac{C_\delta'}{\mathcal{H}f_Q}+\left[\frac{3f+g}{f_Q}\right]C_\delta - D_\theta &= T_\delta \\ -\frac{D_\theta'}{\mathcal{H}f_Q}-\left[\frac{3}{2}\frac{\Omega_m}{f_Q^2}+2\frac{f}{f_Q}\right]D_\theta+\frac{3}{2}\frac{\Omega_m}{f_Q^2}C_\delta &= T_\theta \end{aligned} \tag{3.65}$$

Consequently, the functions C_δ and D_θ may be directly associated with the third-order perturbative kernels. Their time evolution is therefore determined by a closed set of differential equations, from which one obtains the coupled evolution equations for the third-order kernels F_3 and G_3 in interacting dark sector models, given by

$$\begin{aligned} \frac{F_3'}{\mathcal{H}f_Q}+\left[\frac{3f+g}{f_Q}\right]F_3 - G_3 &= \phi \\ -\frac{G_3'}{\mathcal{H}f_Q}-\left[\frac{3}{2}\frac{\Omega_m}{f_Q^2}+2\frac{f}{f_Q}\right]G_3+\frac{3}{2}\frac{\Omega_m}{f_Q^2}F_3 &= -\psi \end{aligned} \tag{3.66}$$

A direct inspection of Eqs. (3.66) shows that the third-order perturbative kernels F_3 and G_3 obey a coupled system of first-order differential equations with explicitly time-dependent coefficients. The presence of the derivatives F_3' and G_3', normalized by the combination $\mathcal{H}f_Q$, indicates that the temporal evolution of the kernels is governed jointly by the background expansion and by the modified growth rate induced by the interacting dark sector.

The coefficients multiplying F_3 and G_3 depend explicitly on the linear growth rate f, the matter density parameter Ω_m, and the interaction function g. In particular, the term proportional to $(3f+g)/f_Q$ in the first equation acts as an effective friction term for F_3, while the explicit coupling between F_3 and G_3 reflects the dynamical interplay between density and velocity perturbations at third order. In the second equation, the factor $\frac{3}{2}\Omega_m/f_Q^2$ governs the gravitational sourcing of the velocity-divergence kernel, whereas the additional contribution proportional to f/f_Q further enhances the explicit time dependence of the system.

The source terms ϕ and ψ encode the nonlinear mode-coupling contributions arising from lower-order perturbations and act as driving terms for the evolution of the third-order kernels. Owing to the explicit time dependence of both the coefficients and the source terms, Eqs. (3.66) do not, in general, admit time-independent solutions. Consequently, the evolution of F_3 and G_3

becomes sensitive to the specific form of the dark sector interaction, rendering the third-order kernels strongly model dependent.

This structure highlights a key departure from the Einstein–de Sitter approximation: in interacting dark sector models, nonlinear mode coupling at third order is directly affected by the dark matter–dark energy interaction and therefore cannot be accurately captured by assuming constant kernels or a separable time and scale dependence.

Is important to comment that since $\phi(\vec{k}_1,\vec{k}_2,\vec{k}_3,\tau)$ and $\psi(\vec{k}_1,\vec{k}_2,\vec{k}_3,\tau)$ is not symmetric under exchange of $\vec{k}_1 \leftrightarrow \vec{k}_2$, $\vec{k}_1 \leftrightarrow \vec{k}_3$ and $\vec{k}_2 \leftrightarrow \vec{k}_3$ we define a symmetrized version $F_3^{(s)}$ and $G_3^{(s)}$ to ensure the correct behavior of the kernel under permutation of inputs. When we symmetrize in ϕ and ψ, we obtain the symmetrized kernel $F_3^{(s)}$ and $G_3^{(s)}$, as discussed in [11]:

$$\begin{aligned}
F_3^{(s)}(\vec{k}_1,\vec{k}_2,\vec{k}_3,\tau) = \frac{1}{3!}\Big[&F_3(\vec{k}_1,\vec{k}_2,\vec{k}_3,\tau) + F_3(\vec{k}_1,\vec{k}_3,\vec{k}_2,\tau) + F_3(\vec{k}_2,\vec{k}_1,\vec{k}_3,\tau)\\
&+F_3(\vec{k}_2,\vec{k}_3,\vec{k}_1,\tau) + F_3(\vec{k}_3,\vec{k}_1,\vec{k}_2,\tau) + F_3(\vec{k}_3,\vec{k}_2,\vec{k}_1,\tau)\Big]\\
G_3^{(s)}(\vec{k}_1,\vec{k}_2,\vec{k}_3,\tau) = \frac{1}{3!}\Big[&G_3(\vec{k}_1,\vec{k}_2,\vec{k}_3,\tau) + G_3(\vec{k}_1,\vec{k}_3,\vec{k}_2,\tau) + G_3(\vec{k}_2,\vec{k}_1,\vec{k}_3,\tau)\\
&+G_3(\vec{k}_2,\vec{k}_3,\vec{k}_1,\tau) + G_3(\vec{k}_3,\vec{k}_1,\vec{k}_2,\tau) + G_3(\vec{k}_3,\vec{k}_2,\vec{k}_1,\tau)\Big]
\end{aligned} \tag{3.67}$$

This results in

$$\begin{aligned}
F_3^{(s)}(\vec{k}_1,\vec{k}_2,\vec{k}_3,\tau) &= \frac{7}{108}\Big[\phi(\vec{k}_1,\vec{k}_2,\vec{k}_3,\tau) + \phi(\vec{k}_1,\vec{k}_3,\vec{k}_2,\tau) + \phi(\vec{k}_2,\vec{k}_1,\vec{k}_3,\tau)\\
&+ \phi(\vec{k}_2,\vec{k}_3,\vec{k}_1,\tau) + \phi(\vec{k}_3,\vec{k}_1,\vec{k}_2,\tau) + \phi(\vec{k}_3,\vec{k}_2,\vec{k}_1,\tau)\Big]\\
&+ \frac{1}{54}\Big[\psi(\vec{k}_1,\vec{k}_2,\vec{k}_3,\tau) + \psi(\vec{k}_1,\vec{k}_3,\vec{k}_2,\tau) + \psi(\vec{k}_2,\vec{k}_1,\vec{k}_3,\tau)\\
&+ \psi(\vec{k}_2,\vec{k}_3,\vec{k}_1,\tau) + \psi(\vec{k}_3,\vec{k}_1,\vec{k}_2,\tau) + \psi(\vec{k}_3,\vec{k}_2,\vec{k}_1,\tau)\Big]\\
G_3^{(s)}(\vec{k}_1,\vec{k}_2,\vec{k}_3,\tau) &= \frac{1}{36}\Big[\phi(\vec{k}_1,\vec{k}_2,\vec{k}_3,\tau) + \phi(\vec{k}_1,\vec{k}_3,\vec{k}_2,\tau) + \phi(\vec{k}_2,\vec{k}_1,\vec{k}_3,\tau)\\
&+ \phi(\vec{k}_2,\vec{k}_3,\vec{k}_1,\tau) + \phi(\vec{k}_3,\vec{k}_1,\vec{k}_2,\tau) + \phi(\vec{k}_3,\vec{k}_2,\vec{k}_1,\tau)\Big]\\
&+ \frac{1}{18}\Big[\psi(\vec{k}_1,\vec{k}_2,\vec{k}_3,\tau) + \psi(\vec{k}_1,\vec{k}_3,\vec{k}_2,\tau) + \psi(\vec{k}_2,\vec{k}_1,\vec{k}_3,\tau)\\
&+ \psi(\vec{k}_2,\vec{k}_3,\vec{k}_1,\tau) + \psi(\vec{k}_3,\vec{k}_1,\vec{k}_2,\tau) + \psi(\vec{k}_3,\vec{k}_2,\vec{k}_1,\tau)\Big]
\end{aligned} \tag{3.68}$$

Having established the evolution equations for the second- and third-order perturbative kernels, we are now in a position to generalize the formalism to arbitrary perturbative order. The results obtained at second and third order already reveal the key structural features introduced by the interacting dark sector (IDS), namely the explicit time dependence of the kernels and the nontrivial coupling between density and velocity perturbations induced by the dark sector interaction.

Motivated by these findings, we proceed to construct the evolution differential equations for the n-th order perturbative kernels in the IDS scenario. At this level, the perturbative hierarchy

naturally takes the form of a coupled system of ordinary differential equations, in which the n-th order kernels are sourced by convolutions of lower-order kernels, weighted by time-dependent coefficients that depend on the background expansion, the linear growth rate, the matter density parameter, and the interaction function characterizing the dark sector coupling.

This generalization makes explicit that the structure observed at second and third order persists at all perturbative orders: the presence of the interaction prevents the separation of time and scale dependence and forbids the existence of time-independent kernel solutions. Consequently, the n-th order evolution equations encode a cumulative memory of the dark sector interaction through the entire perturbative hierarchy. In this framework, nonlinear mode coupling is systematically modified at each order, emphasizing that accurate modeling of structure formation in IDS cosmologies requires a fully time-dependent treatment of the perturbative kernels beyond the standard Einstein–de Sitter approximation.

The derivation of the n-th order evolution differential equations thus provides a consistent and unified description of nonlinear perturbations in interacting dark sector models, forming the basis for higher-order calculations of observables such as the matter power spectrum, bispectrum, and higher-order correlation functions within this extended cosmological framework.

3.4. General case: n-order perturbation equations

The generalization of the perturbative framework to arbitrary order n is well established in the literature and provides a systematic description of nonlinear structure formation. To construct this hierarchy, it is useful to recall the perturbative expansions of the density contrast δ_k and the velocity divergence θ_k in Fourier space. These quantities are expressed as infinite series of perturbative contributions,

$$\delta_k = \sum_{n=1}^{\infty} \delta^{(n)} = D_+\,\delta^{(0)} + D_+^2\,A_\delta + D_+^3\,C_\delta + \cdots\,, \tag{3.69}$$

and

$$\theta_k^{(\Lambda CDM)} = \sum_{n=1}^{\infty} \theta^{(n)} = -\mathcal{H}f\left(D_+\,\delta^{(0)} + D_+^2\,B_\theta + D_+^3\,D_\theta + \cdots\right). \tag{3.70}$$

In these expressions, $\delta^{(n)}$ and $\theta^{(n)}$ denote the n-th order perturbative contributions to the density contrast and velocity divergence, respectively. The linear growth factor D_+ controls the time evolution of perturbations at each order, while the functions A_δ, B_θ, C_δ, and D_θ encode the scale and angular dependence arising from nonlinear mode coupling. The factor $-\mathcal{H}f$ appearing in the expansion of θ_k reflects the relation between the velocity divergence and the growth of density perturbations, with $f \equiv d\ln D_+/d\ln a$ denoting the linear growth rate.

This formulation makes explicit that higher-order contributions scale with increasing powers of the linear growth factor, illustrating the hierarchical nature of the perturbative expansion. Each successive term captures increasingly nonlinear interactions between Fourier modes, sourced by lower-order perturbations through mode-coupling integrals.

For the sake of clarity and notational simplicity, and in anticipation of the general n-th order construction, we adopt in the following a slightly different convention ($\delta_n \equiv -\theta_n$). With this choice, the above expansions can be rewritten in a more compact and systematic form, which will facilitate the derivation of the evolution differential equations at arbitrary perturbative order.

$$\delta_k = \sum_{n=1}^{\infty} D_+^n \delta_n = D_+\delta_1 + D_+^2\delta_2 + \cdots\,, \tag{3.71}$$

$$\theta_k^{(\Lambda CDM)} = \mathcal{H} f \sum_{n=1}^{\infty} D_+^n \theta_n = \mathcal{H} f \left(D_+ \theta_1 + D_+^2 \theta_2 + \cdots \right). \tag{3.72}$$

In the interacting dark sector (IDS) scenario, the perturbative structure remains formally similar to that of the standard case, but with a crucial modification encoded in the growth rate. In particular, the effects of the interaction are absorbed into a generalized growth-rate function f_Q, which replaces the standard linear growth rate f in the evolution of the velocity divergence. As a result, the perturbative expansion of θ_k can be written as

$$\theta_k = \mathcal{H} f_Q \sum_{n=1}^{\infty} D_+^n \, \theta_n = \mathcal{H} f_Q \left(D_+ \theta_1 + D_+^2 \theta_2 + \cdots \right). \tag{3.73}$$

This expression makes explicit that the impact of the dark sector interaction enters the perturbative hierarchy exclusively through the modified growth rate f_Q. Consequently, while the time dependence associated with the linear growth factor D_+ retains the same hierarchical structure as in the noninteracting case, the overall amplitude and evolution of the velocity divergence at each order are directly affected by the interaction.

It is important to emphasize that, for notational convenience, the conventional negative sign relating the velocity divergence to the growth of density perturbations has been absorbed into the definition of the auxiliary kernels θ_n. This choice simplifies the algebraic structure of the higher-order equations, at the cost of modifying the relation between the first-order density and velocity kernels. In the previous convention, one had the simple identification $\delta_1 = \theta_1$. Under the present convention, this relation is replaced by

$$\delta_1 = -\theta_1,$$

which must be consistently taken into account in all subsequent derivations. This redefinition does not alter the physical content of the perturbative expansion, but provides a more convenient framework for extending the formalism to arbitrary perturbative order in interacting dark sector models.

The evolution equations governing perturbations at arbitrary order n can be conveniently expressed in real space through the continuity and Euler equations. In the interacting dark sector framework, these equations take the form

$$\delta' + \theta + \mathcal{H} g \, \delta = -(\nabla^{-1})^i \theta \, \nabla_i \delta - \delta \, \theta, \tag{3.74}$$

$$\theta' + \mathcal{H}\theta + \frac{3}{2}\mathcal{H}^2 \Omega_m \, \delta = -\nabla_i (\nabla^{-1})^j \theta \, \nabla_j (\nabla^{-1})^i \theta - (\nabla^{-1})^i \theta \, \nabla_i \theta. \tag{3.75}$$

The first equation represents the continuity equation and describes the conservation of mass for the dark matter fluid. Relative to the standard case, the interaction with the dark energy sector introduces the additional term $\mathcal{H} g \, \delta$, which acts as an effective source or sink depending on the sign of the coupling function g. The nonlinear terms on the right-hand side arise from the convective derivative and encode mode-coupling effects between density and velocity perturbations. These terms are responsible for the generation of higher-order contributions in the perturbative expansion.

The second equation corresponds to the Euler equation for the velocity divergence. The term proportional to $\mathcal{H}\theta$ represents Hubble friction, while the gravitational sourcing of velocity perturbations is governed by the Poisson term $\frac{3}{2}\mathcal{H}^2 \Omega_m \, \delta$. The nonlinear contributions on the right-hand

side originate from the advective part of the velocity field and describe self-couplings of the velocity divergence. Written in terms of inverse-gradient operators, these terms explicitly highlight the nonlocal nature of the nonlinear interactions in real space.

Together, these equations provide the starting point for constructing the perturbative hierarchy at arbitrary order. When expanded order by order, the nonlinear terms on the right-hand side generate source terms built from products of lower-order perturbations, while the left-hand side governs the time evolution of the n-th order fields. This structure makes explicit how the dark sector interaction modifies the standard fluid equations and propagates its effects throughout the entire perturbative expansion.

By transforming the real-space fluid equations into Fourier space, the nonlinear structure of the perturbative hierarchy becomes explicit. In Fourier space, the continuity and Euler equations for the interacting dark sector scenario read

$$\begin{aligned}
\delta_k' + \theta_k + \mathcal{H} g\, \delta_k &= -\int \frac{d^3k_1}{(2\pi)^3} \int \frac{d^3k_2}{(2\pi)^3} (2\pi)^3 \delta_D(\vec{k} - \vec{k}_1 - \vec{k}_2) \\
&\times \left[\frac{\vec{k}\cdot\vec{k}_1}{k_1^2}\right] \theta(\vec{k}_1)\, \delta(\vec{k}_2), \\
\theta_k' + \mathcal{H}\theta_k + \frac{3}{2}\mathcal{H}^2\Omega_m\, \delta_k &= -\int \frac{d^3k_1}{(2\pi)^3} \int \frac{d^3k_2}{(2\pi)^3} (2\pi)^3 \delta_D(\vec{k} - \vec{k}_1 - \vec{k}_2) \\
&\times \left[\frac{k^2(\vec{k}_1\cdot\vec{k}_2)}{2k_1^2k_2^2}\right] \theta(\vec{k}_1)\, \theta(\vec{k}_2).
\end{aligned} \tag{3.76}$$

In these expressions, the Dirac delta distribution enforces momentum conservation, $\vec{k} = \vec{k}_1 + \vec{k}_2$, reflecting the convolution structure of nonlinear mode coupling in Fourier space. The kernels multiplying the products of perturbations arise from the gradient and inverse-gradient operators present in the real-space equations and encode the angular dependence of the nonlinear interactions between Fourier modes.

To systematically extract the contributions at a given perturbative order, it is convenient to make use of the Cauchy product identity,

$$\sum_{a=1}^{\infty}\sum_{b=1}^{\infty} \theta_a\, \theta_b = \sum_{n=2}^{\infty}\sum_{m=1}^{n-1} \theta_m\, \theta_{n-m}, \tag{3.77}$$

which allows the reorganization of products of perturbative series into contributions of fixed total order n. This identity plays a central role in isolating the source terms that drive the evolution of higher-order perturbations.

Substituting the perturbative expansions of δ_k and θ_k [cf. Eq. (3.71)] into Eq. (3.76), and making systematic use of the Cauchy product identity (3.77), the continuity equation yields, for $n > 1$,

$$\frac{\delta_n'}{\mathcal{H} f_Q} + n\, \delta_n + \theta_n = A_n, \tag{3.78}$$

where A_n denotes the nonlinear source term constructed from convolutions of lower-order density and velocity kernels. This equation makes explicit that the n-th order density perturbation is sourced entirely by nonlinear mode coupling, while its time evolution is governed by the modified growth rate f_Q.

Following the same procedure for the Euler equation, one finds for $n > 1$,

$$\frac{\theta_n'}{\mathcal{H} f_Q} + \left[\frac{3}{2}\frac{\Omega_m}{f_Q^2} + \frac{f}{f_Q}(n-1)\right]\theta_n + \frac{3}{2}\frac{\Omega_m}{f_Q^2}\delta_n = \frac{1}{2}B_n. \tag{3.79}$$

Here, the coefficient multiplying θ_n explicitly depends on the perturbative order n, reflecting the cumulative effect of nonlinear interactions on the velocity divergence. The source term B_n encodes combinations of lower-order velocity kernels and acts as a driving term for the n-th order solution. Together, Eqs. (3.78) and (3.79) define a closed system of evolution equations for the n-th order perturbative kernels in the interacting dark sector scenario, generalizing the standard perturbative hierarchy and making explicit the role of the dark sector interaction at all orders.

It is worth emphasizing that in the limit of vanishing interaction, these equations reduce to the ΛCDM case with time-dependent kernels [Eqs. (3.78) and (3.79)]. Moreover, in the limit $\Omega_m/f^2 = 1$, they recover the Einstein–de Sitter case.

We now express the n-th order density and velocity-divergence perturbations in terms of time-dependent perturbative kernels. In Fourier space, these quantities can be written as

$$\begin{aligned}
\delta_n &= \int \frac{d^3k_1}{(2\pi)^3}\cdots\int \frac{d^3k_n}{(2\pi)^3}(2\pi)^3\delta_D(\vec{k}-\vec{k}_1-\cdots-\vec{k}_n)\,F_n(\vec{k}_1,\ldots,\vec{k}_n,\tau)\,\delta_1(\vec{k}_1)\cdots\delta_1(\vec{k}_n), \\
\theta_n &= -\int \frac{d^3k_1}{(2\pi)^3}\cdots\int \frac{d^3k_n}{(2\pi)^3}(2\pi)^3\delta_D(\vec{k}-\vec{k}_1-\cdots-\vec{k}_n)\,G_n(\vec{k}_1,\ldots,\vec{k}_n,\tau)\,\delta_1(\vec{k}_1)\cdots\delta_1(\vec{k}_n).
\end{aligned} \tag{3.80}$$

These expressions make explicit the convolution structure of nonlinear perturbations: the Dirac delta distribution enforces momentum conservation, while the kernels F_n and G_n encode the full angular, scale, and temporal dependence of the n-th order mode coupling. In contrast to the Einstein–de Sitter approximation, the kernels are explicitly time dependent, reflecting the modified dynamics induced by the interacting dark sector. The minus sign in the definition of θ_n follows from the adopted convention for the velocity divergence and ensures consistency with the lower-order relations.

Substituting Eq. (3.80) into the n-th order continuity and Euler equations, Eqs. (3.78) and (3.79), one obtains a closed system of evolution equations for the n-th order kernels F_n and G_n,

$$\begin{aligned}
\frac{F_n'}{\mathcal{H} f_Q} + \left[\frac{nf+g}{f_Q}\right]F_n - G_n &= \frac{\vec{k}\cdot\vec{k}_1}{k_1^2} \\
&\times \sum_{m=1}^{n-1} G_m(\vec{k}_1,\ldots,\vec{k}_m)\,F_{n-m}(\vec{k}_{m+1},\ldots,\vec{k}_n),
\end{aligned} \tag{3.81}$$

$$\begin{aligned}
-\frac{G_n'}{\mathcal{H} f_Q} - \left[\frac{3}{2}\frac{\Omega_m}{f_Q^2} + \frac{f}{f_Q}(n-1)\right]G_n + \frac{3}{2}\frac{\Omega_m}{f_Q^2}F_n &= -\frac{k^2\,(\vec{k}_1\cdot\vec{k}_2)}{2k_1^2k_2^2} \\
&\times \sum_{m=1}^{n-1} G_m(\vec{k}_1,\ldots,\vec{k}_m)\,G_{n-m}(\vec{k}_{m+1},\ldots,\vec{k}_n).
\end{aligned} \tag{3.82}$$

These equations constitute a central theoretical result of this master's thesis. They provide the general evolution differential equations for the n-th order perturbative kernels in interacting dark sector cosmologies. The structure of the system highlights several key features. First, the

coefficients of the homogeneous terms depend explicitly on the perturbative order n, the linear growth rate f, the matter density parameter Ω_m, and the interaction function g, encapsulated through the modified growth rate f_Q. Second, the source terms on the right-hand side are constructed from convolutions of lower-order kernels, reflecting the hierarchical nature of nonlinear mode coupling.

Importantly, the interaction between dark matter and dark energy enters both through the modified friction terms and through the explicit time dependence of the kernels, implying that the standard assumption of time-independent kernels is no longer valid. As a consequence, Eqs. (3.81) define a fully time-dependent perturbative hierarchy that generalizes the standard cosmological perturbation theory to arbitrary order in the interacting dark sector scenario. This formalism provides a consistent theoretical foundation for computing higher-order observables, such as the bispectrum and trispectrum, within interacting dark sector models.

From the recurrence system in Eq. (3.81), one obtains explicitly, for $n = 2, 3, 4$, the following coupled evolution equations.

Case $n = 2$**.** For $n = 2$ the sums contain only the term $m = 1$:

$$\begin{aligned}
\frac{F_2'}{\mathcal{H} f_Q} + \left[\frac{2f+g}{f_Q}\right] F_2 - G_2 &= \frac{\vec{k}\cdot\vec{k}_1}{k_1^2}\, G_1(\vec{k}_1)\, F_1(\vec{k}_2), \qquad (3.83)\\
-\frac{G_2'}{\mathcal{H} f_Q} - \left[\frac{3}{2}\frac{\Omega_m}{f_Q^2} + \frac{f}{f_Q}\right] G_2 + \frac{3}{2}\frac{\Omega_m}{f_Q^2} F_2 &= -\frac{k^2\,(\vec{k}_1\cdot\vec{k}_2)}{2k_1^2 k_2^2}\, G_1(\vec{k}_1)\, G_1(\vec{k}_2).
\end{aligned}$$

Case $n = 3$**.** For $n = 3$ the sums contain $m = 1, 2$:

$$\begin{aligned}
\frac{F_3'}{\mathcal{H} f_Q} + \left[\frac{3f+g}{f_Q}\right] F_3 - G_3 &= \frac{\vec{k}\cdot\vec{k}_1}{k_1^2}\Big[G_1(\vec{k}_1)\, F_2(\vec{k}_2,\vec{k}_3,\tau) + G_2(\vec{k}_1,\vec{k}_2,\tau)\, F_1(\vec{k}_3)\Big], \qquad (3.84)\\
-\frac{G_3'}{\mathcal{H} f_Q} - \left[\frac{3}{2}\frac{\Omega_m}{f_Q^2} + 2\frac{f}{f_Q}\right] G_3 + \frac{3}{2}\frac{\Omega_m}{f_Q^2} F_3 &= -\frac{k^2\,(\vec{k}_1\cdot\vec{k}_2)}{2k_1^2 k_2^2}\Big[G_1(\vec{k}_1)\, G_2(\vec{k}_2,\vec{k}_3,\tau) + G_2(\vec{k}_1,\vec{k}_2,\tau)\, G_1(\vec{k}_3)\Big].
\end{aligned}$$

Case $n = 4$**.** For $n = 4$ the sums contain $m = 1, 2, 3$:

$$\begin{aligned}
\frac{F_4'}{\mathcal{H} f_Q} + \left[\frac{4f+g}{f_Q}\right] F_4 - G_4 &= \frac{\vec{k}\cdot\vec{k}_1}{k_1^2} \qquad (3.85)\\
&\times\Big[G_1(\vec{k}_1)\, F_3(\vec{k}_2,\vec{k}_3,\vec{k}_4,\tau) + G_2(\vec{k}_1,\vec{k}_2,\tau)\, F_2(\vec{k}_3,\vec{k}_4,\tau)\\
&+G_3(\vec{k}_1,\vec{k}_2,\vec{k}_3,\tau)\, F_1(\vec{k}_4)\Big],\\
-\frac{G_4'}{\mathcal{H} f_Q} - \left[\frac{3}{2}\frac{\Omega_m}{f_Q^2} + 3\frac{f}{f_Q}\right] G_4 + \frac{3}{2}\frac{\Omega_m}{f_Q^2} F_4 &= -\frac{k^2\,(\vec{k}_1\cdot\vec{k}_2)}{2k_1^2 k_2^2}\\
&\times\Big[G_1(\vec{k}_1)\, G_3(\vec{k}_2,\vec{k}_3,\vec{k}_4,\tau) + G_2(\vec{k}_1,\vec{k}_2,\tau)\, G_2(\vec{k}_3,\vec{k}_4,\tau)\\
&+G_3(\vec{k}_1,\vec{k}_2,\vec{k}_3,\tau)\, G_1(\vec{k}_4)\Big].
\end{aligned}$$

In all cases one must keep in mind that $\vec{k} = \vec{k}_1 + \cdots + \vec{k}_n$ is enforced by the Dirac delta distribution in the full convolution representation of the kernels.

In the next section, we present the derivation of the Einstein–de Sitter approximation within the ΛCDM cosmological model, clarifying the assumptions that allow one to approximate the ratio Ω_m/f^2 as being close to unity and discussing the domain of validity of this approximation in the context of perturbation theory.

3.5. Derivation of the Einstein–de Sitter approximation in ΛCDM

The Einstein–de Sitter (EdS) approximation plays a central role in many perturbative approaches to nonlinear structure formation because it provides a simple route to treat the time dependence of higher-order perturbations. In the exact EdS universe, the perturbative kernels are time independent and the growth of structures follows simple power laws. In practice, one often exploits this structure even in ΛCDM by assuming that certain combinations of background and growth functions remain sufficiently close to their EdS values. The main goal of this section is to make explicit how the approximation $\Omega_m/f^2 \simeq 1$ emerges in ΛCDM, and why it is a reasonable (though not exact) working hypothesis for a large fraction of cosmic history. Throughout this derivation, we assume that the matter density parameter $\Omega_m(a)$ and the growth rate $f(a)$ have already been defined in previous sections.

We begin from the linear evolution equation for pressureless matter perturbations in an expanding universe. On sub-horizon scales, within General Relativity, and neglecting pressure and anisotropic stress, the matter density contrast obeys

$$\ddot{\delta} + 2H\dot{\delta} - 4\pi G\rho_m\,\delta = 0. \tag{3.86}$$

This equation encodes the basic physical competition that governs structure formation. The gravitational term proportional to ρ_m drives the growth of overdensities, while the term proportional to H acts as a friction term induced by the expansion, tending to slow down the growth. The relative importance of these two effects changes with time, because both the expansion rate $H(a)$ and the matter density fraction evolve as the Universe transitions from matter domination to dark-energy domination.

To isolate the time dependence, it is convenient to introduce the linear growth factor $D(a)$ through a separable form,

$$\delta(\mathbf{x}, a) = D(a)\,\delta(\mathbf{x}, a_i),$$

where $\delta(\mathbf{x}, a_i)$ represents the initial spatial field at some early epoch a_i, and $D(a)$ carries all the subsequent linear evolution. This separation is possible because, at linear order, different Fourier modes evolve independently and the linear growth is scale independent for cold dark matter in GR on sub-horizon scales. Substituting this definition into the perturbation equation, and changing the time variable from t to $\ln a$ to better track the expansion history, one obtains the standard growth equation

$$\frac{d^2D}{d(\ln a)^2} + \left[2 + \frac{d\ln H}{d\ln a}\right]\frac{dD}{d\ln a} - \frac{3}{2}\Omega_m(a)\,D = 0. \tag{3.87}$$

This form emphasizes that the evolution of $D(a)$ is not determined solely by $\Omega_m(a)$, but also by the logarithmic evolution of the Hubble rate. In other words, the growth of perturbations depends both on how strongly gravity clusters matter (through Ω_m) and on how the expansion stretches comoving scales (through H).

A particularly useful quantity for both theoretical and observational applications is the growth rate,

$$f(a) = \frac{d\ln D}{d\ln a},$$

which measures the fractional change in the amplitude of perturbations per logarithmic interval in scale factor. This function appears directly in redshift-space distortion observables and is therefore a key bridge between theory and data. From a dynamical perspective, expressing the evolution in terms of f is also advantageous because it converts the second-order equation for D into a first-order (but nonlinear) equation for f.

To proceed, we rewrite the second derivative of D in terms of f. Since $dD/d\ln a = fD$, differentiating once more gives

$$\frac{d^2D}{d(\ln a)^2} = \frac{d}{d\ln a}(fD) = D\left(\frac{df}{d\ln a} + f^2\right). \tag{3.88}$$

Substituting this identity into the growth equation and dividing by D yields an exact evolution equation for f,

$$\frac{df}{d\ln a} + f^2 + \left[2 + \frac{d\ln H}{d\ln a}\right] f = \frac{3}{2}\Omega_m(a). \tag{3.89}$$

This equation makes transparent the physical origin of the growth rate: the source term on the right-hand side is proportional to $\Omega_m(a)$, while the "friction" term proportional to $d\ln H/d\ln a$ encodes the impact of the expansion history. In particular, when the Universe accelerates, the expansion rate decreases more slowly with a, increasing the friction term and suppressing the growth.

We now specialize to the ΛCDM model. Neglecting radiation, the Hubble rate is given by

$$H^2(a) = H_0^2\left[\Omega_{m0}a^{-3} + \Omega_{\Lambda 0}\right]. \tag{3.90}$$

This expression explicitly separates the matter contribution, which scales as a^{-3}, from the cosmological constant contribution, which remains constant. It follows that matter dominates at early times, while Λ dominates at late times. Differentiating $\ln H$ with respect to $\ln a$ yields the useful identity

$$\frac{d\ln H}{d\ln a} = -\frac{3}{2}\Omega_m(a), \tag{3.91}$$

which states that the rate of change of the expansion is controlled by the instantaneous matter fraction. Inserting this relation into the exact growth-rate equation leads to the ΛCDM form

$$\frac{df}{d\ln a} + f^2 + \left[2 - \frac{3}{2}\Omega_m(a)\right] f = \frac{3}{2}\Omega_m(a). \tag{3.92}$$

Although this equation must, in general, be solved numerically, it admits accurate analytic approximations that provide intuition and are widely used in the literature.

A particularly successful approximation is the growth-index parametrization, in which f is assumed to track Ω_m through a simple power law,

$$f(a) \simeq \Omega_m(a)^B, \tag{3.93}$$

where B is approximately constant in ΛCDM. The motivation for this ansatz is twofold. First, it reproduces the exact EdS limit: when $\Omega_m \to 1$, one has $f \to 1$ independently of B. Second, it captures the empirical behavior observed in numerical solutions of the growth equation, namely that f closely follows a power of Ω_m over a broad range of redshifts. The remaining task is to determine the value of B that best matches ΛCDM.

To substitute this ansatz into the differential equation, we must express $df/d\ln a$ in terms of Ω_m. Since $f = \Omega_m^B$, we have

$$\frac{df}{d\ln a} = B\Omega_m^{B-1}\frac{d\Omega_m}{d\ln a}. \tag{3.94}$$

Therefore, the key step is to compute $d\Omega_m/d\ln a$ in ΛCDM. Using $\Omega_m(a) = \Omega_{m0}a^{-3}H_0^2/H^2(a)$ and differentiating with respect to $\ln a$, one obtains the standard identity

$$\frac{d\Omega_m}{d\ln a} = -3\,\Omega_m(1-\Omega_m). \tag{3.95}$$

This expression has a simple interpretation: the matter fraction decreases as the Universe expands, and the rate at which it decreases is proportional both to Ω_m itself and to the complementary fraction $1-\Omega_m$ (which is dominated by Λ at late times). Combining Eqs. (3.95) and $f = \Omega_m^B$, we obtain

$$\frac{df}{d\ln a} = -3B\,\Omega_m^B(1-\Omega_m). \tag{3.96}$$

We can now substitute the ansatz into the ΛCDM growth-rate equation. Replacing f by Ω_m^B and $df/d\ln a$ by the expression above yields

$$-3B\,\Omega_m^B(1-\Omega_m) + \Omega_m^{2B} + \left(2 - \frac{3}{2}\Omega_m\right)\Omega_m^B = \frac{3}{2}\Omega_m. \tag{3.97}$$

This is an exact algebraic condition that must hold if the power-law ansatz is to be an exact solution. Since the ansatz is only approximate, Eq. (3.97) should be interpreted as an equation that can be satisfied to a given order in an expansion around an appropriate limit. A convenient way to proceed is to divide both sides by Ω_m^B (with $\Omega_m > 0$), which yields

$$-3B(1-\Omega_m) + \Omega_m^B + 2 - \frac{3}{2}\Omega_m = \frac{3}{2}\Omega_m^{1-B}. \tag{3.98}$$

This form is useful because it isolates the dependence on B in powers of Ω_m and makes clear that the relation becomes exact in the EdS limit $\Omega_m \to 1$.

To extract an analytic value for B in ΛCDM, one expands around the matter-dominated regime, where Ω_m is close to unity. We write

$$\Omega_m = 1-\varepsilon, \qquad 0 < \varepsilon \ll 1, \tag{3.99}$$

so that ε measures the small departure from matter domination. In this regime, it is consistent to expand Ω_m^B and Ω_m^{1-B} to first order in ε,

$$\Omega_m^B \simeq 1 - B\varepsilon, \qquad \Omega_m^{1-B} \simeq 1 - (1-B)\varepsilon. \tag{3.100}$$

Since $1-\Omega_m = \varepsilon$, substituting these expansions into Eq. (3.98) and keeping only terms up to $\mathcal{O}(\varepsilon)$ yields a linear relation for B.

On the left-hand side, we obtain

$$-3B\varepsilon + (1-B\varepsilon) + 2 - \frac{3}{2}(1-\varepsilon) = \frac{3}{2} + \left(-4B + \frac{3}{2}\right)\varepsilon. \tag{3.101}$$

On the right-hand side, we similarly find

$$\frac{3}{2}\left[1-(1-B)\varepsilon\right] = \frac{3}{2} + \left(-\frac{3}{2} + \frac{3}{2}B\right)\varepsilon. \tag{3.102}$$

Equating the coefficients of ε on both sides leads to

$$-4B + \frac{3}{2} = -\frac{3}{2} + \frac{3}{2}B, \tag{3.103}$$

and therefore

$$B = \frac{6}{11} \approx 0.545. \tag{3.104}$$

This is the standard result for ΛCDM (i.e. $w = -1$), often quoted in the approximate form $B \simeq 0.55$. With this value, the growth rate is well approximated by

$$f(a) \simeq \Omega_m(a)^{6/11}. \tag{3.105}$$

Having established the growth-index relation, we can now show explicitly how it motivates the EdS-inspired approximation $\Omega_m/f^2 \simeq 1$. Using $f \simeq \Omega_m^B$, we find

$$\frac{\Omega_m}{f^2} \simeq \frac{\Omega_m}{\Omega_m^{2B}} = \Omega_m^{1-2B}. \tag{3.106}$$

For $B \simeq 6/11$, the exponent is

$$1 - 2B = 1 - \frac{12}{11} = -\frac{1}{11} \approx -0.09, \tag{3.107}$$

so that

$$\frac{\Omega_m}{f^2} \simeq \Omega_m^{-1/11}. \tag{3.108}$$

The crucial point is that the exponent is small in magnitude. Consequently, even when $\Omega_m(a)$ varies substantially between matter domination and the present epoch, the combination Ω_m/f^2 changes only mildly. This is precisely the practical reason why Ω_m/f^2 is often treated as "close to unity" in ΛCDM: it is not exactly one, but it remains sufficiently near one over a broad redshift range to justify using EdS-like time factorization as a controlled approximation in many perturbative applications.

In summary, the EdS-inspired approximation in ΛCDM can be understood as the combination of two ingredients: (i) the exact growth-rate equation derived from the linear growth equation, and (ii) the empirical success of the growth-index ansatz $f \simeq \Omega_m^B$ with $B \simeq 6/11$. Together, these results imply that Ω_m/f^2 evolves slowly and stays near unity, motivating the widespread use of EdS kernels as an efficient approximation for perturbative calculations in the standard cosmological model.

3.6. The ΛCDM and IDS limit of the Einstein–de Sitter approximation

A common simplifying assumption in cosmological perturbation theory is the approximation

$$\frac{\Omega_m}{f^2} \simeq 1, \tag{3.109}$$

is often justified by invoking the Einstein–de Sitter (EdS) limit. In an EdS universe, characterized by $\Omega_m = 1$ and a linear growth rate satisfying $f = 1$, the corresponding relation holds exactly. For this reason, the EdS approximation has been extensively employed in analytical and semi-analytical approaches to nonlinear structure formation, as it allows one to factorize or simplify the time dependence of higher-order perturbative kernels.

The validity and practical implementation of this approximation have been discussed and explored in the literature, for instance in Refs. [12, 11], where the EdS-based treatment serves as a useful reference framework for perturbative calculations beyond linear order.

In the literature, this approximation is frequently assumed to remain valid over a broad range of redshifts, including regimes where dark energy is dynamically relevant. Under this assumption, the time evolution of higher-order kernels is often factorized or treated as effectively constant, greatly simplifying perturbative calculations in the standard ΛCDM cosmology. However, with the advent of precision cosmology and increasingly accurate large-scale structure data, the validity of this approximation deserves careful scrutiny.

In this section, we critically assess the accuracy of the EdS-inspired approximation $\Omega_m/f^2 \approx 1$. We begin by examining the standard ΛCDM model, focusing in particular on its behavior at low redshift, where dark energy dominates the cosmic expansion. We then extend this analysis to interacting dark sector (IDS) models, in which the background and perturbation dynamics are modified by explicit couplings between dark matter and dark energy.

During this investigation, we encounter numerical challenges associated with solving the full time-dependent perturbation equations in ΛCDM and IDS scenarios. To address these issues, we introduce controlled approximations that preserve the essential physics while ensuring numerical stability. These approximations are discussed and validated in detail in the following chapter, where we also demonstrate the robustness of the numerical implementation employed in this work.

Our first key result concerns the accuracy of the EdS approximation within the standard ΛCDM framework. By explicitly computing the quantity Ω_m/f^2 as a function of redshift, we find that it deviates significantly from unity at late times. In particular, at redshift $z = 0$, the deviation reaches approximately 14%, indicating a clear breakdown of the EdS limit in the present-day Universe.

This level of discrepancy is non-negligible in the context of precision cosmology. It implies that EdS-based assumptions, while adequate at high redshift where matter dominates, become increasingly inaccurate as dark energy drives the accelerated expansion. Consequently, perturbative calculations that rely on the EdS approximation may introduce systematic errors when applied to low-redshift observables within the ΛCDM model.

The redshift dependence of this deviation is illustrated in Fig. 3.3, which shows the evolution of Ω_m/f^2 across cosmic time. The figure clearly demonstrates that departures from the EdS value occur not only at late times but also at intermediate redshifts, reinforcing the need for caution when employing EdS-inspired simplifications in analytical treatments.

When interactions in the dark sector are taken into account, deviations from the Einstein–de Sitter approximation become substantially more pronounced than in the standard ΛCDM scenario. In interacting dark sector (IDS) models, both the background evolution and the perturbation equations are modified by additional interaction terms, typically encoded through the functions f_Q and g. These modifications directly affect the growth rate of matter perturbations and, consequently, the quantity Ω_m/f^2.

As shown in Fig. 3.4, the relative deviation of Ω_m/f^2 from unity in IDS models can exceed 120% at low redshifts. This represents a dramatic failure of the EdS approximation, with discrepancies that are an order of magnitude larger than those found in the ΛCDM case. Such large deviations clearly demonstrate that the EdS limit cannot be regarded as a reliable approximation once dark sector interactions are present.

The physical origin of this behavior lies in the direct coupling between dark matter and dark energy. This coupling modifies both the effective friction terms in the perturbation equations and the sourcing of matter fluctuations, leading to a nontrivial redshift dependence of the growth factor and its derivatives. These effects cannot be captured by a simple EdS scaling and invalidate the assumption that Ω_m/f^2 remains close to unity.

From a phenomenological perspective, these results have important implications for analytical

and semi-analytical approaches to large-scale structure formation. Many perturbative calculations rely on EdS-based kernels to simplify the time dependence of higher-order corrections. The large deviations observed here indicate that such approximations may lead to significant systematic biases when applied to interacting dark sector models, particularly in the context of upcoming high-precision galaxy surveys.

In summary, the results presented in Fig. 3.4 provide strong evidence that the Einstein–de Sitter approximation is not applicable to interacting dark sector scenarios at low redshift. The magnitude of the deviations observed in these models strongly motivates the use of fully time-dependent perturbative kernels, reinforcing the theoretical framework developed in the previous chapters of this thesis.

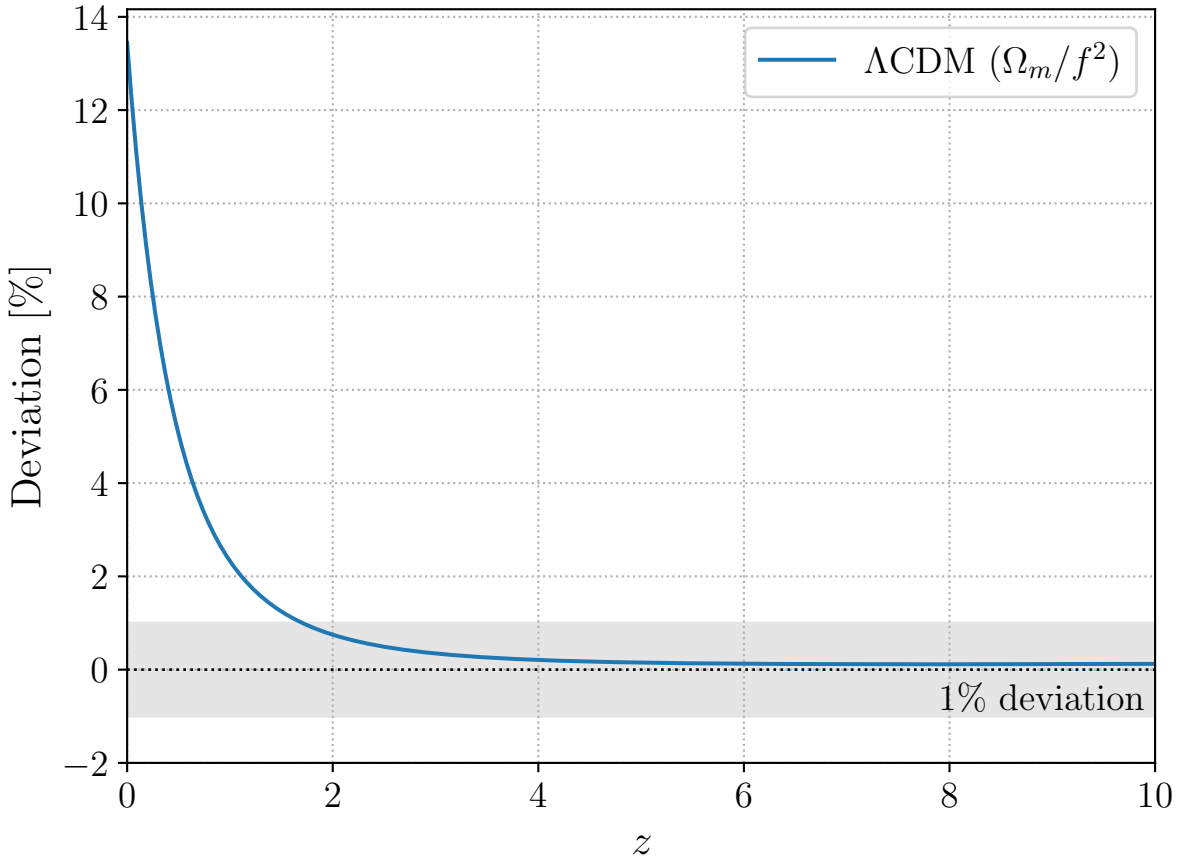

Figure 3.3.: Deviation of the quantity Ω_m/f^2 from unity as a function of redshift, highlighting departures from the Einstein–de Sitter approximation at both high and low redshifts in the ΛCDM model.

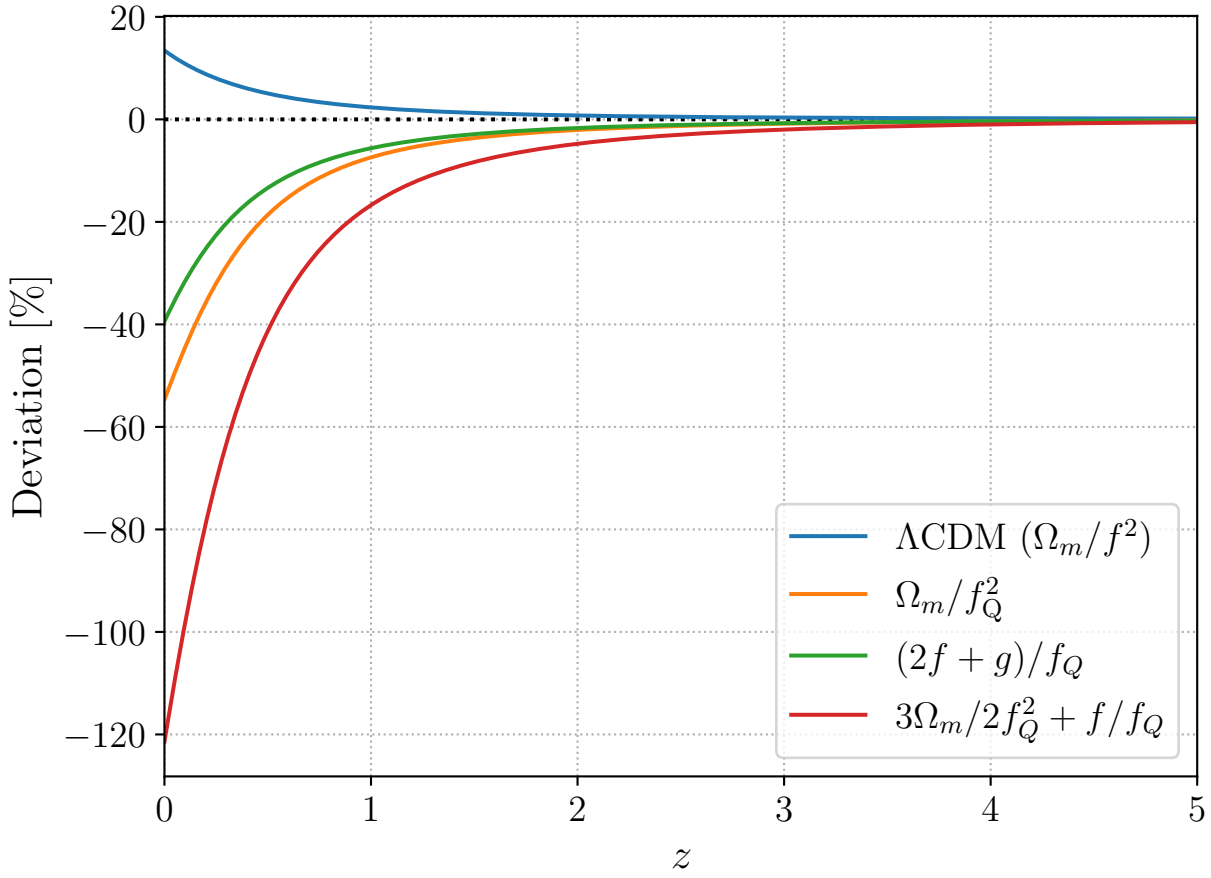

Figure 3.4.: Relative deviations (in percent) of the time-dependent coefficients entering the second-order kernel evolution equations, Eqs. (3.47)–(3.48), as a function of redshift. The curves show the contributions associated with Ω_m/f_Q^2, $(2f+g)/f_Q$, and $3\Omega_m/(2f_Q^2) + f/f_Q$, compared to their corresponding ΛCDM limits. These terms explicitly appear in the friction and coupling coefficients of the F_2 and G_2 equations and quantify how the interaction in the dark sector modifies the temporal evolution of the kernels. The large deviations at low redshift indicate that the Einstein–de Sitter approximation becomes inadequate in interacting models, highlighting the necessity of retaining the full time dependence of the kernels when solving Eqs. (3.47)–(3.48).

Statistical Measures of Structure

The perturbation variables introduced thus far—such as δ, ψ, and θ, together with their Fourier counterparts—must be understood as intrinsically stochastic quantities. They are random variables: at any specific point in space–time one cannot deterministically predict whether the density contrast assumes the value 0, -0.01, or any other number. What the Einstein equations provide is not the specific realization of these quantities, but rather the law governing their temporal evolution; for example, in the linear regime $\delta \propto a$. Consequently, if δ happens to vanish initially at a given spatial location, it will remain zero throughout the evolution. Conversely, if the initial density contrast is negative, indicating an underdense region, this underdensity will deepen over time until the region effectively becomes empty. If the region is initially overdense, δ will grow monotonically until it eventually leaves the linear regime.

Because the perturbation fields are random fields defined over space, a statistical description is required. In practice, instead of analyzing the specific realization $\delta(\boldsymbol{x}, \tau)$, one studies its statistical moments, particularly the mean and the variance. In configuration space, the variance of the density contrast as a function of spatial separation,

$$\langle \delta(\boldsymbol{x})\, \delta(\boldsymbol{x} + \boldsymbol{r}) \rangle,$$

defines the two-point correlation function. In Fourier space, the analogous quantity,

$$\langle |\delta(\boldsymbol{k})|^2 \rangle,$$

defines the matter power spectrum. The mean, however, is trivial: by definition of the density contrast,

$$\langle \delta \rangle = 0,$$

since δ measures deviations from the cosmic mean density. As all other scalar perturbation variables are proportional to δ in the linear regime, one similarly has $\langle \Psi \rangle = \langle \Phi \rangle = \langle \theta \rangle = 0$, and so on. Hence, it is the variance that contains the physically relevant information. Higher-order moments can in principle be considered, and are indeed used in many contexts. Nevertheless, a key assumption motivated by inflation is that the primordial fluctuations are Gaussian distributed. For a Gaussian random field, the variance fully characterizes the distribution: all odd moments vanish, while even moments can be expressed as combinations of $\langle \delta^2 \rangle$ (e.g., $\langle \delta^4 \rangle = 3\langle \delta^2 \rangle^2$). This justifies the central role of quadratic statistics—the correlation function and the power spectrum—in modern cosmology [13].

As structure formation progresses, however, the initially small fluctuations grow and eventually enter the nonlinear regime, at which point their Gaussian nature is no longer preserved. This is easy to understand qualitatively: if an initially negative δ decreases, the density contrast is bounded below by $\delta = -1$, corresponding to a completely empty region; meanwhile, a positive δ

can grow without bound as the region collapses and forms nonlinear structures such as galaxies, stars, or black holes. The resulting distribution of overdensities and underdensities therefore becomes skewed and decidedly non-Gaussian. Determining this fully nonlinear distribution analytically is extremely challenging and typically requires numerical N-body simulations to compute with accuracy.

4.1. Statistical Properties of the Density Field

The large–scale distribution of matter in the Universe is most naturally described using the language of random fields. Since the observed structure originates from the gravitational amplification of small primordial perturbations, a single realization of the density contrast is less informative than its statistical properties. Statistical descriptors such as ensemble averages, variances, and correlation functions encode the information contained in $\delta(\vec{x})$. Among them, the most widely used are the N–point correlation functions and their Fourier counterparts, the power spectra. They form the backbone of modern observational cosmology, bridging theory and measurements from galaxy surveys and the cosmic microwave background.

Below we summarize the essentials of this statistical framework, beginning with basic definitions, then introducing correlation functions, and finally presenting their spectral representations.

4.1.1. Averages, Variances, and Moments

Statistical quantities play a central role in the description of cosmological perturbations, which are intrinsically stochastic in nature. We begin by considering a single real-valued random variable x, characterized by a probability distribution function (PDF) $f(x)$. The normalization condition,

$$1 = \int f(x)\, dx, \tag{4.1}$$

ensures that the total probability of all possible outcomes of the random variable is unity.

The first moment of the distribution defines the *mean* (or expectation value) of x,

$$\langle x \rangle = \int x\, f(x)\, dx, \tag{4.2}$$

which represents the average value obtained after many realizations of the random variable. In physical applications, such as cosmology, the mean often corresponds to the background or homogeneous component of a quantity.

The second (raw) moment is given by

$$\langle x^2 \rangle = \int x^2\, f(x)\, dx, \tag{4.3}$$

and measures the average of the squared variable. While this quantity already contains information about the spread of the distribution, it does not isolate fluctuations around the mean.

More generally, the expectation value of any function $g(x)$ of the random variable is defined as

$$\langle g(x) \rangle = \int g(x)\, f(x)\, dx. \tag{4.4}$$

This definition allows one to compute ensemble averages of arbitrary observables constructed from the underlying random variable.

The hierarchy of statistical moments provides a systematic characterization of the distribution. The n-th (raw) moment is defined as

$$\overline{M}_n = \int x^n \, f(x) \, dx, \tag{4.5}$$

and encodes information about the overall shape of the distribution. In contrast, the n-th *central moment*,

$$M_n = \int (x - \langle x \rangle)^n \, f(x) \, dx, \tag{4.6}$$

quantifies fluctuations relative to the mean value. Central moments are particularly useful because they are insensitive to shifts of the distribution.

The second central moment,

$$M_2 = \int (x - \langle x \rangle)^2 \, f(x) \, dx, \tag{4.7}$$

is known as the *variance* and measures the typical amplitude of fluctuations around the mean. Its square root defines the standard deviation, which sets the characteristic scale of dispersion of the random variable.

When dealing with a set of random variables x_i, it is important to quantify not only their individual variances but also how they fluctuate jointly. This information is encoded in the *covariance matrix*,

$$C_{ij} = \langle x_i x_j \rangle, \tag{4.8}$$

which measures the degree of correlation between different variables. In cosmological applications, the covariance matrix plays a fundamental role in characterizing correlations between different modes or observables and forms the basis for statistical inference and parameter estimation.

4.1.2. The Two-Point Correlation Function

A key descriptor of the density field is the two–point correlation function, defined as the ensemble average

$$\xi(\vec{r}) = \langle \delta(\vec{x}) \delta(\vec{x} + \vec{r}) \rangle. \tag{4.9}$$

Statistical homogeneity ensures that ξ depends only on the separation $\vec{r}$, and isotropy implies dependence only on $r = |\vec{r}|$.

In practice, $\xi(r)$ measures the excess probability over random of finding matter separated by r. Equivalently, it can be interpreted as the "conditional density contrast," i.e., the fractional excess of the average density measured at distance r from a randomly selected particle.

4.1.3. The N-Point Correlation Functions and the Hierarchical Ansatz

The statistical properties of the matter density field beyond the linear regime are fully characterized by its hierarchy of correlation functions. The N-point correlation function is defined as

$$\xi_N(\vec{x}_1, \ldots, \vec{x}_N) = \langle \delta(\vec{x}_1) \cdots \delta(\vec{x}_N) \rangle, \tag{4.10}$$

where $\delta(\vec{x})$ denotes the matter density contrast and angular brackets represent an ensemble average. This quantity measures the joint probability of finding correlated density fluctuations at the spatial positions $\vec{x}_1, \ldots, \vec{x}_N$. While the two-point function encodes information about

the variance and spatial clustering of matter, higher-order correlation functions probe genuinely non-Gaussian features generated by nonlinear gravitational evolution.

The lowest-order statistic sensitive to non-Gaussianity is the three-point correlation function, defined as

$$\zeta(\vec{x}_1, \vec{x}_2, \vec{x}_3) = \langle \delta(\vec{x}_1)\, \delta(\vec{x}_2)\, \delta(\vec{x}_3) \rangle. \tag{4.11}$$

This quantity captures the leading-order mode coupling induced by nonlinear dynamics. In Fourier space, its counterpart is the bispectrum, which plays a central role in constraining gravitational clustering, biasing, and possible deviations from standard cosmological models.

In regimes where gravitational clustering follows a hierarchical pattern, the higher-order correlation functions can be expressed approximately as products of lower-order ones. This behavior emerges naturally in perturbation theory and reflects the dominance of tree-level contributions in the weakly nonlinear regime. Under this assumption, the three-point correlation function can be written in the form

$$\zeta_{123} = \tilde{Q} \left[\xi_{12}\xi_{23} + \xi_{12}\xi_{13} + \xi_{13}\xi_{23} \right], \tag{4.12}$$

where $\xi_{ij} \equiv \xi_2(|\vec{x}_i - \vec{x}_j|)$ denotes the two-point correlation function evaluated at the separation between points $\vec{x}_i$ and $\vec{x}_j$. The parameter $\tilde{Q}$, often referred to as the reduced three-point amplitude, is approximately constant on large scales and encodes the strength of nonlinear mode coupling.

This hierarchical ansatz provides a compact and physically motivated description of higher-order clustering. In standard gravitational perturbation theory, $\tilde{Q}$ is predicted to depend weakly on scale and configuration in the quasi-linear regime, approaching a constant value in the Einstein–de Sitter limit. Observationally, this scaling behavior has been extensively tested in galaxy surveys and numerical simulations, showing good agreement with theoretical expectations over a wide range of scales (see, e.g., [11, 20]). As such, the hierarchical ansatz serves as a useful bridge between perturbative calculations and measurable higher-order statistics in large-scale structure studies.

4.1.4. The Power Spectrum

The statistical properties of the matter density field are most conveniently described in Fourier space. We begin by defining the Fourier transform of the density contrast $\delta(\vec{x}) \equiv [\rho(\vec{x}) - \bar{\rho}]/\bar{\rho}$ as

$$\delta(\vec{k}) = \int d^3x\, \delta(\vec{x})\, e^{-i\vec{k}\cdot\vec{x}}, \tag{4.13}$$

where $\vec{k}$ denotes the comoving wavevector associated with a given spatial scale, and the exponential factor $e^{-i\vec{k}\cdot\vec{x}}$ projects the real-space density field onto plane-wave modes. The Fourier amplitude $\delta(\vec{k})$ therefore quantifies the contribution of fluctuations with wavelength $\lambda = 2\pi/|\vec{k}|$ to the total density field.

The corresponding inverse Fourier transform,

$$\delta(\vec{x}) = \int \frac{d^3k}{(2\pi)^3}\, \delta(\vec{k})\, e^{i\vec{k}\cdot\vec{x}}, \tag{4.14}$$

reconstructs the real-space density contrast by superposing all Fourier modes, weighted by their amplitudes and phases. The normalization factor $(2\pi)^{-3}$ ensures the consistency of the forward and inverse transformations.

Under the assumptions of statistical homogeneity and isotropy, the ensemble average of the product of two Fourier modes takes the form

$$\langle \delta(\vec{k})\delta^*(\vec{k}')\rangle = (2\pi)^3\,\delta_D(\vec{k}-\vec{k}')\,P(k), \tag{4.15}$$

where $\langle\cdots\rangle$ denotes an ensemble average over realizations of the density field, δ_D is the Dirac delta distribution, and $P(k)$ is the matter power spectrum. The Dirac delta enforces momentum conservation, implying that modes with different wavevectors are uncorrelated, while statistical isotropy ensures that $P(k)$ depends only on the magnitude $k = |\vec{k}|$. This relation serves as the *definition* of the power spectrum.

Physically, the power spectrum $P(k)$ measures the variance of density fluctuations per unit logarithmic interval in wavenumber and encodes how power is distributed across spatial scales. Large values of $P(k)$ indicate enhanced clustering at the corresponding scale, whereas smaller values signal suppressed fluctuations.

The real-space two-point correlation function $\xi(r)$, which quantifies the excess probability of finding matter pairs separated by a distance $r = |\vec{r}|$, is obtained as the inverse Fourier transform of the power spectrum,

$$\xi(r) = \int \frac{d^3k}{(2\pi)^3}\,P(k)\,e^{i\vec{k}\cdot\vec{r}}. \tag{4.16}$$

This expression makes explicit the equivalence between the power spectrum in Fourier space and the correlation function in real space, with the two descriptions containing the same statistical information about the density field.

In the linear regime of structure formation, different Fourier modes evolve independently under gravitational instability. As a result, the power spectrum provides a direct and powerful link between early-Universe physics—such as the primordial fluctuations generated during inflation—and late-time observables, including galaxy clustering, weak gravitational lensing, and cosmic microwave background anisotropies. For this reason, the power spectrum plays a central role in both theoretical modeling and observational analyses of large-scale structure.

4.2. Growth of structure: linear theory

The evolution of cosmological perturbations is not uniform across cosmic history but can be naturally divided into three characteristic stages, each governed by the dominant physical processes of the corresponding epoch. During the radiation–dominated era, perturbations in the matter component are strongly influenced by relativistic species, leading to a suppression of growth on subhorizon scales. As the Universe transitions to matter domination, gravitational instability becomes the driving mechanism, allowing perturbations to grow more efficiently. Finally, in the late–time acceleration stage dominated by dark energy, the growth of structures is significantly slowed down, leaving observable imprints in the large–scale distribution of matter.

A central tool in describing this evolution is the transfer function, which encapsulates how primordial fluctuations are mapped into their present–day amplitudes across different scales. The transfer function effectively encodes the memory of the different physical processes that occurred during each stage of cosmic evolution, including horizon crossing, the damping effects of radiation pressure, and the transition to matter domination. When combined with the primordial power spectrum, it provides the linear matter power spectrum, which serves as the theoretical bridge between early Universe models and late–time large–scale structure observations.

In what follows, we present a detailed discussion of these two fundamental elements. We first outline the three main stages of perturbation evolution, emphasizing the role of background

dynamics in shaping the growth of inhomogeneities. We then introduce the concept of the transfer function and show how it quantifies the scale dependence of perturbation growth, thereby linking the initial conditions of inflationary cosmology with current observations of cosmic structure.

4.2.1. The Transfer Function

The transfer function, $T(k)$, is a fundamental quantity in cosmology that describes how primordial perturbations evolve under the influence of cosmic expansion and microphysical processes. It relates the initial density perturbations, generated in the early Universe, to their subsequent evolution across different cosmological epochs.

Formally, the transfer function is defined as

$$T(k) = \frac{\delta(k, a)}{\delta_p(k)}, \tag{4.17}$$

where $\delta(k, a)$ denotes the Fourier mode of the density contrast at scale factor a, and $\delta_p(k)$ is the primordial amplitude of the same mode. By construction, $T(k) \to 1$ on very large scales ($k \to 0$), since those modes remain unaffected by causal microphysics before horizon entry. On small scales ($k \gg k_{eq}$), the transfer function deviates from unity due to the suppression of growth during the radiation-dominated era and other physical effects such as baryonic acoustic oscillations.

Within the cold dark matter (CDM) paradigm, the linear transfer function provides a convenient way to encode the scale-dependent growth of density perturbations from the early Universe to late times. A widely used analytical fitting formula for the CDM transfer function was derived by Bardeen, Bond, Kaiser, and Szalay (BBKS) [11], and is given by

$$T(k) = \frac{\ln(1 + 2.34q)}{2.34q} \left[1 + 3.89q + (16.1q)^2 + (5.46q)^3 + (6.71q)^4\right]^{-1/4}, \tag{4.18}$$

where the dimensionless wavenumber q is defined as

$$q = \frac{k}{\Omega_m h^2, \mathrm{Mpc}^{-1}}. \tag{4.19}$$

This fitting function was obtained by matching numerical solutions of the linear perturbation equations in a Universe dominated by cold dark matter, neglecting baryonic acoustic oscillations and assuming adiabatic initial conditions [11, 20].

The BBKS transfer function encapsulates the essential physical effect of horizon crossing in different cosmological epochs. Perturbation modes with wavelengths that enter the horizon during the radiation-dominated era experience suppressed growth due to radiation pressure, while modes entering after matter–radiation equality grow unimpeded. As a result, the transfer function imprints a characteristic scale dependence on the matter power spectrum, preserving a memory of the transition from radiation to matter domination and linking early-Universe physics to the observed large-scale structure [26, 21].

Despite its simplicity and historical importance, the BBKS approximation has well-known limitations. In particular, it does not accurately capture baryonic effects, such as baryon acoustic oscillations, nor does it fully account for massive neutrinos or dark energy dynamics. Consequently, while it provides valuable intuition and is often used for analytic estimates, more precise calculations require numerical Boltzmann solvers.

In this work, we therefore adopt the transfer function computed using the `CLASS` (*Cosmic Linear Anisotropy Solving System*) code [31]. The use of `CLASS` ensures a self-consistent and

accurate treatment of all relevant physical components, including radiation, baryons, cold dark matter, neutrinos, and dark energy, as well as their interactions and relativistic effects. This approach guarantees reliable predictions for the transfer function across the wide range of scales and redshifts relevant for our analysis.

4.2.2. The Primordial Power Spectrum

The primordial power spectrum provides a statistical description of the initial density fluctuations generated in the early Universe, commonly associated with a phase of cosmic inflation. These primordial perturbations are assumed to form a nearly Gaussian random field and to obey statistical homogeneity and isotropy. Under these assumptions, all the statistical information of the primordial density field is fully encoded in its two-point correlation function in Fourier space.

The primordial power spectrum $P_p(k)$ is defined through the ensemble average

$$\langle \delta_p(\vec{k})\, \delta_p^*(\vec{k}')\rangle = (2\pi)^3\, \delta_D(\vec{k}-\vec{k}')\, P_p(k), \tag{4.20}$$

where $\delta_p(\vec{k})$ denotes the primordial density contrast in Fourier space, and δ_D is the Dirac delta distribution enforcing translational invariance and momentum conservation. Statistical isotropy further implies that $P_p(k)$ depends only on the magnitude of the wavevector, $k = |\vec{k}|$.

In the simplest inflationary scenarios, the primordial power spectrum is well approximated by a nearly scale-invariant power-law form,

$$P_p(k) = A_s \left(\frac{k}{k_*}\right)^{n_s-1}, \tag{4.21}$$

where A_s is the amplitude of the primordial scalar perturbations, n_s is the scalar spectral index, and k_* is a reference pivot scale. Exact scale invariance corresponds to $n_s = 1$, while the small deviation from unity observed in current data reflects the mild scale dependence predicted by realistic inflationary models.

In this work, rather than adopting an idealized analytic parametrization, we employ the primordial power spectrum computed with the Boltzmann solver `CLASS`. This choice ensures a consistent and high-precision treatment of the initial conditions, incorporating the full set of cosmological parameters and accurately propagating the primordial fluctuations through the radiation-dominated era. The use of `CLASS` therefore provides a robust and self-consistent foundation for the nonlinear perturbative analysis developed throughout this dissertation.

4.2.3. Linear Power Spectrum

The linear matter power spectrum plays a central role in connecting the primordial density fluctuations generated in the early Universe to the large-scale distribution of matter observed at later times. Within linear perturbation theory, different Fourier modes evolve independently, and the time evolution of matter fluctuations is fully described by a scale-independent growth factor. This property allows for a clear separation between the primordial initial conditions and the subsequent gravitational amplification of structures.

In this work, the linear matter power spectrum is expressed as

$$P_L(k,a) = D_+^2(a)\, P_p(k), \tag{4.22}$$

where $P_p(k)$ denotes the primordial power spectrum and $D_+(a)$ is the linear growth factor, normalized such that $D_+(a=1) = 1$. The quantity $P_L(k,a)$ therefore characterizes the variance

of matter density fluctuations in Fourier space at a given cosmic time, explicitly describing how the primordial perturbations are amplified by gravitational instability in the linear regime.

At this level of description, the shape of the power spectrum is entirely inherited from the primordial fluctuations, while its overall amplitude evolves proportionally to the square of the growth factor. This factorization reflects a fundamental feature of linear theory: the growth of cosmic structures is governed by the background expansion history and the gravitational dynamics of the model, but remains independent of scale. As a consequence, all scale dependence is fixed by the initial conditions, whereas time evolution is encoded solely in $D_+(a)$.

Crucially, the linear growth factor is not universal, but depends on the underlying cosmological model. Different scenarios—such as the standard ΛCDM model, interacting dark sector models, or theories of modified gravity—predict distinct expansion histories and growth rates for matter perturbations. Even when the same primordial power spectrum is assumed, these differences lead to model-dependent modifications in the amplitude of the linear matter power spectrum. This behavior is explicitly illustrated in Fig. 4.1, where the linear power spectra computed with `CLASS` exhibit clear deviations between ΛCDM and interacting dark sector models, arising solely from their different growth histories.

In the context of this work, the model dependence of the growth factor is of particular importance, as it directly impacts both the linear power spectrum and the higher-order, nonlinear corrections discussed in subsequent sections. An accurate determination of $D_+(a)$ for each cosmological model under consideration is therefore essential for a consistent comparison between theoretical predictions and observational data from large-scale structure surveys.

For further details on linear perturbation theory and the construction of the linear matter power spectrum, the reader is referred to Refs. [26, 28, 11]. In the next section, we move beyond the linear description and investigate how nonlinear effects modify the growth of cosmic structures.

4.3. Growth of Structure: Beyond Linear Theory

In order to study the growth of cosmic structures beyond the linear regime, it becomes essential to analyze higher-order correlation functions of the primordial fluctuations. While the linear theory is entirely characterized by the two-point correlation function or, equivalently, the power spectrum, the nonlinear regime involves mode couplings that give rise to nontrivial higher-order statistics, such as the bispectrum and trispectrum. The computation of these quantities often requires systematic techniques to reduce products of random fields into sums over their fundamental correlators.

A central tool in this context is Wick's theorem, which provides a prescription to express n-point correlation functions of Gaussian random fields in terms of products of two-point functions. Since the initial density perturbations generated in the early Universe are well described by a Gaussian random field, Wick's theorem ensures that all statistical information at leading order is encoded in the two-point function alone. This property drastically simplifies the evaluation of ensemble averages in perturbation theory and underpins much of the formalism employed in standard cosmological perturbation theory.

Beyond its technical utility, Wick's theorem also highlights the transition between Gaussian initial conditions and the emergence of non-Gaussian signatures generated by nonlinear gravitational evolution. As we extend the perturbative analysis to second and higher orders, the theorem allows us to systematically track how mode coupling leads to deviations from Gaussianity, thereby providing insight into the formation of the large-scale structure observed in the Universe today.

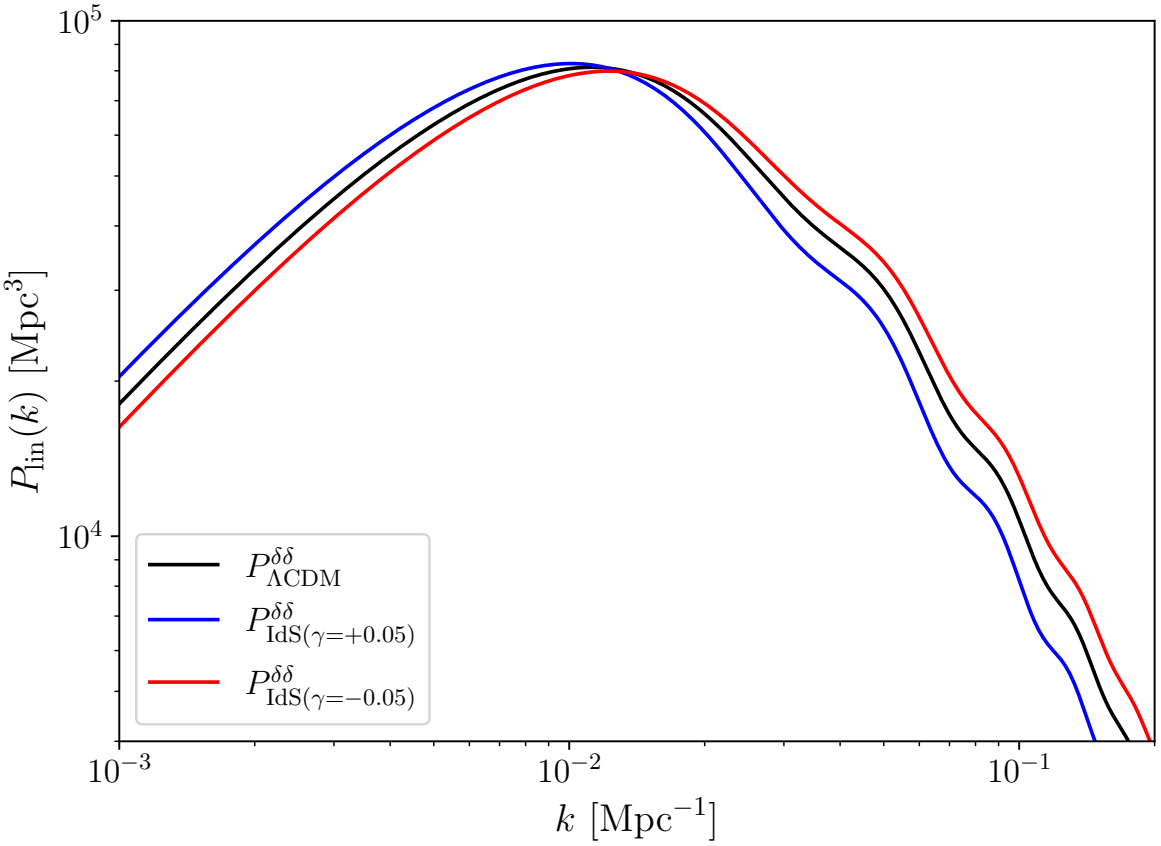

Figure 4.1.: Linear matter power spectrum $P_{\rm L}(k)$ at $z = 0$ computed with the Boltzmann code `CLASS` for the standard ΛCDM model and for interacting dark sector (IDS) scenarios with interaction parameters $\gamma = \pm 0.05$. All spectra are obtained using the same primordial initial conditions, so that the differences in amplitude and scale dependence arise solely from the modified background evolution and growth history induced by the dark sector interaction. The deviations with respect to ΛCDM illustrate how interactions in the dark sector alter the linear growth of matter perturbations, even at the level of the linear power spectrum.

4.3.1. Wick Theorem

In order to incorporate nonlinear effects in the evolution of cosmic density perturbations, the matter overdensity field $\delta_m(\vec{k}, a)$ is expanded perturbatively in powers of the linear density contrast,

$$\delta_m(\vec{k}, a) = \delta^{(1)}(\vec{k}, a) + \delta^{(2)}(\vec{k}, a) + \delta^{(3)}(\vec{k}, a) + \cdots , \tag{4.23}$$

where $\delta^{(n)}$ denotes the n-th order contribution in standard perturbation theory. Each term $\delta^{(n)}$ scales as the n-th power of the linear density field and encodes mode-coupling effects generated by nonlinear gravitational evolution.

The two-point correlation function of the matter overdensity in Fourier space can then be written as

$$\langle \delta_m(\vec{k}, a)\, \delta_m(\vec{k}', a) \rangle = \sum_{n+l \text{ even}} \left\langle \delta^{(n)}(\vec{k}, a)\, \delta^{(l)}(\vec{k}', a) \right\rangle , \tag{4.24}$$

where the sum runs over pairs of perturbative orders whose total order $n+l$ is even. This restriction follows from the assumption that the primordial density field is Gaussian and statistically homogeneous and isotropic. Under these conditions, expectation values involving an odd number of linear density fields vanish identically.

To make this structure explicit, we expand the correlator up to third order,

$$\begin{aligned} &\left\langle \big(\delta^{(1)}_{\vec{k}} + \delta^{(2)}_{\vec{k}} + \delta^{(3)}_{\vec{k}}\big)\big(\delta^{(1)}_{\vec{k}'} + \delta^{(2)}_{\vec{k}'} + \delta^{(3)}_{\vec{k}'}\big) \right\rangle \\ &= \langle \delta^{(1)}_{\vec{k}} \delta^{(1)}_{\vec{k}'} \rangle + \langle \delta^{(1)}_{\vec{k}} \delta^{(2)}_{\vec{k}'} \rangle + \langle \delta^{(1)}_{\vec{k}} \delta^{(3)}_{\vec{k}'} \rangle + \langle \delta^{(2)}_{\vec{k}} \delta^{(1)}_{\vec{k}'} \rangle \\ &\quad + \langle \delta^{(2)}_{\vec{k}} \delta^{(2)}_{\vec{k}'} \rangle + \langle \delta^{(2)}_{\vec{k}} \delta^{(3)}_{\vec{k}'} \rangle + \langle \delta^{(3)}_{\vec{k}} \delta^{(1)}_{\vec{k}'} \rangle + \langle \delta^{(3)}_{\vec{k}} \delta^{(2)}_{\vec{k}'} \rangle + \langle \delta^{(3)}_{\vec{k}} \delta^{(3)}_{\vec{k}'} \rangle . \end{aligned} \tag{4.25}$$

The evaluation of these expectation values relies on Wick's theorem, which states that ensemble averages of products of Gaussian random fields can be decomposed into sums of products of two-point correlators. Since the linear density field $\delta^{(1)}$ is assumed to be Gaussian, all correlators involving an odd total number of linear fields vanish. As a consequence, mixed terms such as

$$\langle \delta^{(1)}_{\vec{k}} \delta^{(2)}_{\vec{k}'} \rangle = \langle \delta^{(2)}_{\vec{k}} \delta^{(1)}_{\vec{k}'} \rangle = \langle \delta^{(2)}_{\vec{k}} \delta^{(3)}_{\vec{k}'} \rangle = \langle \delta^{(3)}_{\vec{k}} \delta^{(2)}_{\vec{k}'} \rangle = 0 \tag{4.26}$$

vanish identically.

Retaining only the nonzero contributions up to fourth order in the linear density field, the two-point correlator reduces to

$$\langle \delta_m(\vec{k}, a)\, \delta_m(\vec{k}', a) \rangle = \langle \delta^{(1)}_{\vec{k}} \delta^{(1)}_{\vec{k}'} \rangle + \langle \delta^{(2)}_{\vec{k}} \delta^{(2)}_{\vec{k}'} \rangle + 2\, \langle \delta^{(1)}_{\vec{k}} \delta^{(3)}_{\vec{k}'} \rangle + \mathcal{O}(\delta^6). \tag{4.27}$$

The first term corresponds to the linear power spectrum, while the remaining two terms represent the leading nonlinear corrections at one-loop order. Specifically, $\langle \delta^{(2)} \delta^{(2)} \rangle$ gives rise to the P_{22} contribution, whereas $\langle \delta^{(1)} \delta^{(3)} \rangle$ generates the P_{13} term. Together, these corrections capture the lowest-order effects of mode coupling induced by nonlinear gravitational evolution and form the basis for the one-loop matter power spectrum analyzed in this work.

4.3.2. One Loop Power Spectrum

Finally, the total matter power spectrum can be written as an expansion in powers of the linear spectrum, incorporating higher-order (nonlinear) corrections:

$$P(k, a) = P_L(k, a) + P^{NLO}(k, a) + \cdots , \tag{4.28}$$

where $P^{NLO}(k,a)$ denotes the next-to-leading order correction, such as the one-loop correction in standard perturbation theory. This expansion becomes essential on smaller scales where nonlinear clustering becomes significant. Here, $P(k,a)$ is the total power spectrum at a given scale k and scale factor a. The first term, $P_L(k,a)$, represents the linear contribution, while the second term, $P^{NLO}(k,a)$, corresponds to the next-to-leading-order nonlinear correction. The ellipsis indicates additional higher-order contributions that are not explicitly shown.

The one-loop nonlinear part of the power spectrum can be expressed as:

$$P^{NLO}(k,a) = P^{(22)}(k,a) + 2P^{(13)}(k,a) \tag{4.29}$$

Here, $P^{(22)}(k,a)$ and $P^{(13)}(k,a)$ denote the second- and third-order correction terms, respectively. In the next subsection we will discuss how to obtain these fundamental perturbative equations.

4.3.3. Diagrammatic Representation in Large-Scale Structure

The nonlinear corrections to the matter power spectrum can be systematically described within the framework of Standard Perturbation Theory (SPT). At next-to-leading order, two distinct contributions appear:

- $P^{(22)}(k,a)$, which originates from second-order density fields contracted with each other, representing a two-particle loop contribution;
- $P^{(13)}(k,a)$, which arises from the contraction of a third-order field with the linear density field, representing a one-particle loop correction to the linear power spectrum.

To keep track of these terms and their combinatorial structure, one often employs diagrammatic techniques analogous to Feynman diagrams in quantum field theory. In the context of Large-Scale Structure (LSS), these diagrams provide an intuitive bookkeeping device rather than a fundamental quantum interpretation. Each line corresponds to a linear density field (or propagator), while vertices encode the mode-coupling kernels F_n that arise in perturbation theory.

For example, the $P^{(22)}$ term is represented by a diagram with two second-order vertices connected by an internal loop momentum $\vec{p}$, symbolizing the coupling of two linear modes into the external mode $\vec{k}$. On the other hand, the $P^{(13)}$ term is depicted as a diagram where a third-order vertex couples to a single linear leg, effectively representing a correction to the propagation of the linear density field itself as we can see in Figure 4.2 and Figure 4.3.

These diagrammatic rules significantly simplify the derivation of higher-order correlators. They allow one to visually identify the origin of different contributions to the power spectrum and to generalize the perturbative expansion to arbitrary loop orders. In this sense, Feynman-like diagrams serve as a bridge between the formal structure of SPT and its practical computation, making them a central tool in the study of nonlinearities in cosmic structure formation.

4.3.4. Auto and Cross Power Spectrum

Each of these terms depends solely on the second- and third-order kernels, given by:

$$\begin{aligned} P^{(22)}_{\delta\delta}(k,a) &= 2\int \frac{d^3p}{(2\pi)^3}\left[F_2(\vec{p},\vec{k}-\vec{p})\right]^2 P_L(p,a)P_L(|\vec{k}-\vec{p}|,a) \\ P^{(13)}_{\delta\delta}(k,a) &= 3P_L(k,a)\int \frac{d^3p}{(2\pi)^3}F_3(p,-p,k)P_L(p,a) \end{aligned} \tag{4.30}$$

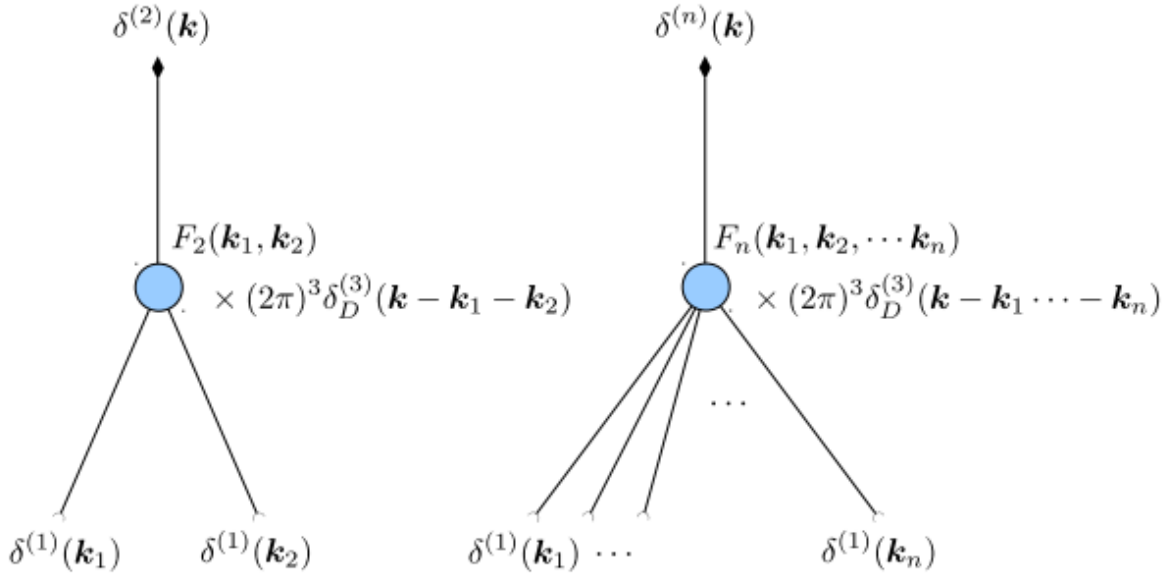

Figure 4.2.: Diagrammatic representation of the second-order density field $\delta^{(2)}$ (left) and the n^{th} order density field (right). In each case, the final density field is connected to n initial density fields by the interaction kernel F_n (with $n = 2$ in the case of $\delta^{(2)}$. Analogous diagrams describe the velocity divergence $\theta^{(n)}$ in terms of kernels G_n. Here we suppress the time arguments for clarity

In the first expression, $P^{(22)}(k, a)$, the second-order kernel F_2 acts as a weighting factor involving the linear power spectrum P_L at the scales p and $|\vec{k} - \vec{p}|$. The prefactor 2 arises from the symmetry of particle exchange in the loop, reflecting the combinatorial nature of such processes.

In the second expression, $P^{(13)}(k, a)$, the third-order kernel F_3 incorporates the contribution of an additional particle, and the prefactor 3 results from the combination of the three particles involved. This shows how the nonlinear density perturbations are linked to the linear fluctuations, emphasizing the connection between different length scales in the process of cosmic structure formation.

These expressions are essential for understanding how primordial fluctuations evolve into the observable structures we see today, such as galaxies and galaxy clusters. We can show that nonlinear effects become increasingly important in the ΛCDM model.

Similarly, one-loop contributions can also be computed for the cross power spectrum between the density contrast δ and the velocity divergence θ, as well as for the auto spectrum of θ. These terms follow analogous expressions with the replacement of density kernels F_n by the corresponding velocity kernels G_n.

The inclusion of these higher-order corrections is crucial for accurately describing the clustering of matter on mildly non-linear scales, where linear theory is no longer sufficient but full numerical simulations are not always practical. Thus, the “22” and “13” components represent the first step in bridging the gap between linear theory and the fully non-linear regime of structure formation.

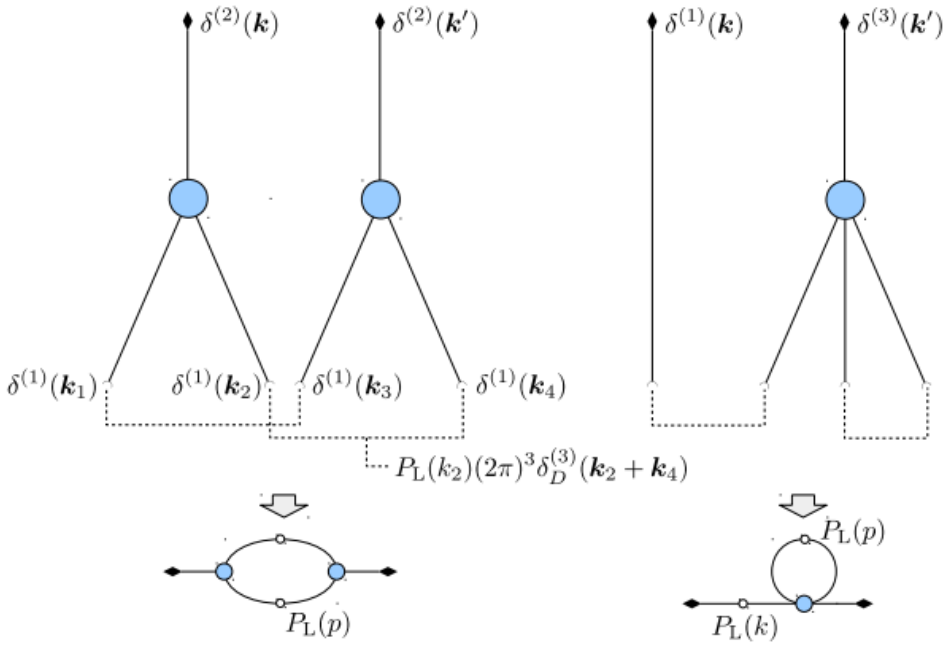

Figure 4.3.: Diagrammatic representation of the next-to-leading order contributions to the matter power spectrum. The terms arise from contractions of nonlinear density fields, which can be expressed in terms of linear fields connected by dashed lines. By Wick's theorem, each connection corresponds to a linear matter power spectrum and a Dirac delta function. The lower part of the diagram introduces a simplified and economical representation, where the connection of two linear fields is depicted by an open circle, each circle corresponding to a linear power spectrum. In this form, it becomes evident why these contributions are referred to as "1-loop" corrections: each loop represents one integral over the internal wavenumber p, also called the loop momentum.

For the density–velocity cross spectrum one finds

$$P_{\delta\theta}^{(22)}(k,a) = 2\int \frac{d^3p}{(2\pi)^3}\, F_2\big(\vec{p},\vec{k}-\vec{p}\big)\, G_2\big(\vec{p},\vec{k}-\vec{p}\big)\, P_L\big(p,a\big)\, P_L\big(|\vec{k}-\vec{p}|,a\big), \tag{4.31}$$

$$P_{\delta\theta}^{(13)}(k,a) = 3\, P_L(k,a)\int \frac{d^3p}{(2\pi)^3}\, \Big[\, F_3\big(\vec{p},-\vec{p},\vec{k}\big) + G_3\big(\vec{p},-\vec{p},\vec{k}\big)\,\Big]\, P_L(p,a), \tag{4.32}$$

where the 22-term arises from the coupling of two second-order fields and the 13-term collects the contributions linear–cubic in the perturbative expansion (the sum in the 13 expression displays explicitly the two possible pairings, $\langle\delta^{(1)}\theta^{(3)}\rangle$ and $\langle\delta^{(3)}\theta^{(1)}\rangle$).

For the velocity–velocity auto spectrum the analogous expressions read

$$P_{\theta\theta}^{(22)}(k,a) = 2\int \frac{d^3p}{(2\pi)^3}\, \big[G_2\big(\vec{p},\vec{k}-\vec{p}\big)\big]^2\, P_L\big(p,a\big)\, P_L\big(|\vec{k}-\vec{p}|,a\big), \tag{4.33}$$

$$P_{\theta\theta}^{(13)}(k,a) = 3\, P_L(k,a)\int \frac{d^3p}{(2\pi)^3}\, G_3\big(\vec{p},-\vec{p},\vec{k}\big)\, P_L(p,a). \tag{4.34}$$

4.3.5. Reduced Bispectrum

Within the framework of Standard Perturbation Theory (SPT), the bispectrum constitutes the leading-order statistic that captures departures from Gaussianity in the matter density field. It arises at second order in the perturbative expansion of the density contrast $\delta(\vec{k})$ and is generated by nonlinear mode coupling between three Fourier modes $\vec{k}_1$, $\vec{k}_2$, and $\vec{k}_3$, which satisfy the closure condition $\vec{k}_1 + \vec{k}_2 + \vec{k}_3 = 0$ as a consequence of momentum conservation.

At tree level, the matter bispectrum is determined by the second-order perturbative kernel F_2, which encodes the nonlinear coupling between pairs of linear density perturbations. In general, F_2 depends on the magnitudes of the interacting wavevectors and on the angle θ between them. Importantly, the time evolution of this kernel is not universal: while in the Einstein–de Sitter (EdS) approximation F_2 is time independent, in more general cosmological models its evolution acquires an explicit dependence on cosmic time and on the underlying dynamics of the model.

For illustrative purposes, we consider isosceles configurations with $|\vec{k}_1| = |\vec{k}_2|$ and varying opening angle θ. In this case, the relevant second-order kernels take the form

$$F_2(\vec{k}_1, \vec{k}_2) \equiv F_{212}(\theta) = \frac{5}{7} + \frac{5}{4}\cos\theta + \frac{2}{7}\cos^2\theta, \tag{4.35}$$

$$F_2(\vec{k}_1, \vec{k}_3) \equiv F_{213}(\theta) = \frac{5}{7} - \frac{9}{20}(2 + \cos\theta) + \frac{2}{35}(2 + \cos\theta)^2, \tag{4.36}$$

$$F_2(\vec{k}_2, \vec{k}_3) \equiv F_{223}(\theta) = \frac{5}{7} - \frac{3}{5}(1 + 2\cos\theta) + \frac{2}{35}(1 + 2\cos\theta)^2. \tag{4.37}$$

The tree-level bispectrum is then constructed as the symmetrized sum over all pairwise mode couplings,

$$B(k_1, k_2, k_3) = 2F_2(\vec{k}_1, \vec{k}_2)P_L(k_1)P_L(k_2) + 2F_2(\vec{k}_1, \vec{k}_3)P_L(k_1)P_L(k_3) + 2F_2(\vec{k}_2, \vec{k}_3)P_L(k_2)P_L(k_3), \tag{4.38}$$

where $P_L(k, a)$ denotes the linear matter power spectrum.

For the specific configuration considered in this work, the bispectrum can be written as

$$B(\theta, a) = 2\Big[F_{212}(\theta)P_L(2, a)P_L(1, a) + F_{213}(\theta)P_L(2, a)P_L(\sqrt{5}, a) + F_{223}(\theta)P_L(1, a)P_L(\sqrt{5}, a)\Big], \tag{4.39}$$

explicitly displaying its dependence on the opening angle θ and on the cosmic scale factor a.

In order to isolate the dependence on triangle shape and to reduce sensitivity to the overall amplitude of the power spectrum, it is customary to introduce the reduced bispectrum,

$$\tilde{Q}^{(0)} = \frac{B(\theta, a)}{P_L(\vec{k}_1, a)P_L(\vec{k}_2, a) + P_L(\vec{k}_1, a)P_L(\vec{k}_3, a) + P_L(\vec{k}_2, a)P_L(\vec{k}_3, a)}. \tag{4.40}$$

In the EdS approximation, where the second-order kernel F_2 is assumed to be time independent and universal, the reduced bispectrum becomes effectively insensitive to the underlying cosmological model. In this case, all explicit model dependence cancels out, and $\tilde{Q}^{(0)}$ depends only on the geometry of the triangle formed by the wavevectors. This property has motivated the widespread use of the reduced bispectrum as a robust, nearly model-independent observable in large-scale structure analyses.

However, this simplification no longer holds when the full time dependence of the perturbative kernels is taken into account. In more general cosmological scenarios—such as interacting dark sector models—the evolution of F_2 depends explicitly on the background dynamics and on the growth history of perturbations. As a consequence, the reduced bispectrum acquires a genuine

model dependence, even at tree level. This effect is clearly evidenced in Fig. 5.8, where the reduced bispectrum exhibits significant deviations between different cosmological models once the temporal evolution of the kernels is properly included.

The results presented here demonstrate that the reduced bispectrum is not a universal quantity, but rather a sensitive probe of the underlying cosmological model when time-dependent kernels are employed. This sensitivity highlights the limitations of the EdS approximation and underscores the importance of using fully time-evolved perturbative kernels in precision studies of higher-order statistics. The reduced bispectrum therefore provides a powerful diagnostic for distinguishing between ΛCDM and alternative cosmological scenarios, offering direct insight into the nonlinear dynamics governing structure formation.

Results

In this chapter, we present the main conclusions of the work together with a set of relevant findings that emerged throughout the analysis. After obtaining the analytical expressions for the perturbative kernels, our goal was to solve the corresponding evolution equations and extract quantitative results for the time-dependent coefficients. However, during this process, we encountered several numerical difficulties. Consequently, this work proposes an alternative method that simplifies the solution of these equations and avoids the instabilities that arise in the standard numerical procedure.

5.1. Numerical Computation of Kernels

In this section, we present the numerical results for the time-dependent perturbative kernels derived in the previous sections. The purpose of this analysis is twofold: first, to describe in a clear and systematic manner the numerical strategy adopted to solve the kernel evolution equations, and second, to assess the impact of time dependence in both the standard ΛCDM cosmology and in interacting dark sector (IDS) models.

Our numerical approach is based on a recursive, grid-based integration of the coupled systems of ordinary differential equations governing the perturbative kernels. This strategy naturally follows the hierarchical structure of cosmological perturbation theory. We begin at second order by solving the coupled equations for the kernels F_2 and G_2, given in Eqs. (3.47) and (3.48). The equations are integrated on a two-dimensional grid spanning wavenumber and redshift,

$$k \in [10^{-3},\, 10]\,\mathrm{Mpc}^{-1}, \qquad z \in [0,\, 50].$$

Once the numerical solutions are obtained on the grid, the kernels are interpolated to arbitrary configurations, as required by the convolution integrals entering higher-order perturbative calculations.

The interpolated second-order kernels are then used as inputs for the third-order evolution equations. Since the source terms of the third-order system depend explicitly on F_2 and G_2, the solution naturally proceeds in a recursive manner. Using the same grid-based integration and interpolation strategy, we solve the coupled equations for the third-order kernels F_3 and G_3, given in Eqs. (3.66). This procedure ensures a consistent and fully time-dependent treatment of the perturbative hierarchy at each order.

Before turning to interacting dark sector models, we first apply this numerical framework to the ΛCDM case. This step serves as a validation of our numerical implementation and as a benchmark against the well-known Einstein–de Sitter (EdS) kernels. In Fig. 5.1, we show the ratio of the numerically computed second-order kernels F_2 and G_2 in ΛCDM to their EdS

counterparts, focusing on the equilateral configuration $k_1 = k_2$, corresponding to $r = 1$. To guide the eye, a shaded grey band indicating a 1% deviation from the EdS prediction is included in the figure.

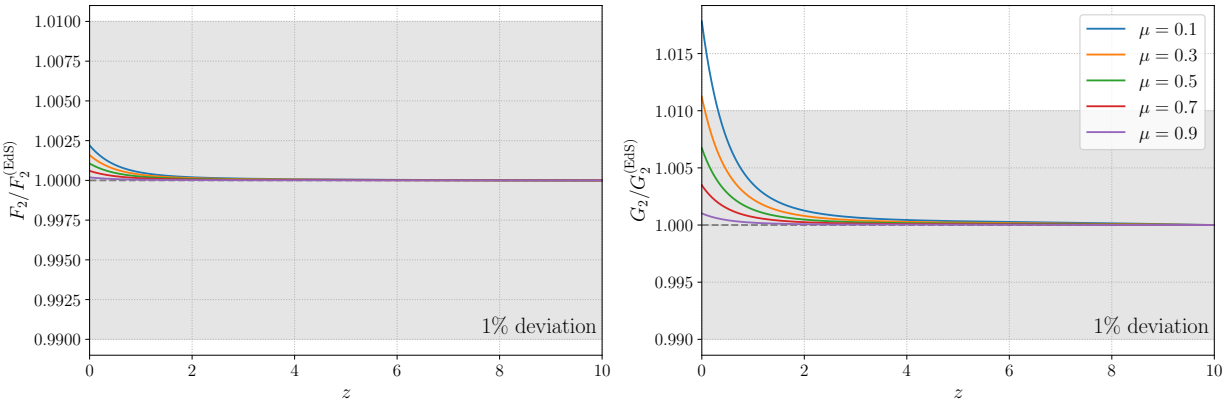

Figure 5.1.: Deviation of the second-order kernels F_2 (left) and G_2 (right) in the ΛCDM model relative to their Einstein–de Sitter counterparts, shown as a function of redshift for the equilateral configuration ($r = 1$).

While the equilateral configuration suffices to illustrate the main qualitative behavior, a more comprehensive exploration of triangle shapes is required in order to probe the dependence of the kernels on both scale ratios and relative orientations of the wavevectors. For this reason, a broader set of configurations is presented in Appendix C, covering

$$r = \{0.1,\ 2,\ 5,\ 10\}, \qquad \mu = \{0.1,\ 0.3,\ 0.5,\ 0.7,\ 0.9\},$$

where $r \equiv k_2/k_1$ controls the relative magnitudes of the interacting modes, and μ denotes the cosine of the angle between the wavevectors, defined as

$$\mu \equiv \frac{\mathbf{k}_1 \cdot \mathbf{k}_2}{k_1 k_2}. \tag{5.1}$$

Therefore, varying μ corresponds to scanning different relative orientations between $\mathbf{k}_1$ and $\mathbf{k}_2$, ranging from nearly orthogonal configurations ($\mu \approx 0$) to nearly collinear ones ($\mu \approx 1$). Together, the parameters r and μ allow one to explore squeezed, equilateral, and elongated triangle configurations across a wide range of geometries in Fourier space.

In all configurations analyzed, the deviations from the EdS kernels remain small across the full redshift interval, typically at or below the percent level.

We now extend the analysis to the third-order kernels in the ΛCDM model. In Fig. 5.2, we present the ratios of the numerically computed F_3 and G_3 kernels to their EdS counterparts for the equilateral configuration $k_1 = k_2 = k_3$, corresponding to $r_2 = r_3 = 1$. Different relative orientations are probed by varying the angular cosines μ_{12} and μ_{13} within the set $\{0.1, 0.5, 0.9\}$.

As in the second-order case, the deviations of F_3 remain sub-percent over the entire redshift range, while the deviations of G_3 are slightly larger, reaching the level of $\sim 1\%$. Given the increasing complexity of the vector configurations entering the third-order kernels and the recursive structure of the perturbative hierarchy, we restrict the third-order analysis to this representative configuration.

Taken together, these results confirm that, although the ΛCDM kernels are formally time dependent, the EdS approximation provides an excellent description of their evolution. This

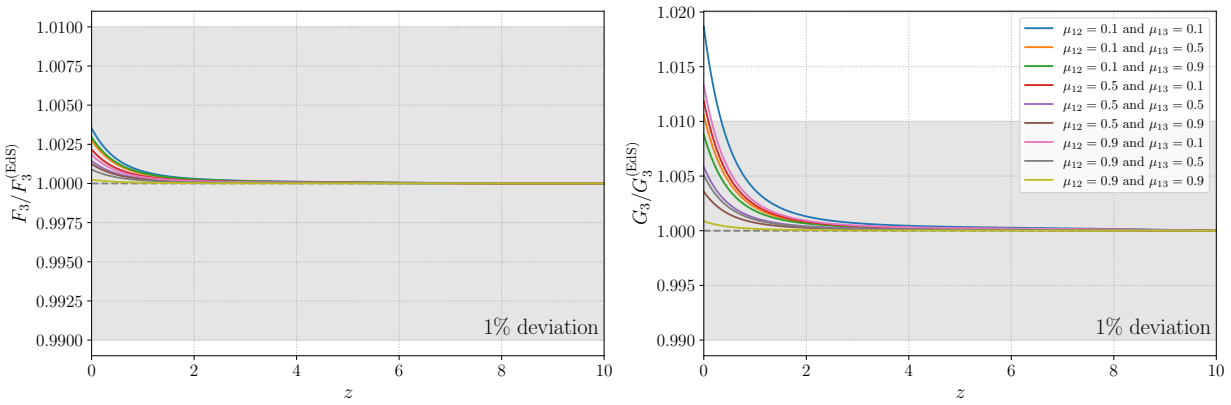

Figure 5.2.: Deviation of the third-order kernels F_3 (left) and G_3 (right) in the ΛCDM model relative to their Einstein–de Sitter counterparts, shown as a function of redshift for the equilateral configuration ($r_2 = r_3 = 1$).

agreement serves as an important consistency check of our numerical pipeline and validates the recursive grid-based integration and interpolation procedure adopted in this work.

We now repeat the same analysis for the interacting dark sector (IDS) scenario, using exactly the same set of triangle configurations adopted in the ΛCDM validation. Figure 5.3 shows the ratios of the second-order kernels F_2 and G_2 in the IDS model relative to their EdS counterparts for the equilateral configuration, while results for additional triangle shapes and orientations are presented in Appendix C.

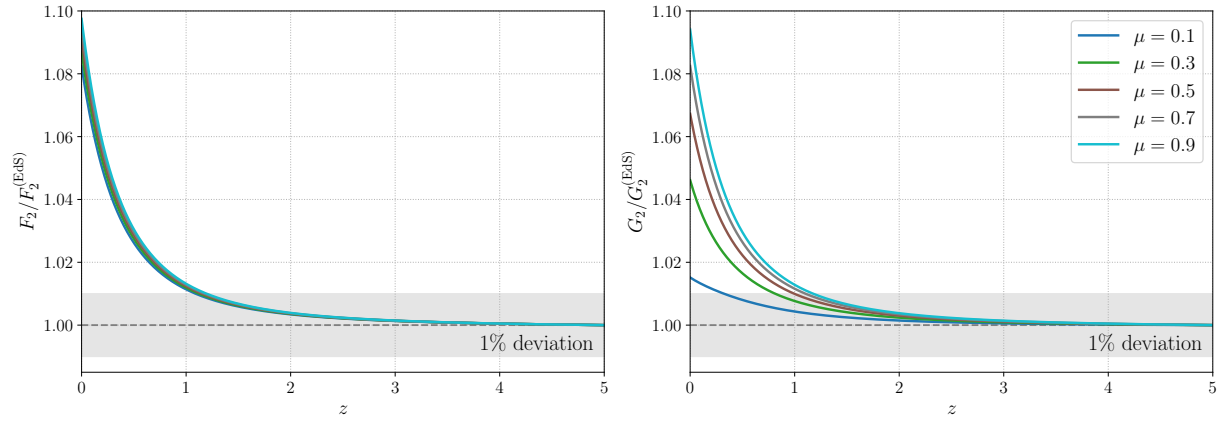

Figure 5.3.: Deviation of the second-order kernels F_2 (left) and G_2 (right) in interacting dark sector models relative to their Einstein–de Sitter counterparts, shown as a function of redshift for the equilateral configuration ($r = 1$).

In contrast to the ΛCDM case, the IDS kernels exhibit significantly larger deviations. Depending on the triangle shape and orientation, departures from the EdS limit reach the few-percent level and can approach $\sim 10\%$ at low redshift.

We finally extend the analysis to the third-order kernels in the IDS scenario. In Fig. 5.4, we display the ratios of the F_3 and G_3 kernels to their EdS counterparts for the equilateral configuration $k_1 = k_2 = k_3$ ($r_2 = r_3 = 1$), varying the relative orientations through μ_{12} and μ_{13}. Additional configurations obtained by permuting r_2, $r_3 \in \{0.1, 2, 10\}$ are collected in Appendix C.

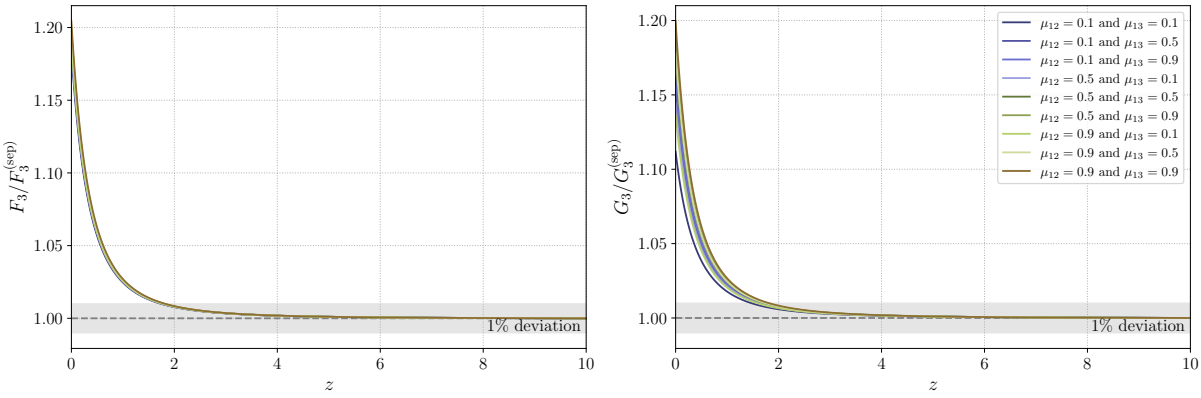

Figure 5.4.: Deviation of the third-order kernels F_3 (left) and G_3 (right) in interacting dark sector models relative to their Einstein–de Sitter counterparts, shown as a function of redshift for the equilateral configuration ($r = 1$).

Compared to the second-order case, the impact of the interaction is even more pronounced at third order. The deviations of F_3 and G_3 from their EdS limits reach several percent at low redshift. This behavior is physically expected, since at third order the time dependence induced by the interaction enters not only through the kernel evolution coefficients, but also through the source terms, which explicitly depend on the lower-order kernels F_2 and G_2. As a result, the interaction-driven time dependence propagates cumulatively along the perturbative hierarchy.

These numerical findings are fully consistent with the theoretical analysis presented in Sec. 3.6. The presence of a dark sector interaction modifies the effective growth rate and introduces explicit time dependence in the coefficients governing the kernel evolution, leading to a breakdown of the EdS approximation even for relatively small couplings. Retaining the full time dependence of the perturbative kernels is therefore essential for a consistent one-loop description of nonlinear structure formation in interacting dark sector cosmologies.

5.2. Numerical Computation of One-Loop Power Spectrum Contributions

A further major numerical challenge addressed in this work concerns the evaluation of the one-loop contributions to the matter power spectrum, schematically represented by integrals of the form given in Eq. (4.30). From a numerical standpoint, the direct computation of these loop integrals in Cartesian momentum space is both computationally demanding and susceptible to spurious divergences, which arise from cancellations between different regions of the integrand and from the highly oscillatory behavior of the kernel functions.

To overcome these difficulties, we adopt a more suitable parametrization of the loop momentum by rewriting the integration variable $\vec{p}$ in terms of the dimensionless variables (r, x), defined as

$$r \equiv \frac{p}{k}, \qquad x \equiv \cos\theta = \hat{p} \cdot \hat{k}, \qquad |\vec{k} - \vec{p}| = k\sqrt{1 + r^2 - 2rx}. \tag{5.2}$$

Here, r measures the magnitude of the loop momentum relative to the external scale k, while x encodes the angular dependence between the vectors $\vec{p}$ and $\vec{k}$. This change of variables makes the physical structure of the integrals more transparent, separating radial and angular contributions and explicitly exposing the dependence on the external wavenumber.

Under this transformation, the integration measure simplifies considerably. Writing the volume element in spherical coordinates and expressing it in terms of the new variables, one finds

$$d^3p = p^2\, dp\, d\Omega = k^3 r^2\, dr\, dx\, d\mathcal{A}. \tag{5.3}$$

This form is particularly convenient for numerical implementation, as it reduces the original three-dimensional integral to a two-dimensional integral over r and x, with the azimuthal angle $\mathcal{A}$ contributing only a trivial factor.

Using these variables, the one-loop contribution $P^{(22)}$, which arises from the autocorrelation of second-order density perturbations, can be rewritten as

$$\begin{aligned} P^{(22)}_{\delta\delta}(k,a) &= 2\int \frac{d^3p}{(2\pi)^3}\left[F_2(\vec{p},\vec{k}-\vec{p};a)\right]^2 P_L(p,a)\, P_L(|\vec{k}-\vec{p}|,a) \\ &= \frac{k^3}{2\pi^2}\int_0^\infty dr\, r^2 \int_{-1}^1 dx\, \left[F_2\Big(kr,\ k\sqrt{1+r^2-2rx};a\Big)\right]^2 \\ &\times\ P_L(kr,a)\, P_L\Big(k\sqrt{1+r^2-2rx},a\Big). \end{aligned} \tag{5.4}$$

In this expression, the dependence on the internal momentum configurations is entirely captured by the variables r and x, while the linear power spectra P_L weight the contribution of each mode to the loop integral. The prefactor $k^3/(2\pi^2)$ arises from the angular integration and ensures the correct normalization.

Similarly, the $P^{(13)}$ contribution, which describes the coupling between first- and third-order density perturbations, can be expressed as

$$\begin{aligned} P^{(13)}_{\delta\delta}(k,a) &= 3\, P_L(k,a)\int \frac{d^3p}{(2\pi)^3}\, F_3(\vec{p},-\vec{p},\vec{k};a)\, P_L(p,a) \\ &= \frac{3\,k^3}{2\pi^2}\, P_L(k,a)\int_0^\infty dr\, r^2\, F_3(kr,-kr,k;a)\ P_L(kr,a). \end{aligned} \tag{5.5}$$

Here, the angular dependence is entirely absorbed into the kernel F_3, evaluated in the specific folded configuration $(\vec{p},-\vec{p},\vec{k})$, which naturally emerges in the structure of the $P^{(13)}$ term.

It is important to emphasize that this change of variables is not novel and has been widely employed in the literature. Several studies have adopted equivalent parametrizations when computing one-loop corrections to the matter power spectrum, as they allow one to isolate the angular dependence, improve numerical stability, and avoid artificial divergences associated with Cartesian momentum integrations [13, 12, 11]. The present analysis follows this well-established strategy, which has proven to be both efficient and robust across a broad class of cosmological models.

We developed a numerical code named SPTIDS, which has been made publicly available on GitHub so that any interested reader may incorporate it into their own research for more details see Appendix B. Using this tool, we computed the power spectrum for both the standard scenario and for the interacting dark sector model considered in this work. For the ΛCDM case, the results show that allowing the kernels to vary in time leads to a percent-level deviation when compared with the EdS approximation. In contrast, for the interacting model characterized by $Q = 3\gamma H\rho_\Lambda$, the discrepancy relative to the EdS-based solution becomes significantly larger, exceeding five percent. This behavior indicates that the commonly used approximation $\Omega_m/f^2 \simeq 1$ is not valid in cosmological scenarios that include interactions within the dark sector.

5.3. One-Loop Matter Power Spectrum in the Interacting Dark Sector Model

One of the main results of this dissertation is the computation and analysis of the one-loop matter power spectrum in cosmological models with an interacting dark sector. This calculation provides a concrete quantitative assessment of how dark sector interactions modify the nonlinear growth of cosmic structures and, crucially, demonstrates the limitations of commonly adopted approximations based on time-independent perturbative kernels. The results presented in this section establish that a fully time-dependent treatment of the perturbative kernels is not merely a refinement, but a necessary ingredient for accurately describing nonlinear clustering in interacting scenarios.

The nonlinear matter power spectrum is constructed by including the leading one-loop corrections to the linear spectrum, which encode mode-coupling effects arising from second- and third-order perturbations. In order to render the numerical computation tractable while preserving the dominant physical contributions, we employ an angular-averaged formulation of the perturbative kernels. This approach allows for a stable and computationally efficient evaluation of the one-loop terms, while retaining sensitivity to the time evolution of the kernels induced by the interaction in the dark sector.

The resulting spectra for the standard ΛCDM model are shown in Fig. 5.5. In the upper panel, the total nonlinear power spectrum $P_{\rm NL}$ is compared with its counterpart $P_{\rm NL}^{\rm (EdS)}$ obtained under the Einstein–de Sitter (EdS) approximation, together with the linear power spectrum $P_{\rm lin}$. The lower panel displays the ratio $P_{\rm NL}/P_{\rm NL}^{\rm (EdS)}$, which provides a direct measure of the impact of the time dependence of the perturbative kernels. In the ΛCDM case, this ratio remains close to unity over most of the probed scales, indicating that the EdS approximation captures the dominant nonlinear behavior with reasonable accuracy, although small but systematic deviations already emerge in the mildly nonlinear regime.

A markedly different behavior is observed in the interacting dark sector scenario, as shown in Fig. 5.6. The upper panel presents the total nonlinear power spectrum in the IDS model, again contrasting the fully time-dependent result $P_{\rm NL}$ with the EdS-based spectrum $P_{\rm NL}^{\rm (EdS)}$ and the corresponding linear spectrum. The most striking feature appears in the lower panel, where the ratio $P_{\rm NL}/P_{\rm NL}^{\rm (EdS)}$ exhibits substantial deviations from unity across a wide range of scales. These deviations reach and exceed the level of 15%, clearly demonstrating that the EdS approximation breaks down once dark sector interactions are introduced. Unlike the ΛCDM case, the discrepancy is not confined to deeply nonlinear scales, but extends into the mildly nonlinear regime, underscoring the strong sensitivity of the power spectrum to the temporal evolution of the perturbative kernels.

This pronounced departure constitutes one of the central findings of this dissertation. It provides direct numerical evidence that interacting dark sector models intrinsically require time-dependent perturbative kernels for a consistent description of nonlinear structure formation. The assumption of time-independent kernels, implicit in the EdS approximation, leads to systematic errors that are well above the precision targets of current and forthcoming large-scale structure surveys. Consequently, any perturbative framework aimed at confronting interacting dark sector models with observational data must abandon the EdS assumption in favor of a fully time-resolved treatment.

A direct comparison between the nonlinear corrections in the IDS and ΛCDM models is presented in Fig. 5.7. This figure highlights that the post–Newtonian leading-order (PNLO) contributions are significantly enhanced in the interacting case, reflecting the cumulative impact

of dark sector interactions on mode coupling and nonlinear growth. At the same time, this comparison illustrates the numerical challenges associated with summing multiple nonlinear contributions, reinforcing the importance of the approximation strategies developed in this work to ensure numerical stability and physical consistency.

In summary, the computation of the one-loop matter power spectrum in interacting dark sector models represents a key numerical achievement of this dissertation. The results presented here demonstrate that dark sector interactions leave a substantial imprint on nonlinear clustering and render the Einstein–de Sitter approximation inadequate. This finding provides strong motivation for the development and application of fully time-dependent perturbative approaches in precision cosmology.

In the following section, the analysis is extended beyond two-point statistics to the matter bispectrum. As the lowest-order statistic that directly probes mode coupling and genuinely nonlinear gravitational effects, the bispectrum is expected to be even more sensitive to the time dependence of perturbative kernels induced by dark sector interactions. This extension will allow us to further assess the distinctive nonlinear signatures of interacting dark sector models and their potential observational relevance.

In the following section, we extend the analysis beyond two-point statistics and investigate the impact of interacting dark sector (IDS) models on the matter bispectrum. As the lowest-order statistic sensitive to mode coupling and genuinely nonlinear gravitational effects, the bispectrum provides a complementary and more stringent probe of departures from the standard ΛCDM scenario. In particular, it is expected to be especially sensitive to modifications in the time evolution of perturbative kernels induced by dark sector interactions. By analyzing the bispectrum within the same fully time-dependent perturbative framework developed in this work, we aim to assess how IDS models modify the amplitude and shape dependence of three-point correlations, and to identify distinctive nonlinear signatures that may serve as observational discriminants in the era of precision cosmology.

5.4. Bispectrum in the Interacting Dark Sector Model

In order to further investigate the impact of dark sector interactions on nonlinear structure formation, we now turn our attention to the matter bispectrum. As the lowest-order statistic that directly probes mode coupling and genuinely nonlinear gravitational effects, the bispectrum provides a natural extension of the power spectrum analysis and a more sensitive diagnostic of deviations from the standard ΛCDM scenario.

Adopting an interaction parameter $\gamma = 0.05$, we compute the matter bispectrum within the interacting dark sector (IDS) model and present the results in Fig. 5.8. The calculation is performed using the reduced bispectrum defined in Eq. 4.40, which isolates the nonlinear contributions by factoring out the overall power spectrum dependence. This formulation allows for a clearer comparison between different cosmological models and highlights the intrinsic non-Gaussian features generated by gravitational evolution.

As shown in Fig. 5.8, the presence of dark sector interactions leads to a clear enhancement of the bispectrum amplitude relative to the standard ΛCDM prediction. This enhancement is a direct consequence of the modified growth history induced by the interaction, which amplifies nonlinear mode coupling and accelerates the formation of inhomogeneities. In contrast to the power spectrum, where interaction effects may partially mimic changes in background parameters, the bispectrum responds more directly to the altered dynamics of perturbations, making the impact of the interaction particularly evident.

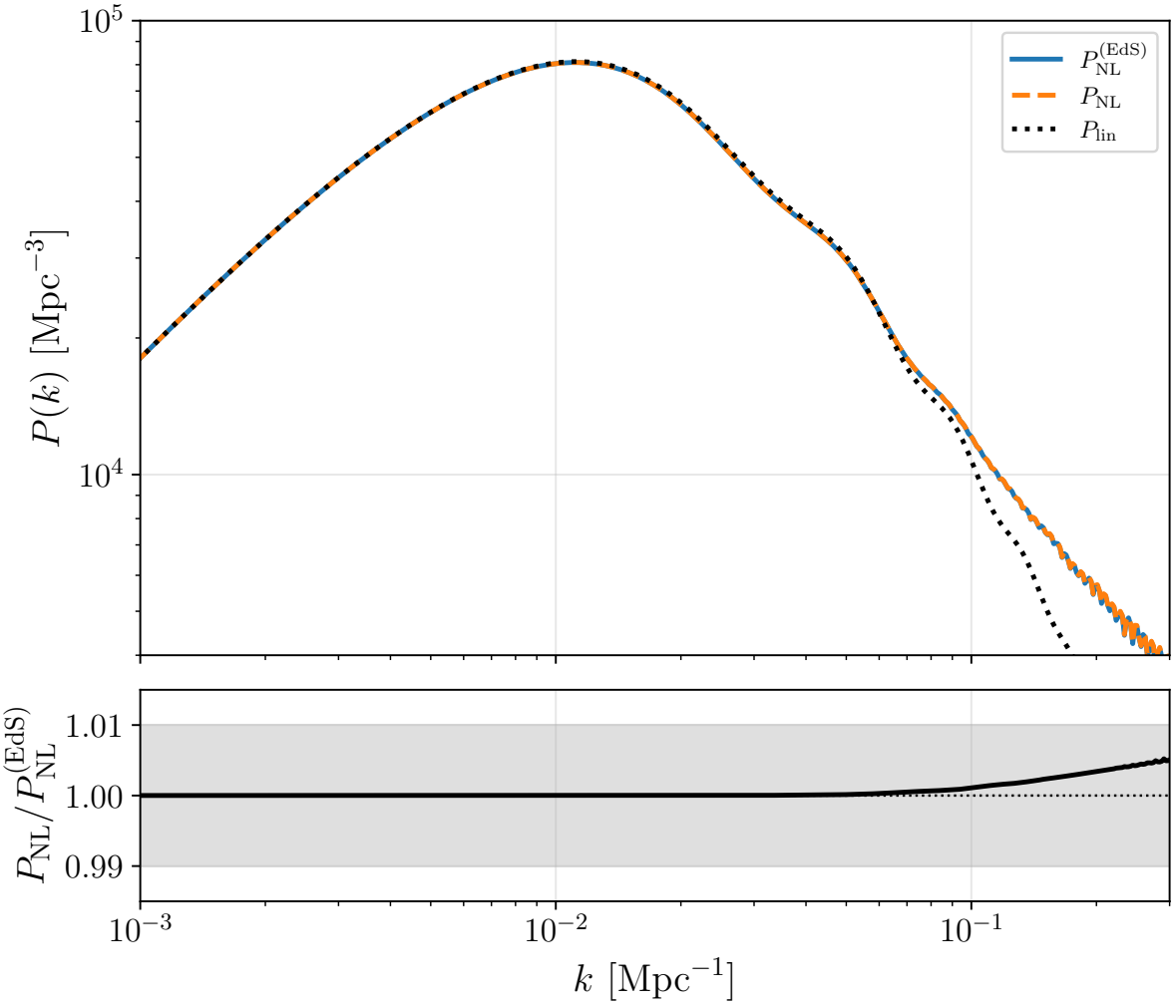

Figure 5.5.: Total matter power spectrum in the ΛCDM model. The curve $P_{\rm NL}^{\rm (EdS)}$ denotes the nonlinear power spectrum computed using the Einstein–de Sitter approximation, while $P_{\rm NL}$ includes the effects of the time dependence of the perturbative kernels. The dotted line corresponds to the linear ΛCDM power spectrum. The lower panel shows the ratio $P_{\rm NL}/P_{\rm NL}^{\rm (EdS)}$, highlighting the deviations induced by the temporal evolution of the kernels with respect to the EdS approximation, particularly on nonlinear scales.

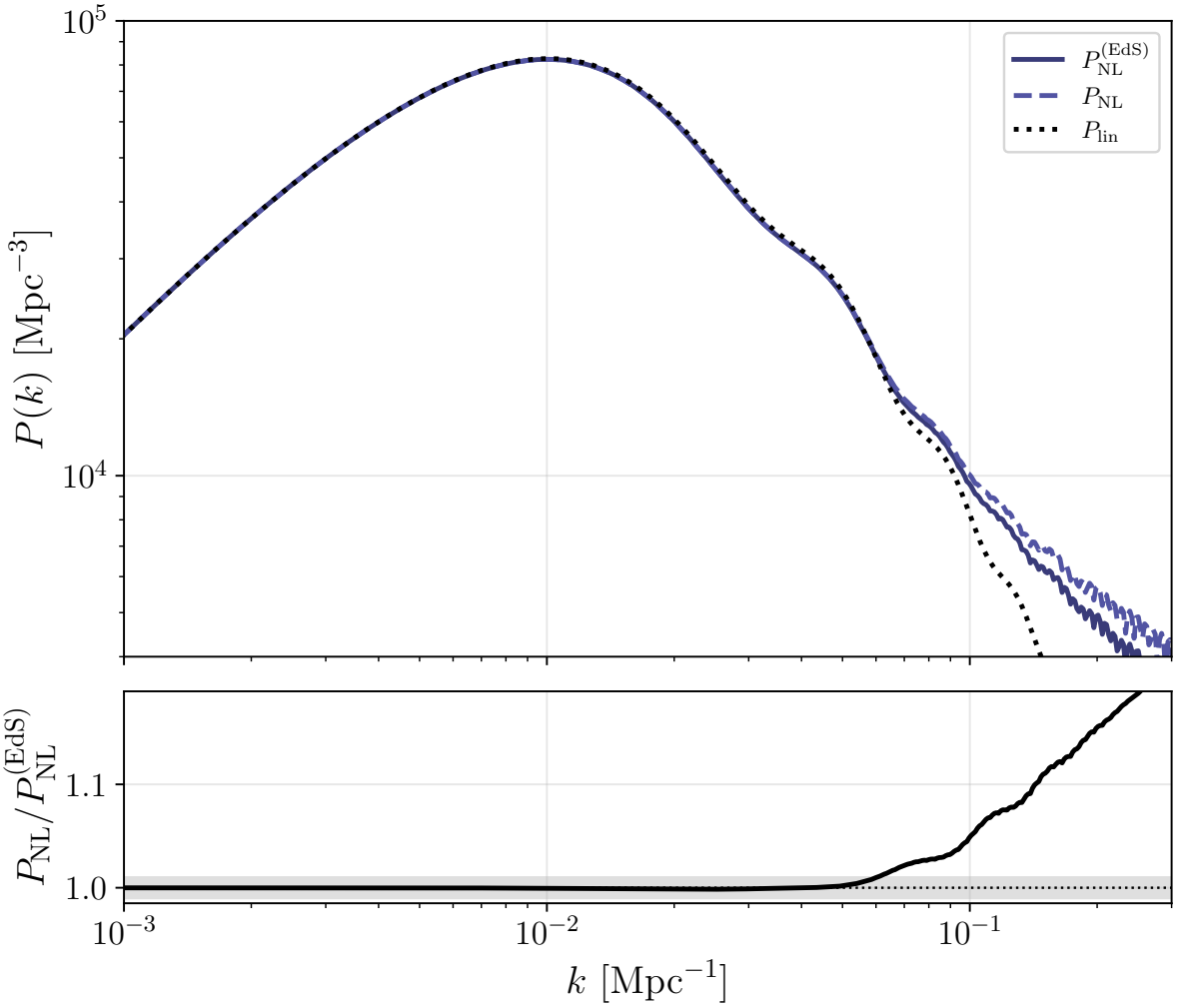

Figure 5.6.: Total matter power spectrum in the interacting dark sector (IDS) model for $\gamma = +0.05$. The curve $P_{\rm NL}^{\rm (EdS)}$ represents the nonlinear power spectrum obtained under the Einstein–de Sitter approximation, whereas $P_{\rm NL}$ includes the full time dependence of the perturbative kernels induced by the dark sector interaction. The dotted line corresponds to the linear power spectrum in the IDS scenario. The lower panel shows the ratio $P_{\rm NL}/P_{\rm NL}^{\rm (EdS)}$ and reveals a pronounced departure from unity when compared to the ΛCDM case. This behavior indicates that dark sector interactions significantly modify the nonlinear evolution of density perturbations, enhancing the sensitivity of the power spectrum to the temporal evolution of the kernels and leading to stronger deviations from the Einstein–de Sitter approximation, especially on nonlinear scales.

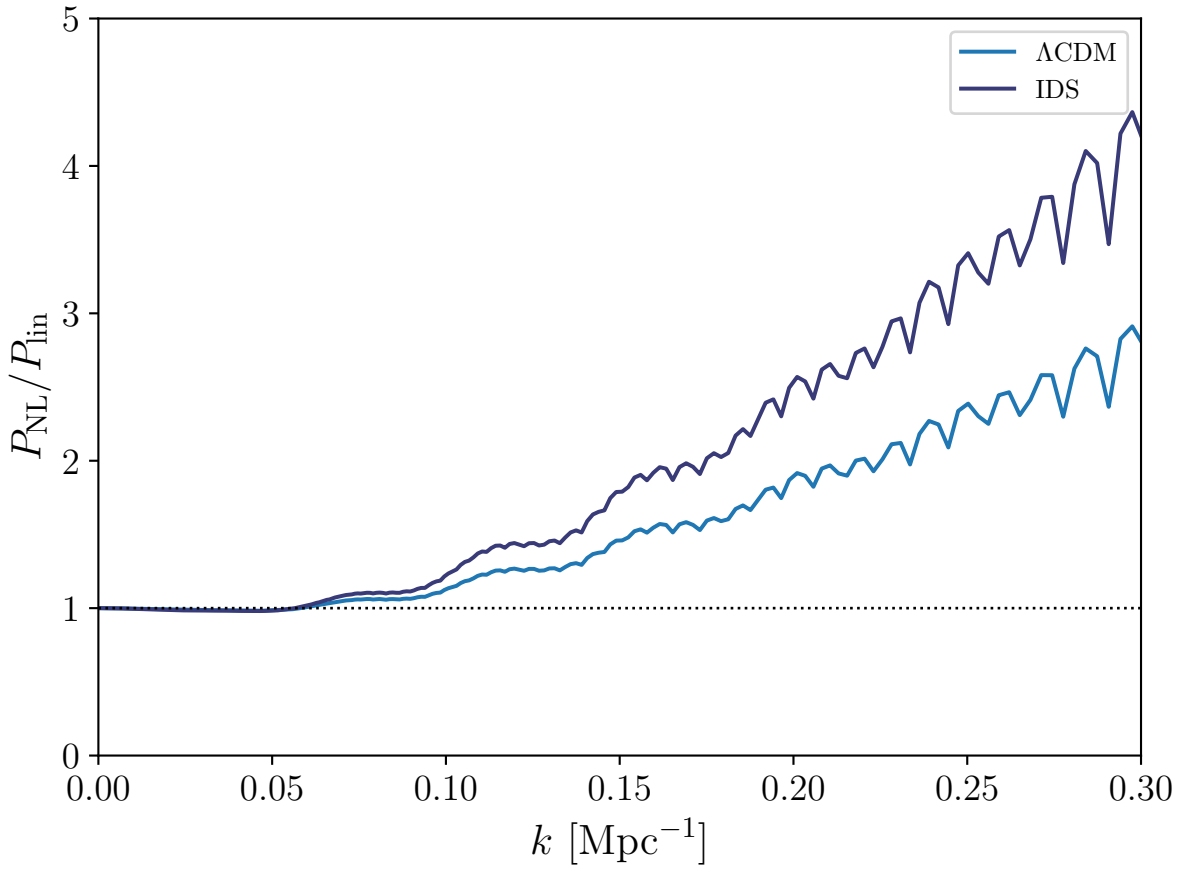

Figure 5.7.: Comparison of post–Newtonian leading-order (PNLO) corrections between the standard ΛCDM model and the Interacting Dark Sector (IDS) scenario. The figure shows that in the IDS model, the PNLO corrections are significantly enhanced, reflecting the stronger impact of dark sector interactions on the nonlinear evolution of cosmic structures.

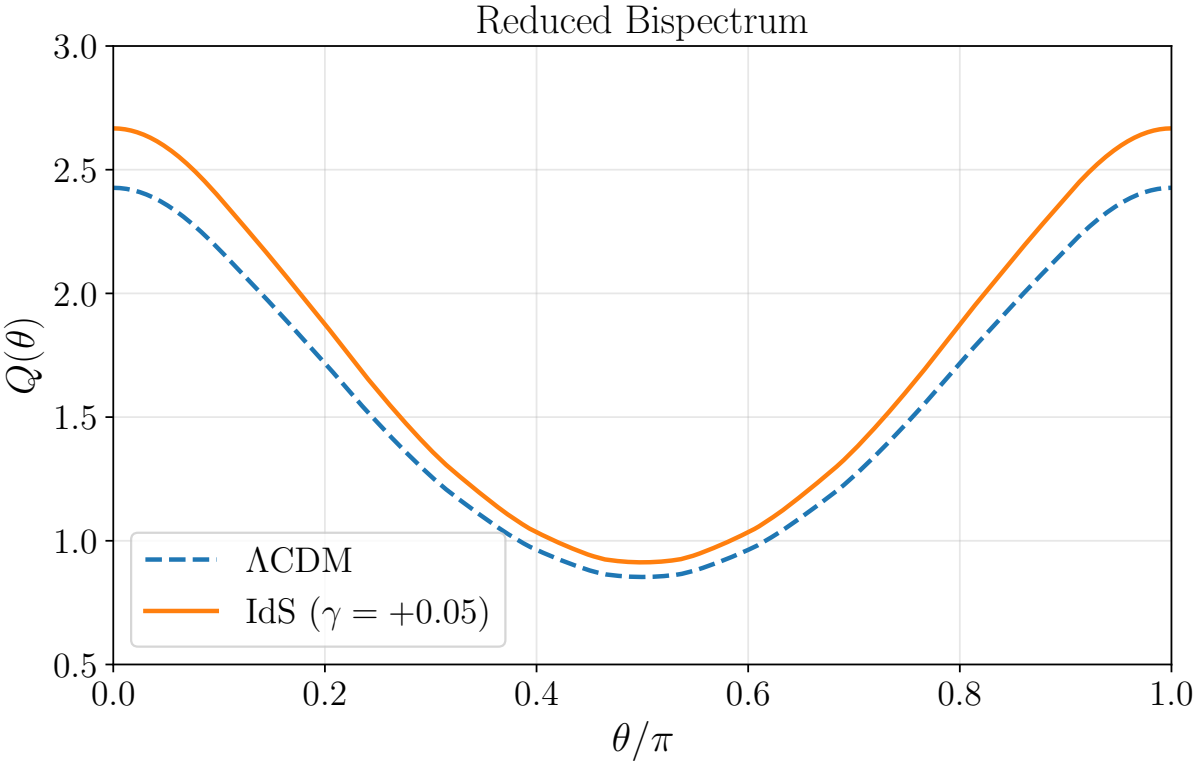

Figure 5.8.: Comparison of the bispectrum between the standard ΛCDM model and the Interacting Dark Sector (IDS) model. The presence of interactions in the dark sector enhances the growth of inhomogeneities, leading to an overall increase in the bispectrum amplitude. This highlights the significant effect that dark sector interactions can have on higher-order correlations in the matter distribution.

The observed differences demonstrate that the IDS model leaves a distinctive imprint on the three-point correlation function of the matter density field. This result indicates that higher-order statistics are especially well suited to capture the effects of dark matter–dark energy interactions, as they probe combinations of perturbative kernels whose time evolution is directly modified by the interaction terms. Consequently, the bispectrum provides an additional and complementary avenue for testing interacting cosmologies beyond what can be achieved with two-point statistics alone.

Overall, this analysis shows that the effects of dark sector interactions are not only present but clearly visible in the bispectrum, reinforcing the importance of incorporating higher-order statistics in precision cosmology studies. These findings support the use of the bispectrum as a powerful observational discriminator between the standard ΛCDM model and alternative scenarios with interacting dark components, particularly in the context of current and forthcoming large-scale structure surveys.

5.5. Directions for Future Research

The work developed in this dissertation establishes a consistent and fully time-dependent perturbative framework for cosmological models with interactions in the dark sector, enabling the

explicit computation of both the matter power spectrum and the matter bispectrum beyond the standard Einstein–de Sitter approximation. It is important to stress, however, that the perturbative results derived here are strictly valid for modes that enter the horizon during the matter-dominated era, where the underlying assumptions of the formalism remain well justified. Outside this regime, additional physical effects may alter the dynamical evolution and require further refinement of the treatment.

The analysis demonstrates that dark sector interactions leave measurable imprints on nonlinear clustering statistics, particularly at the level of higher-order correlations. A key theoretical result of this dissertation is the explicit identification of the nontrivial time dependence of perturbative kernels in interacting models, which prevents the simple factorization typically assumed under the Einstein–de Sitter approximation.

A natural and essential continuation of this research is the direct confrontation of these theoretical predictions with observational data. In practice, this involves modeling the clustering of galaxies, which act as biased tracers of the underlying matter distribution, and consistently incorporating redshift-space distortions, survey geometry, and observational systematics. This data-driven perspective will form the central objective of the forthcoming doctoral project, where the formalism developed here will be embedded into likelihood-based analyses tailored to current and upcoming galaxy surveys. Such an approach will allow a quantitative assessment of the observational viability of interacting dark sector models and of their distinguishability from the standard ΛCDM scenario.

From a theoretical standpoint, the perturbative structure derived in this dissertation allows, in principle, the computation of statistical quantities at arbitrary loop order. This opens the possibility of investigating both the numerical convergence of the implemented algorithms and the convergence of the perturbative expansion itself. These two aspects are conceptually distinct: numerical convergence refers to the stability and precision of the integration procedures and discretization schemes employed, whereas perturbative convergence concerns the hierarchy of loop corrections and the regime in which higher-order contributions remain subdominant. In interacting dark sector models, modified growth histories may shift the onset of nonlinearity and alter the relative importance of loop terms, making a systematic study of convergence particularly relevant.

Furthermore, although the present treatment relies primarily on the fluid description truncated at the lowest moments, the formalism can be consistently extended using kinetic theory. By starting from the Boltzmann equation and deriving the evolution of perturbations beyond the approximation based solely on the first moments of the distribution function, it becomes possible to capture additional physical effects and assess the validity of the fluid truncation in interacting scenarios.

Another aspect that deserves further investigation concerns the coupling between scalar perturbations and vector modes. While vector perturbations typically decay in standard cosmology and are therefore neglected at linear order, interactions in the dark sector may, in principle, induce nontrivial mode couplings. A systematic study of these effects would clarify whether additional degrees of freedom contribute to nonlinear clustering observables.

Beyond two- and three-point statistics, the framework developed here can be naturally extended to higher-order statistical moments of the matter density field, such as skewness and kurtosis. These observables probe increasingly nonlinear combinations of perturbations and may be especially sensitive to departures from standard gravitational dynamics. The nonlinear effects identified throughout this work suggest that higher-order statistics may serve as powerful discriminators between cosmological models, particularly in scenarios where degeneracies persist at the level of lower-order correlations.

Taken together, these considerations indicate that the results obtained in this dissertation represent not an endpoint, but rather the foundation of a broader research program. By combining fully time-dependent perturbation theory, a systematic study of convergence properties, kinetic-theory extensions, and observational data analysis, future work aims to deepen our understanding of structure formation in interacting dark sector models and to explore new strategies for breaking degeneracies associated with dark energy in the era of precision cosmology.

Virtues of Fourier Space

One of the key advantages of Fourier analysis in cosmology is its ability to simplify the treatment of differential equations governing perturbations. In real space, fields such as the density contrast and velocity divergence are coupled through partial derivatives, making the system highly non-trivial to solve. By contrast, in Fourier space, spatial derivatives are mapped into multiplicative factors of the wavenumber vector. This transformation diagonalizes the equations with respect to modes of different scales, allowing each Fourier mode to evolve independently at linear order.

Formally, a scalar field $f(\vec{x})$ in configuration space can be expressed in Fourier space as

$$f(\vec{x}) = \int \frac{d^3k}{(2\pi)^3} f(\vec{k})\, e^{i\vec{k}\cdot\vec{x}}, \tag{A.1}$$

with the inverse relation given by

$$f(\vec{k}) = \int d^3x\, f(\vec{x})\, e^{-i\vec{k}\cdot\vec{x}}. \tag{A.2}$$

A.1. Fourier-Space Representation of Gradient and Inverse-Gradient Operators

The crucial simplification arises because the gradient operator acts as

$$\nabla \quad \longrightarrow \quad i\vec{k}, \tag{A.3}$$

$$\nabla^{-1} \quad \longrightarrow \quad -\frac{i\vec{k}}{|k|^2}, \tag{A.4}$$

so that partial differential equations in real space reduce to ordinary differential equations in Fourier space. This property not only facilitates analytical calculations, but also underlies the efficiency of numerical approaches, where the evolution of perturbations is computed mode by mode.

The Fourier space formalism is therefore not merely a mathematical convenience; it provides a natural language for describing the growth of cosmic structures. By decoupling the evolution of modes at linear order, it allows a transparent connection between the initial conditions of the Universe and the statistical properties of large-scale structure observed today.

A.2. Dirac's Delta in the Fourier Space

It is worth emphasizing that the Dirac delta function possesses remarkable properties that will prove useful in the calculations carried out in this work. This mathematical tool is extensively employed in quantum field theory, and the manipulations we shall perform share strong similarities with those found in that context. In particular, it is important to recall that the integral of a Dirac delta function in real space yields the value of the integrand evaluated at the argument specified by the delta function, as expressed in the equation below,

$$f(\vec{a}) = \int d^3k f(\vec{k})\delta_D(\vec{k} - \vec{a}) \tag{A.5}$$

An important property of the Dirac delta distribution is its representation in Fourier space. In three dimensions, the delta function in real space can be expressed as the Fourier transform of a constant function, namely

$$\delta_D(\vec{k} - \vec{a}) = \int \frac{d^3k}{(2\pi)^3}\, e^{i(\vec{k}-\vec{a})\cdot\vec{x}}. \tag{A.6}$$

This relation highlights the dual role of the Dirac delta in connecting configuration space and Fourier space. It enforces translational invariance by ensuring that the correlation between two points depends only on their separation. Furthermore, the Fourier representation of the delta function is frequently used in cosmology and quantum field theory, since it allows spatial integrals involving convolutions to be rewritten in momentum space as simple algebraic products. This property will be extensively employed in the calculations developed in this work, simplifying the treatment of perturbative quantities by exploiting the natural diagonalization provided by Fourier modes

The SPTIDS code

The code developed as part of this work is publicly available and can be accessed through the following repository: https://github.com/Matheus-Mello123/Matheus-Mestrado.git . This repository contains all scripts, CLASS files, data processing routines, and supplementary materials necessary to reproduce the results presented in this study. In order to execute the computational routines correctly, it is required to utilize the provided CLASS definitions and run the scripts using the Python programming language. Users are encouraged to consult the repository for implementation details, and the code is made available under an open-access framework to promote transparency, reproducibility, and further research, allowing other researchers to fully reproduce and extend the results of this work.

Additional triangle configurations for the kernels

In this Appendix, we present an extended set of triangle configurations employed in the analysis of the second-order perturbative kernels F_2 and G_2. These configurations complement the representative cases discussed in Sec. 5.1 and allow us to assess the robustness of our conclusions against variations in triangle geometry in Fourier space.

For the F_2–G_2 system, the geometry of a triangle formed by two wavevectors $\mathbf{k}_1$ and $\mathbf{k}_2$ is fully characterized by two parameters: the ratio of their magnitudes,

$$r \equiv \frac{k_2}{k_1}, \tag{C.1}$$

and the cosine of the angle between them,

$$\mu \equiv \hat{\mathbf{k}}_1 \cdot \hat{\mathbf{k}}_2. \tag{C.2}$$

These parameters provide an intuitive and convenient way to classify different triangle shapes. Small values of r correspond to squeezed configurations, $r \simeq 1$ describes equilateral triangles, while large values of r represent elongated configurations. Similarly, varying μ allows us to probe different relative orientations between the wavevectors.

In order to explore a broad and representative range of triangle geometries, including squeezed, equilateral, moderately elongated, and highly elongated configurations, we consider the following discrete set of values:

$$r \in \{0.1,\, 2,\, 10\}, \tag{C.3}$$

$$\mu \in \{0.1,\, 0.3,\, 0.5,\, 0.7,\, 0.9\}. \tag{C.4}$$

This choice allows us to systematically investigate the dependence of the second-order kernels on both the relative scale and the angular configuration of the interacting modes.

We begin by presenting the results obtained in the ΛCDM model. Figure C.1 shows the ratios of the numerically computed second-order kernels F_2 and G_2 to their corresponding Einstein–de Sitter (EdS) limits as functions of redshift, for the full set of triangle configurations defined above. For all triangle shapes and orientations considered, the deviations from the EdS kernels remain small, typically at or below the percent level throughout the entire redshift range analyzed.

These results confirm that, although the second-order kernels in ΛCDM are formally time dependent, the EdS approximation provides an excellent description of their evolution across a wide variety of triangle geometries. The extended analysis presented here therefore reinforces the conclusions drawn in Sec. 5.1, demonstrating that they are robust and not sensitive to the specific choice of triangle configuration.

We now turn to the IDS scenario. In Fig. C.2, we show the ratios of the numerically computed second-order kernels to their corresponding EdS limits as functions of redshift for the same extended set of triangle configurations adopted in the ΛCDM analysis. In clear contrast with the standard case, the IDS kernels display substantially larger departures from the EdS approximation. The deviations exhibit a pronounced dependence on redshift, reaching the few-percent level for several configurations and approaching 10% at low redshift in almost all cases. Confirming the analysis made in Sec. 5.1, this behavior is a clear manifestation of the interaction-induced modification of the effective growth rate f_Q and the resulting explicit time dependence of the kernel evolution coefficients.

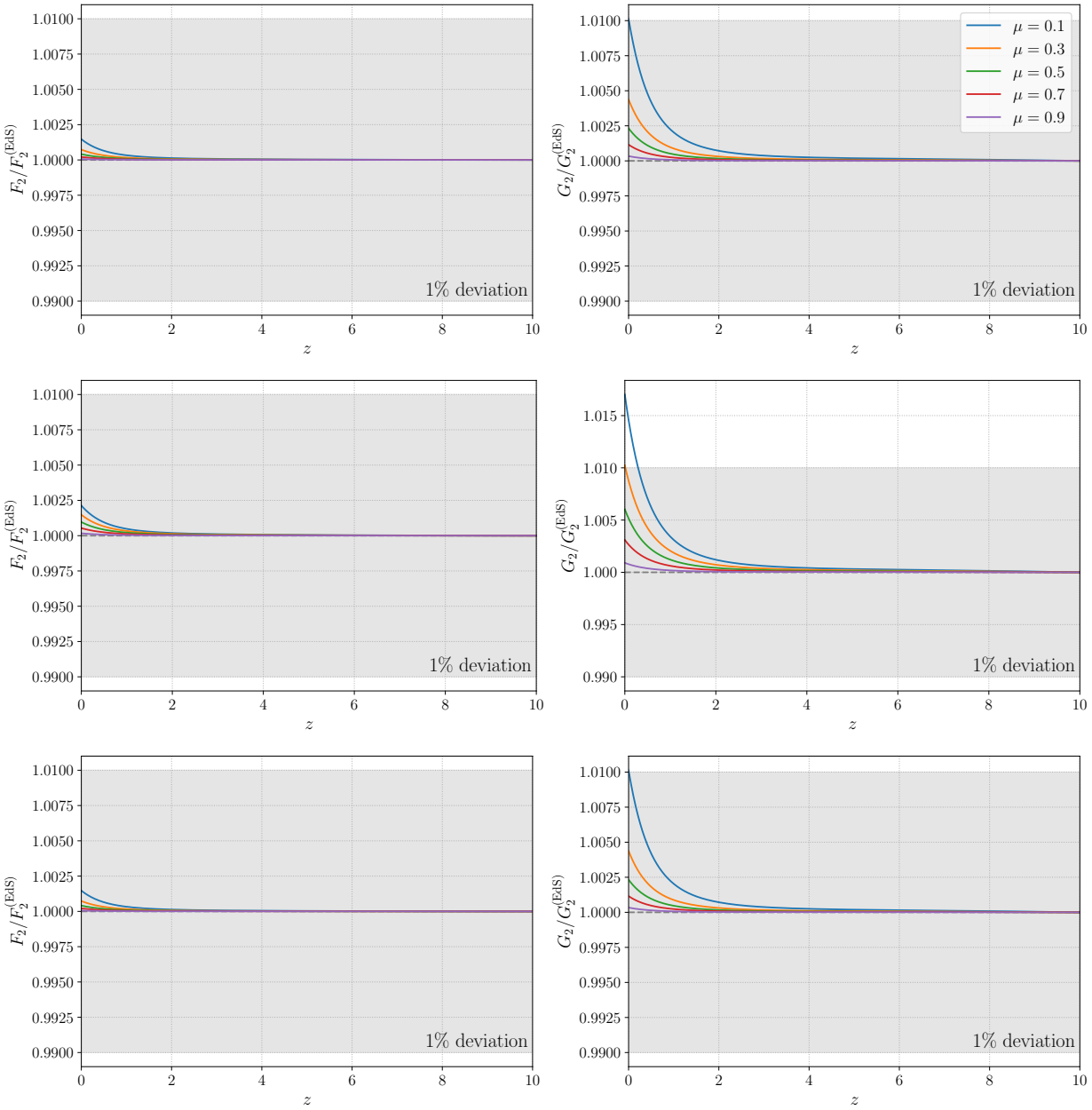

Figure C.1.: Same as Fig. 5.1, but for additional triangle configurations. **(i) Top row:** $r = 0.1$ (squeezed configuration). **(ii) Middle row:** $r = 2$ (moderately elongated configuration). **(iii) Bottom row:** $r = 10$ (highly elongated configuration).

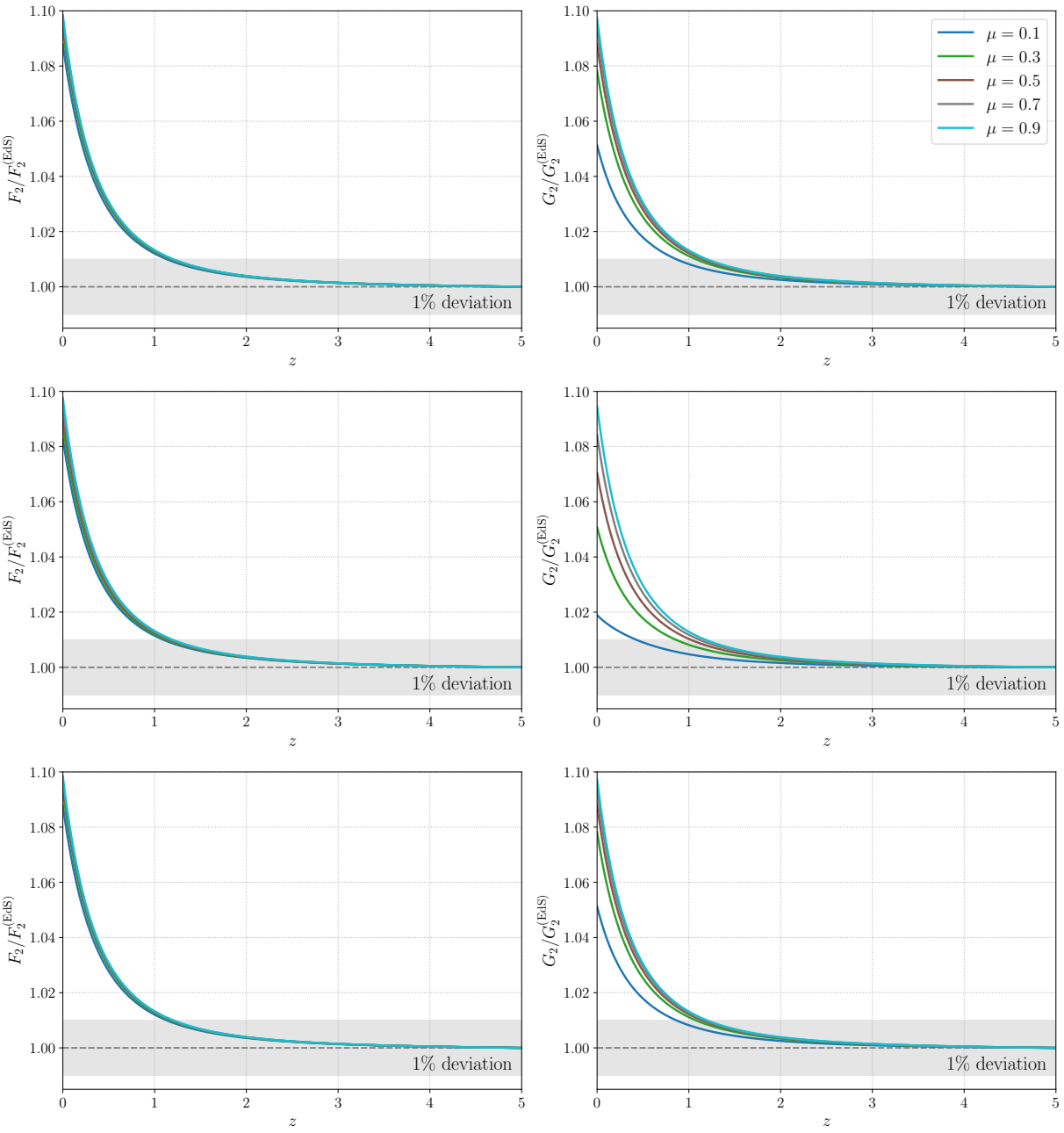

Figure C.2.: Same as Fig. 5.3, but for additional triangle configurations in the IDS scenario. **(i) Top row:** $r = 0.1$ (squeezed configuration). **(ii) Middle row:** $r = 2$ (moderately elongated configuration). **(iii) Bottom row:** $r = 10$ (highly elongated configuration).

Bibliography

[1] M. S. Turner. *The Road to Precision Cosmology*. Annual Review of Nuclear and Particle Science **72** 1 (2022). To appear in Annual Review of Nuclear and Particle Science; also available as arXiv preprint. arXiv:2201.04741. Cited on page 1.

[2] P. Collaboration. *Planck 2018 results. VI. Cosmological parameters*. Astron. Astrophys. **641** A6 (2020). URL: https://arxiv.org/pdf/1807.06209. Cited on pages 1, 3, 5, 6, 23, and 24.

[3] M. Blanton and S. Collaboration. *Sloan Digital Sky Survey: Mapping the Universe*. Astron. J. **154** 28 (2017). URL: https://arxiv.org/pdf/1703.00052. Cited on page 1.

[4] A. G. Riess et al. *A Comprehensive Measurement of the Local Value of the Hubble Constant*. Astrophys. J. Lett. **934** L7 (2021). URL: https://arxiv.org/pdf/2112.04510. Cited on pages 1, 23, and 27.

[5] D. Collaboration. *DESI 2024 VI: Cosmological Constraints from the Measurements of Baryon Acoustic Oscillations*. arXiv e-prints (2024). Versão 3 disponível. URL: https://arxiv.org/abs/2404.03002 arXiv:2404.03002. Cited on pages 1 and 5.

[6] M. Asgari et al. *KiDS-1000 Cosmology: Cosmic shear constraints and comparison between two-point statistics*. Astron. Astrophys. **645** A104 (2021). URL: https://arxiv.org/pdf/2007.15633. Cited on page 1.

[7] D. Collaboration. *Dark Energy Survey Year 3 Results: Cosmological Constraints from Galaxy Clustering and Weak Lensing*. Phys. Rev. D **105** 023520 (2022). URL: https://arxiv.org/pdf/2105.13549. Cited on page 1.

[8] E. D. Valentino et al. *In the Realm of the Hubble Tension — a Review of Solutions*. Class. Quant. Grav. **38** 153001 (2021). URL: https://arxiv.org/pdf/2103.01183. Cited on pages 1 and 25.

[9] V. Poulin et al. *Early Dark Energy Can Resolve The Hubble Tension*. Phys. Rev. Lett. **122** 221301 (2019). URL: https://arxiv.org/pdf/1811.04083. Cited on pages 1 and 25.

[10] E. D. Valentino, A. Melchiorri, O. Mena, and S. Vagnozzi. *Non-Minimal Dark Sector Physics and Cosmological Tensions*. Phys. Rev. D **101** 063502 (2020). URL: https://arxiv.org/pdf/1910.09853. Cited on pages 1, 26, and 30.

[11] F. Bernardeau, S. Colombi, E. Gaztañaga, and R. Scoccimarro. *Large-Scale Structure of the Universe and Cosmological Perturbation Theory*. Phys. Rep. **367** 1 (2002). URL: https://arxiv.org/pdf/astro-ph/0112551. Cited on pages 2, 3, 59, 68, 75, 77, 79, and 91.

[12] M. Pietroni. *Flowing with Time: a New Approach to Nonlinear Cosmological Perturbations*. JCAP **2008** 036 (2008). URL: https://arxiv.org/pdf/0806.0971. Cited on pages 2, 68, and 91.

[13] L. Amendola. *Coupled Quintessence*. Phys. Rev. D **62** 043511 (2000). Cited on pages 2, 6, 35, 72, and 91.

[14] B. Wang, E. Abdalla, F. Atrio-Barandela, and D. Pavón. *Dark Matter and Dark Energy Interactions: Theoretical Challenges, Cosmological Implications and Observational Signatures*. Rep. Prog. Phys. **79** 096901 (2016). URL: https://arxiv.org/pdf/1603.08299. Cited on pages 2 and 29.

[15] Y. L. Bolotin, A. Kostenko, O. A. Lemets, and D. A. Yerokhin. *Cosmological Evolution With Interaction Between Dark Energy and Dark Matter*. Int. J. Mod. Phys. D **24** 1530007 (2015). Cited on pages 2 and 35.

[16] W. Yang, S. Pan, E. D. Valentino, R. C. Nunes, and D. F. Mota. *Dark Sector Interaction and Cosmic Tensions*. Phys. Rev. D **101** 083509 (2020). URL: https://arxiv.org/pdf/2001.10852. Cited on pages 2 and 30.

[17] V. Petri, V. Marra, and R. von Marttens. *Dark Degeneracy in DESI DR2: Interacting or Evolving Dark Energy?* arXiv preprint (2025). Acessado em 2 de setembro de 2025. URL: https://arxiv.org/pdf/2508.17955 arXiv:2508.17955. Cited on page 2.

[18] J. Valiviita, E. Majerotto, and R. Maartens. *Instability in Interacting Dark Energy and Dark Matter Fluids*. J. Cosmol. Astropart. Phys. **07** 020 (2008). URL: https://arxiv.org/pdf/0804.0232. Cited on pages 2, 29, and 30.

[19] E. Majerotto, J. Valiviita, and R. Maartens. *Adiabatic Initial Conditions for Perturbations in Interacting Dark Energy Models*. Mon. Not. R. Astron. Soc. **402** 2344 (2010). URL: https://arxiv.org/pdf/0907.4981. Cited on pages 2 and 30.

[20] P. J. E. Peebles. *Principles of Physical Cosmology*. Princeton University Press 1993. Cited on pages 2, 6, 75, and 77.

[21] V. Mukhanov. *Physical Foundations of Cosmology*. Cambridge University Press 2005. Cited on pages 2, 6, and 77.

[22] J. M. Bardeen. *Gauge-invariant cosmological perturbations*. Phys. Rev. D **22** 1882 (1980). Cited on page 2.

[23] C.-P. Ma and E. Bertschinger. *Cosmological Perturbation Theory in the Synchronous and Conformal Newtonian Gauges*. Astrophys. J. **455** 7 (1995). Cited on page 2.

[24] B. Wang, E. Abdalla, F. Atrio-Barandela, and D. Pavón. *Dark Matter and Dark Energy Interactions: Theoretical Challenges, Cosmological Implications and Observational Signatures*. Reports on Progress in Physics **79** 096901 (2016). Cited on pages 2 and 35.

[25] E. D. Valentino, A. Melchiorri, and J. Silk. *Planck Evidence for a Closed Universe and a Possible Crisis for Cosmology*. Nature Astronomy **4** 196 (2020). URL: https://arxiv.org/pdf/1911.02087. Cited on pages 2 and 30.

[26] S. Dodelson. *Modern Cosmology*. Academic Press 1 edition 2003. Cited on pages 2, 3, 5, 6, 9, 11, 32, 77, and 79.

[27] S. Weinberg. *Cosmology*. Oxford University Press 2008. Cited on pages 2 and 5.

[28] D. Baumann. *Cosmology*. Cambridge University 2013. Lecture Notes, available at `https://cmb.wintherscoming.no/pdfs/baumann.pdf`. Cited on pages 2, 9, 10, 11, 32, and 79.

[29] D. W. Hogg, D. J. Eisenstein, M. R. Blanton, N. A. Bahcall, J. Brinkmann, J. E. Gunn, and D. P. Schneider. *Cosmic homogeneity demonstrated with luminous red galaxies*. Astrophys. J. **624** 54 (2005). Cited on page 6.

[30] P. K. Aluri et al. *Is the Observable Universe Consistent with the Cosmological Principle?* Class. Quant. Grav. **40** 094001 (2023). URL: `https://arxiv.org/pdf/2207.05765`. Cited on page 25.

[31] D. Blas, J. Lesgourgues, and T. Tram. *The Cosmic Linear Anisotropy Solving System (CLASS)*. JCAP **07** 034 (2011). Cited on page 77.